

**AFWAL-TM-84-203**

PREDICTION OF AERODYNAMIC DRAG

CHARLES E. JOBE



AERODYNAMICS & AIRFRAME BRANCH

AEROMECHANICS DIVISION

JULY 1984

19970612 029

APPROVED FOR PUBLIC RELEASE; DISTRIBUTION  
IS UNLIMITED

**FLIGHT DYNAMICS LABORATORY  
AIR FORCE WRIGHT AERONAUTICAL LABORATORIES  
WRIGHT-PATTERSON AIR FORCE BASE, OHIO 45433**

DTIC QUALITY INSPECTED 1

**REPORT DOCUMENTATION PAGE**

*Form Approved*  
OMB No. 0704-0188

Public reporting burden for this collection of information is estimated to average 1 hour per response, including the time for reviewing instructions, searching existing data sources, gathering and maintaining the data needed, and completing and reviewing the collection of information. Send comments regarding this burden estimate or any other aspect of this collection of information, including suggestions for reducing this burden, to Washington Headquarters Services, Directorate for Information Operations and Reports, 1215 Jefferson Davis Highway, Suite 1204, Arlington, VA 22202-4302, and to the Office of Management and Budget, Paperwork Reduction Project (0704-0188), Washington, DC 20503.

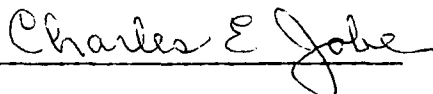
|  |   |  |   |  |
|--|---|--|---|--|
| 1. AGENCY USE ONLY (Leave blank)   |   | 2. REPORT DATE<br>JULY 1984                                | 3. REPORT TYPE AND DATES COVERED<br>FINAL REPORT JULY 1984                |  |
| 4. TITLE AND SUBTITLE<br>PREDICTION OF AERODYNAMIC DRAG  |   |  | 5. FUNDING NUMBERS  |  |
| 6. AUTHOR(S)<br>CHARLES E. JOBE  |   |  |   |  |
| 7. PERFORMING ORGANIZATION NAME(S) AND ADDRESS(ES)<br>AERODYNAMICS AND AIRFRAME BRANCH<br>AEROMECHANICS DIVISION<br>FLIGHT DYNAMICS LABORATORY<br>AIR FORCE WRIGHT AERONAUTICAL LABORATORIES<br>WRIGHT-PATTERSON AFB OH 45433  |   |  | 8. PERFORMING ORGANIZATION<br>REPORT NUMBER                               |  |
| 9. SPONSORING/MONITORING AGENCY NAME(S) AND ADDRESS(ES)<br>FLIGHT DYNAMICS DIRECTORATE<br>WRIGHT LABORATORY<br>AIR FORCE MATERIEL COMMAND<br>WRIGHT-PATTERSON AFB OH 45433-7562<br>POC: Dr Charles E. Jobe, WL/FIGC, 937-255-8484; DSN 785-255-8484  |   |  | 10. SPONSORING/MONITORING<br>AGENCY REPORT NUMBER<br><br>AFWAL-TM-884-203 |  |
| 11. SUPPLEMENTARY NOTES  |   |  |   |  |
| 12a. DISTRIBUTION AVAILABILITY STATEMENT<br><br>APPROVED FOR PUBLIC RELEASE; DISTRIBUTION IS UNLIMITED   |   |  | 12b. DISTRIBUTION CODE  |  |
| 13. ABSTRACT (Maximum 200 words)<br><br>Drag prediction is the most important and challenging problem in aerodynamics. Experimental, empirical, analytical and numerical approaches, singly and in concert, have addressed this problem with varying degrees of success (and notable failures). This report reviews the published material on drag prediction through January 1984., The subject of wind tunnel to flight drag correlation will be reviewed in a later report. |   |  |   |  |
| 14. SUBJECT TERMS<br>Drag Prediction   |   |  | 15. NUMBER OF PAGES<br>210  |  |
|  |   |  | 16. PRICE CODE  |  |
| 17. SECURITY CLASSIFICATION<br>OF REPORT<br>UNCLASSIFIED   | 18. SECURITY CLASSIFICATION<br>OF THIS PAGE<br>UNCLASSIFIED | 19. SECURITY CLASSIFICATION<br>OF ABSTRACT<br>UNCLASSIFIED | 20. LIMITATION OF ABSTRACT<br>SAR   |  |

FOREWARD

This report was prepared by Charles E. Jobe of the Aerodynamics and Airframe Branch, Aeromechanics Division, Flight Dynamics Laboratory, Wright-Patterson AFB, Ohio. The work was performed under Work Unit 24041048, Advanced Methods for Aerodynamic Prediction.

Drag prediction is the most important and challenging problem in aerodynamics. Experimental, empirical, analytical and numerical approaches, singly and in concert, have addressed this problem with varying degrees of success (and notable failures). This report reviews the published material on drag prediction through January 1984. The subject of wind tunnel to flight drag correlation will be reviewed in a later report.

This report has been reviewed and is approved.



CHARLES E. JOBE

Technical Manager

Aerodynamic Methods Group



TOMMY J. KENT, MAJ, USAF

Chief, Aerodynamics and

Airframe Branch

## PREDICTION OF AERODYNAMIC DRAG

|       |   |    |
|-------|---|----|
| 1     | Introduction                                | 1  |
| 1.1   | Drag  | 4  |
| 1.2   | Level of Drag Prediction Detail             | 5  |
| 1.2.1 | The Preliminary Design Phase                | 6  |
| 1.2.2 | The Detailed Design Phase                   | 6  |
| 1.2.3 | The Final Design Phase                      | 7  |
| 2     | Subsonic Drag                               | 11 |
| 2.1   | Empirical Correlations                      | 12 |
| 2.1.1 | Bomber/Transport Aircraft                   | 13 |
| 2.1.2 | Fighter/Attack Aircraft                     | 14 |
| 2.2   | Detailed Drag Estimates - Component Buildup | 16 |
| 2.2.1 | Friction Drag                               | 17 |
| 2.2.2 | Form Drag                                   | 19 |
| 2.2.3 | Interference Drag                           | 21 |
| 2.2.4 | Camber Drag                                 | 22 |
| 2.2.5 | Base Drag                                   | 23 |
| 2.2.6 | Miscellaneous Drag                          | 23 |
| 2.2.7 | Drag Due to Lift                            | 23 |
| 3     | Transonic Drag                              | 30 |
| 3.1   | The Drag Rise                               | 30 |
| 3.2   | Detailed Drag Estimates - Component Buildup | 31 |
| 3.2.1 | Zero-Lift Drag                              | 31 |
| 3.2.2 | Drag Due to Lift                            | 33 |
| 3.3   | Numerical Transonic Aerodynamics            | 33 |
| 4     | Supersonic Drag                             | 36 |
| 4.1   | Friction Drag                               | 37 |
| 4.2   | Wave Drag                                   | 39 |
| 4.3   | Lift-Induced Drag                           | 42 |
| 5     | Numerical Aerodynamics                      | 49 |
|       | Bibliography                                |    |

| <u>FIGURE</u> | <u>TITLE</u>  |
|---------------|---|
| 1             | Test Approach   |
| 2             | Transport Aircraft Drag Buildup   |
| 3             | Probable Error During Design  |
| 4             | Drag Data Scatter About Drag Polar Fairings with Mach Number                                |
| 5             | Typical Aircraft Drag Breakdowns  |
| 6             | Components of Aircraft Drag   |
| 7             | Equivalent Skin Friction  |
| 8             | Subsonic Parasite Drag - Bomber/Transport   |
| 9             | Subsonic Parasite Drag - Fighter/Attack   |
| 10            | Relative Wing Size  |
| 11            | Equivalent Body Shape   |
| 12            | Equivalent Body Concept   |
| 13            | Aerodynamic Cleanness   |
| 14            | Comparison of Empirical Flat Plate Skin Friction Formulae for Incompressible Turbulent Flow |
| 15            | Summary of Experimental Research on Flat Plate Skin Friction, Incompressible Speeds         |
| 16            | Fuselage Profile Drag - Bodies of Revolution  |
| 17            | Fuselage Shape Factors $M \leq 0.70$  |
| 18            | Airfoil Shape Factors   |
| 19            | Lift and Speed Regions for Calculation of Drag Due to Lift                                  |
| 20            | The Subsonic Drag Polar   |
| 21            | Drag Predictions Using Panel Methods  |
| 22            | Effects of Engine Power on Lift and Drag of Various Aircraft Components                     |
| 23            | Historic Correlation of Transonic Drag Rise   |
| 24            | Transonic Drag Buildup  |

|    |  |
|----|--|
| 25 | F-5 $C_L$ versus $C_D$ ; $M = 0.9$   |
| 26 | Total Forces and Moments Comparison Between Different Computer Programs  |
| 27 | Correlation of Calculated and Measured Wing-Body Drag Divergence Mach Number, Compressibility Drag, and Drag Rise for Three Supercritical Wings. |
| 28 | Supersonic Drag Buildup  |
| 29 | Supersonic Skin Friction   |
| 30 | Supercruiser Type Configuration - Test Theory Comparison   |
| 31 | Experimental and Theoretical Drag Polars of Supersonic - Cruise Airplanes $R_c = 4.8 \times 10^6$  |
| 32 | Leading Edge Suction Effects, LES 216  |
| 33 | Drag Polars, CDAF Configuration  |
| 34 | $5C^3$ , Drag Performance  |
| 35 | Supersonic Volumetric Efficiency   |
| 36 | Zero Lift Drag Buildup   |
| 37 | Zero Lift Drag Comparison  |

TABLE

TITLE

1

Drag Scatter

2

Aircraft Characteristics - Fighter/Attack Geometry

## Prediction of Aerodynamic Drag

### 1 INTRODUCTION

The state-of-the-art in aircraft drag prediction was defined as of 1973 by the AGARD conference entitled "Aerodynamic Drag."<sup>20</sup> This chapter draws heavily on that work and attempts to update, to the extent possible, those portions relevant to aircraft drag prediction at subsonic, transonic and supersonic speeds. Special drag prediction problems peculiar to short take-off and landing (STOL) designs, such as jet flap thrust recovery, and energy efficient aircraft concepts, for example laminar flow control, are beyond the scope of this chapter; as are drag due to speed brakes and fighter aircraft weapons carriage. Certainly, a sound physical understanding of drag will be required before drag prediction becomes a science.

The assessments, projections and conclusions in this chapter agree, in general, with those of Wood<sup>161</sup> who briefly addressed four relevant questions.

- "1. How well do ground based estimates for drag polars and engine characteristics correlate to flight test results?
2. In what areas do performance prediction techniques work best or worst, and why?
3. What are the differences in the way various manufacturers (airframe or engine) predict drag polars and engine characteristics?
4. Are there portions of various performance prediction techniques that could or should be combined to form a better or best method?"



Wood's answer to question one is, very well for up-and-away flight; however, his survey of twelve commercial transport aircraft showed six predictions were low (as much as 22%), four were high (up to 10%), and two were exact. The second question received a similar answer: predictions are best for up-and-away flight in the clean aircraft configuration. An entire symposium would be needed to address questions three and four unless the simple answer that no single methodology is best for every situation is accepted. Wood also observed that, "the quality of the estimate is more a function of the time and care taken to include all the details and higher-order terms than it is of the particular equations used."

Williams'<sup>158</sup> synthesis of responses to the AGARD-FMP questionnaire on prediction techniques and flight correlation is also worthy of detailed study. The five questions asked of experts in six NATO countries were:

- "1. What are the advantages/disadvantages of different prediction techniques?
2. What portions of the flight regime cannot/should not be addressed by ground-based techniques?
3. Are there areas where analytical prediction can be better than wind tunnel and/or simulation results; or vice-versa?
4. Are there methods of reducing differences between prediction and flight test results?
5. Are there any new prediction techniques that should be emphasized?"

Williams' section on background to prediction/design needs and discussion of increasing technical demands is also especially relevant to the understanding of drag prediction.

The initial sections of this chapter describe drag prediction methods typically used to define the most promising configuration for further, detailed analysis and wind tunnel testing. These methods are mainly empirical in origin, although numerical aerodynamics is presently providing timely data for this phase of design in some organizations. The latter sections of the report describe drag prediction methods based on wind tunnel results from models specifically constructed for the particular design project and guided by aerodynamic theory, known as "wind tunnel to flight correlations." Rooney<sup>119,120</sup> and Craig<sup>34</sup> have recently published detailed accounts of the meticulous testing performed to correlate the wind tunnel and flight measured aerodynamic drag of the Tomahawk Cruise Missile. The size of this missile permitted wind tunnel testing of the full-scale vehicle -- yet discrepancies remained. These correlations and many others for all types of aircraft and missiles form the basis of evaluation for a new design.

Despite many recent advances, it is generally conceded that accurate drag predictions, based entirely on the solution of the equations of motion, or some reduced form thereof; are, at present, limited to the prediction of drag due to lift in the linear range and supersonic wave drag for a limited class of slender configurations. All other drag predictions ultimately depend on empirical correlations. Progress in computational fluid dynamics or, more generally, numerical aerodynamics, has been tremendous in the last decade and will continue into the future due to the introduction of new computers, faster, more accurate solution algorithms, improved resolution of grids and new turbulence models.<sup>73</sup> However, except for the isolated cases of drag-due-to-lift at small angle of attack and supersonic wave drag for smooth slender bodies, drag prediction is beyond the capability of current numerical aerodynamic methods.

The aerodynamics of the aerodynamic reference model<sup>147</sup>, usually a sub-scale wind tunnel wing-body model with flow-through nacelles and reference nozzles are considered initially. This is one of many models tested during an aircraft development program, Fig. 1, and the basic model for drag prediction. The uncorrected airplane lift, drag, and pitching moment characteristics are derived from tests of this model. Drag corrections to account for the differences between the data from this model and the actual flight vehicle are discussed in the latter sections of this chapter. The methods of properly combining these drag data, including thrust effects, are the subject of this book.

### 1.1 Drag

The resultant aerodynamic force caused by a flight vehicle's motion with respect to the atmosphere is the summation of the normal, pressure forces, and the tangential skin friction forces acting on the vehicle's surface. This resultant force is conventionally resolved into lift and drag components in the vehicle's plane of symmetry. The lift force is the aerodynamic reaction perpendicular to the free-stream velocity direction which is the level equilibrium flight path direction. Lift is not directly a subject of this chapter; however, drag, the component of the total force that opposes motion in the equilibrium flight path direction, approximately follows a parabolic variation with lift for heavier-than-air flight as shown in Figure 2. Thus, the relative state of motion of the vehicle (equilibrium, or accelerated flight) is determined by the lift force, which is an appropriate multiple of the vehicle's weight, and the throttle-dependent thrust force.

Aircraft normally spend ninety percent of their flight time on nominally straight, unaccelerated flight paths where all the forces are in static equilibrium. This is the cruise condition that is usually considered the

standard condition for the design of an airplane. This chapter is mainly concerned with cruise drag prediction (Fig. 2) because of the importance of this flight condition. Drag prediction for accelerated flight (take-off, landing, maneuver) will be treated as an important, although ancillary, issue.

The parabolic variation of drag with lift, or angle of attack, appropriately additive to the zero lift drag is shown in Fig. 2. Drag is produced by the tangential (skin friction) and normal (pressure) forces acting on the vehicle's surface due to relative fluid motion from a basic fluid mechanics standpoint. Total drag has been dissected into a multitude of various components, depending on the phase of the design process, the aircraft mission and configuration, the experimental data available and the persuasion of the drag analyst. A properly defined, consistent reference condition for the entire aircraft and propulsion system is crucial to the correct final comparison of theoretical, empirical, ground and flight test data in the latter design stages for performance guarantees. The operating reference condition is straight-forward for commercial transports with a single, known cruise design point; however, military fighter aircraft with multiple design points pose severe additional problems. It is often difficult to define an operating reference condition in this case. Additionally, the variation in installed flight test thrust permitted in military engines of the same family can be an order of magnitude greater than that permitted in engines slated for commercial applications.

## 1.2 Level of Drag Prediction Detail

Three somewhat distinct levels of drag prediction sophistication and reliability are usually described by authors on this subject.<sup>20, 106, 110, 125, 167</sup> In reality, drag predictions are updated continuously throughout the

entire design cycle of an aircraft as data from numerical methods and wind tunnel tests become available. However, decisions that affect the final design are made based on the best available information at many stages of the design process.

#### 1.2.1 The Preliminary Design Phase.

This is the beginning of the design process. It has also been called the feasibility<sup>20</sup> and conceptual<sup>167</sup> design phase. Primarily empirical methods are used to assess the relative merits of many design concepts against the mission specifications generated by an apparent market opportunity or military statement of operational need. Drag prediction error, as measured with respect to future flight test data, is highest due to method error and geometric uncertainty in the configuration definition<sup>13</sup>, Fig. 3. Relative accuracy in the methodology is necessary at this stage in order to select the most efficient configuration to meet the design objectives. Absolute accuracy is desirable in order to give equal consideration to all new concepts and areas of the design space or mission profile. Promising new concepts could be excluded from further consideration at this stage if drag methodology incorrectly predicts that the mission cannot be achieved. An overall drag target or maximum drag level is determined during this design phase. Several compilations of drag prediction methodology are available<sup>4, 63, 101, 107, 122, 135</sup> for rapid performance assessment. Each has its own peculiarities and limitations. Additionally, each airframe manufacturer has compiled large drag handbooks that are highly valued and extremely proprietary.

#### 1.2.2 The Detailed Design Phase.

Drag validation becomes a more specialized and detailed continuous process. This phase has also been called the development<sup>20</sup>, preliminary<sup>124</sup>, and project definition<sup>109</sup> phase. Estimates and assumptions are gradually replaced by

predictions supported by intensive wind tunnel test data on the determinate aircraft design, as derived from the clean wing reference configuration and aerodynamic reference configuration models, Fig. 1. Drag sub-targets for each component of the configuration, consistent with the overall target, are assessed and synthesized. In some development programs, prototype flight test data provides the basis for diagnostics, reassessments, and analysis if drag improvements are found to be necessary.

### 1.2.3 The Final Design Phase.

Production aircraft performance guarantees with error bounds are made. This is also the pre-production<sup>20</sup> or wind tunnel to flight correlation<sup>104</sup> phase. A detailed analysis and interpretation of the prototype test performance is conducted. The drag predictive model is calibrated by reference to the prototype data. An excellent description of this process and its difficulties has been published by Rooney<sup>119</sup> and Craig<sup>34</sup> for the Tomahawk missile.

Theory, empirical methods, and ground and flight test measurements are continuously intertwined throughout the design, development and production phases of an aircraft's life. Each drag prediction method contains its unique strengths and weaknesses.

Strictly empirical methods, conventionally based on flight test data, include the real aircraft effects of flow separations, Reynolds number, gaps, steps, protuberances, rigging, etc., but are not readily generalized. Problems have even arisen when these methods are applied to aircraft of the same family from which the data base was generated.<sup>158</sup>

Current theoretical methods that utilize large computers are capable of immediate generalization to almost any configuration, but are limited in accuracy because of the lack of real aircraft effects. Prediction of the drag-due-to-lift is usually quite accurate up to drag levels where flow

separations become significant. Prediction of the zero-lift-drag remains empirical.

Progressive wind tunnel development programs contain a greater degree of reality than theoretical methods, lack some real aircraft effects, and are costly and time consuming. Correct interpretation of the data remains an art, particularly when wall effects, Reynolds number scaling and propulsion system model data are included. Systematic total drag measurement errors greater than one percent cannot be tolerated if drag prediction methods for the smaller drag components are to be validated.<sup>19</sup>

A typical breakdown of flight test drag data is shown in Fig. 2. The industry standard for drag measurement ( $\pm 3\%$  accuracy) is seldom achieved, even under carefully controlled conditions.<sup>118</sup> From these data, drag correlations for each drag component are made and drag design charts are constructed as a basis for the preliminary design empirical method. The preliminary design study is considered as the reference point for judgment on program success. The initial decisions on wing area, aspect ratio, thickness ratio and matching engine cycle and thrust requirements are based on early lift-to-drag (L/D) estimates. A lower bound for L/D must be estimated in order to assure that the propulsion system will provide the power necessary at the airplane critical flight condition. Misjudgements at this design stage will result in an inefficient engine-airplane that is noncompetitive.

The designer encounters errors from two sources at this stage; errors due to lack of configuration geometric definition, and errors due to inaccurate methods. These errors have been estimated by Bowes<sup>13</sup> for long-range subsonic transports and are summarized in Fig. 3. He also suggests an aerodynamicist's rating scale, where  $M_{DD}$  is the drag divergence Mach Number. The need for an accurate force and moment model as early as possible in the design cycle is clearly evident, from the following tables.

| <u>L/D Level Achieved</u> | <u>M<sub>DD</sub></u> | <u>Rating</u> |
|---------------------------|-----------------------|---------------|
| ± 3%                      | ± .002                | Amazing       |
| ± 5%                      | ± .004                | Very Good     |
| ± 7%                      | ± .006                | Average       |
| ± 10%                     | ± .010                | Below Average |

Most commercial aircraft flying today fit within this table; however, military programs have been far less successful in achieving these accuracy levels.

This may be due, in part, to the less precise flight test data recorded from the older military aircraft as shown in the following table.

TABLE 1 DRAG SCATTER

| <u>Aircraft</u> | <u>Flight Test Data Scatter</u>       | <u>Ref</u> |
|-----------------|---------------------------------------|------------|
| B-747           | ± 1% (drag)                           | 13         |
| C-5A            | ± 3.5% (C <sub>Dp</sub> ) ± 2% (drag) | 86         |
| C-141           | ± 3.3% (drag)                         | 86         |
| B-707           | ± 5% (drag)                           | 13         |
| DC-10-30        | ± 3.5% (range factor)                 | 44         |
| F-14            | ± 1% (C <sub>Do</sub> )               | 118        |
| F-15            | ± 20% (drag)                          | 173        |
| YF-16           | ± 5% (drag)                           | 18         |
| F-16            | ± 12% (C <sub>Dmin</sub> )            | 152        |
| F-18            | ± 20% (drag)                          |            |
| Tomahawk        | ±1.5% (drag)                          | 34         |
| Tornado         | ± 3% (drag) ± 1% (C <sub>Do</sub> )   | 71         |
| Alpha-Jet       | ± 5% (drag)                           | 124        |



The table should not be read such that the data scatter is constant for a given aircraft throughout the flight envelope. The scatter stated is representative of the cruise condition. Fig. 4, from Arnaiz's<sup>3</sup> study of the XB-70 flight test data, clearly demonstrates this point by showing the actual number of occurrences of scatter and the estimated scatter plotted against Mach number. The drag uncertainty estimates were obtained by combining many individual errors in weight, Mach number, static pressure, angle of attack, thrust, acceleration, etc., in a root-sum-square calculation.

Performance estimates for military aircraft are more accurate than Table 1 indicates, since the major problems occur when one attempts to isolate the thrust and drag components from the measured performance data. Current steady-state, level flight test data indicate that a repeatability of  $\pm 1\%$  can be achieved if meticulous care is exercised during the engine calibration and flight test processes. This level of accuracy must be attained<sup>159</sup> in order to obtain useful correlations for the smaller drag components shown in Fig. 2. These component correlations, necessary to develop accurate prediction methods, are based on convention, tradition, and aerodynamic theory.

Flight test data are, however, not presently capable of resolving drag into components. The accuracy of each component cannot be checked since only total drag, deduced from performance measurements, is available. Additional instrumentation that could resolve drag into components is superfluous to aircraft performance guarantees and is usually not included on the flight test aircraft because of the additional cost to the development program. This is particularly true of military aircraft development programs where budget cuts are traditional and there is little interest in developing drag prediction methodology for the next aircraft program.

The relative size of each drag component varies with aircraft type and flight condition. Representative examples of the cruise drag and take-off drag breakdowns for four different aircraft types are shown in Fig. 5 from Butler<sup>19</sup>. The drag breakdown also varies with aircraft range and purpose (military or civilian transport) within each aircraft type.

The conventional approach to drag estimation is to estimate and sum the zero lift drag of each major physical component of the aircraft with allowances for interference effects and other small contributions and then add the drag due to lift. Their summation is intrinsically inaccurate since aircraft components are mounted at incidence to each other so each is not at zero lift simultaneously. Butler<sup>19</sup> suggests that this classification of aircraft drag into components independent of, and dependent on, lift should be rejected and drag could be estimated by compounding elements arising from different basic causes associated with fluid dynamics as shown in Fig. 6.

Currently, each manufacturer has a methodology, or drag handbook, by which a thorough drag estimate is made. There is no single, industry-wide drag handbook. Manufacturers may even use several drag accounting breakdowns (depending on the customer) for the same airplane. There exist several basic sources for fundamental drag level prediction; however, total drag comparisons, between prediction and test, require accurate flight data and expert analysis and are highly proprietary to each manufacturer.<sup>161</sup>

## 2 Subsonic Drag

The aircraft drag at subsonic speeds, here taken to be less than the drag divergence Mach number, is traditionally decomposed into lift-induced drag and minimum drag. Minimum drag is further divided into friction drag, profile drag, and interference drag.

The accuracy of the drag divergence Mach number,  $M_{DD}$  prediction varies widely with configuration. Rooney's<sup>119</sup> detailed assessment of the Tomahawk flight test data indicates that  $M_{DD}$  cannot be accurately predicted while Henne, Dahlin and Peavey<sup>57</sup> conclude that a substantial capability exists for the determination of drag divergence Mach number for transport type geometries. The determination of drag levels and increments is rated marginal. McGeer and Shevell<sup>94</sup> were able to correlate transonic drag rise data for peaky type airfoils on older Douglas transport aircraft wings. Their correlation was not accurate for the Boeing 747 or the F-111A/TACT aircraft, however.

## 2.1 Empirical Correlations (C.R. James)

In the preliminary design phase, gross or overall correlations are used to estimate the size and geometric features of the aircraft. These correlations are traditionally based on wind tunnel and flight test data from older, successful aircraft. The key to this method is to obtain sufficient, relevant data from aircraft of the same general type (bomber, transport or fighter, etc.) being designed in order to form trends and extrapolations with confidence. Data collections of this type are continuously sought and maintained within the preliminary design groups of the aircraft industry. The data from a single airframe manufacturer, for a particular series of aircraft similar to the new design, usually produces the most accurate drag prediction.

Correlations of flight test data based on aircraft geometry provide insight as to the relative importance of factors influencing subsonic minimum drag. This section treats two types of aircraft: bomber/transport and fighter/attack. Minimum drag is related to wetted area through the use of an equivalent skin friction coefficient,  $C_{fe}$ . Fig. 7 compares flight derived values of  $C_{fe}$  with incompressible flat plate turbulent flow skin friction

coefficients for jet aircraft of both types. This comparison shows that, in general, about two-thirds of subsonic minimum drag may be attributed to skin friction. The balance is due to form drag and interference. Form drag results from flow over curved surfaces and flow separation induced by viscous effects. Interference drag is the result of mutual interaction of the flow fields developed by the major configuration components. The equivalent skin friction coefficient,  $C_{fe}$ , is a convenient method to relate total drag (including form and interference drag) to wetted area:

$$C_{fe} = \frac{D}{q S_{wet}}$$

where  $D$  = Minimum drag, lb

$q$  = Dynamic pressure, lb/sq ft

$S_{wet}$  = Total wetted area, sq ft

The quantity  $D/q$  is defined as equivalent parasite area,  $f$ .

### 2.1.1 Bomber/Transport Aircraft

The relationship of  $C_{fe}$  and  $f$  to wetted area is illustrated in Fig. 8. Experimental points derived from flight tests of several transport and bombers are indicated. Wetted areas vary from approximately 5800 square feet for the Breguet 941 to 33,000 square feet for the C-5A. Equivalent skin friction coefficients vary from 0.0027 for the C-5A to 0.0060 for the C-130. The variation in  $C_{fe}$  reflects factors which influence form and interference drag as well as Reynold's number effects resulting from variations in aircraft size. For example, the three turboprop military transports (Br 941, C-130, and C-133) exhibit values of  $C_{fe}$  in the 0.0050 to 0.0060 range. These aircraft have upswept afterbodies characteristic of rear loading arrangements and consequently incur form drag penalties which increase  $C_{fe}$ . Interference effects of nacelles and propeller slip streams also contribute to the higher

drag levels. Jet transports (737, 727, and DC-8), with a higher degree of aerodynamic cleanness, are in the 0.0030 range. The C-5A, because of its size, operates at higher Reynolds numbers and has the lowest  $C_{fe}$  of the transports evaluated. The low  $C_{fe}$  of the C-5A is due to its aerodynamic cleanness and very low aftbody drag increment, despite its military upsweep.

### 2.1.1 Fighter/Attack Aircraft

Correlation of flight test data of fighter/attack aircraft provides additional insight as to the relative importance of factors influencing subsonic minimum drag. This section illustrates effects of four parameters: wetted area, relative wing size, fuselage shape, and aerodynamic cleanness. Correlations were developed from flight tests of eight jet fighters. In table 2 the aircraft and some key parameters are listed. Wetted areas vary from slightly over 1100 square feet for the F-84G to approximately 2100 square feet for the F-4E. Equivalent fuselage fineness ratios vary from about 4.5 for the F-86H to 9.3 for the F-18. These aircraft have single engines with the exception of the F-4E/J, F-14 and F-18. The relationship between  $f$ ,  $C_{fe}$ , and wetted area is illustrated on Fig. 9. Experimental points derived from flight tests of the aircraft listed on Table 2 are indicated on this figure. Equivalent skin friction coefficients vary from 0.0032 for the F-8D to 0.0052 for the F-4E/J. The variation in  $C_{fe}$  results primarily from factors which influence form and interference drag. Significant factors are: (1) relative wing size, (2) fuselage shape, and (3) aerodynamic cleanness.

The effect of relative wing size is illustrated in Fig. 10. The ratio of the equivalent skin friction coefficient,  $C_{fe}$ , to the incompressible mean flat plate value,  $C_{f_{ico}}$ , is shown as a function of  $\delta$ , the ratio of the total wetted area to wing wetted area. The increase in this ratio with increasing

TABLE 2  
 AIRCRAFT CHARACTERISTICS  
 FIGHTER/ATTACK GEOMETRY

| MODEL<br>DESIGNATION | AREAS (SQ. FT.)   |                 | EQUIVALENT                    |
|----------------------|-------------------|-----------------|-------------------------------|
|                      | WING<br>REFERENCE | TOTAL<br>WETTED | FUSELAGE<br>FINENESS<br>RATIO |
| A-7A                 | 375               | 1691            | 6.43                          |
| F-4E/J               | 530               | 2092            | 5.88                          |
| F-8D                 | 375               | 1821            | 8.16                          |
| F-84F                | 325               | 1257            | 5.92                          |
| F-84G                | 260               | 1104            | 5.08                          |
| F-86H                | 313               | 1186            | 4.57                          |
| F-100D               | 400               | 1571            | 6.61                          |
| F-105D               | 385               | 1907            | 8.86                          |
| F-18                 | 400               | 2046            | 9.28                          |
| F-14                 | 565               | 3097            | 8.22                          |

$\delta$  reflects the fact that wing surface tolerances are normally held much tighter than other components, and protuberances, roughness, and leakage penalties are smaller for the wing than for other components.

An important factor affecting fuselage drag is the degree of pressure or form drag developed due to flow separation induced by viscous effects. In general, flow separation is more pronounced with bodies of low fineness ratio. This effect is illustrated in Fig. 11 by defining an equivalent body which includes frontal areas of the fuselage, canopy, and wing to establish an equivalent fuselage fineness ratio. In Fig. 12 this parameter is illustrated and defined. A form factor,  $F_B$ , is defined from the empirical expression:

$$F_B = 1.02 \left[ 1 + \frac{1.5}{(\ell/d)^{1.5}} + \frac{7}{.6(\ell/d)^3 (1-M^2)} \right]$$

Mach number,  $M$ , accounts for compressibility effects, Fig. 11 also includes an aerodynamic cleanness factor,  $\omega$ , which is related empirically to relative wing size, Fig. 13.

The aerodynamic cleanness factor accounts for form drag and interference effects not treated by fuselage shape parameters. Examples are form and interference drag for wings and tails, protuberance and leakage drag, manufacturing tolerance effects, and surface roughness. The magnitude of  $\omega$  and the variation with relative wing size is shown in Fig. 13. Separate trend lines are identified as a function of the number of inlet and exit flows. The lower line is determined by the single inlet-single nozzle configurations, the middle line by the data from the F-105D with two inlets and one exit nozzle, and the upper line by the data from the F-4/J, F-14 and F-18 with two inlets and two nozzles.

These correlations suggest an initial approach for estimating subsonic minimum drag for similar fighter/attack configurations:

1. Calculate the wetted area and a characteristic length for each component.
2. Calculate an area weighted mean length,  $l_m$ , for the complete configuration or estimate  $l_m$  from experience.
3. Use this mean length to calculate Reynold's number at the flight condition to be evaluated.
4. Determine an incompressible skin friction coefficient,  $C_{f_{ico}}$ , using this Reynold's number. The Karman-Schoenherr equation for turbulent flow or a similar expression may be used.
5. Calculate the wetted area ratio,  $\delta$ , and use Fig. 13 to establish the value of  $\omega$  for the appropriate inlet/nozzle arrangement.
6. Calculate the equivalent fuselage fineness ratio,  $1/d$ , and determine the form factor,  $F_B$ .
7. Determine equivalent parasite area,  $f$ , from the expression:

$$f = C_{f_{ico}} \times \omega \times F_B \times S_{wet}$$

A similar approach developed for bomber/transport would highlight those factors influencing subsonic minimum drag for this type of aircraft.

## 2.2 Detailed Drag Estimates - Component Buildup

As the design project progresses, the geometric definition of the aircraft is formed and more detailed drag prediction methods are used to assess drag targets or design goals for each aircraft component. These goals must be consistent with the overall drag target previously determined since the total configuration drag is the sum of the component drags including interference effects.



Each component may have an initial run of laminar flow, followed by a transition zone and fully developed turbulent flow thereafter. The extent of each flow region is difficult to determine with precision. Fully turbulent flow was usually assumed from the leading edge aft on full-scale flight vehicles at altitudes below about twenty kilometers. The smoothness and rigidity of newer composite materials may provide longer runs of laminar flow on future flight vehicles. Transition is usually fixed by trip strips or grit on subscale wind tunnel models that are tested at lower Reynolds numbers. The positioning and selection of boundary-layer trip strips that accurately simulate full-scale conditions is an art.<sup>8, 14, 15</sup>

### 2.2.1 Friction Drag

There exists little controversy concerning calculation of the average laminar skin friction on one side of a doubly infinite flat plate. It is given by Blasius<sup>9</sup> formula from his exact solution to the laminar boundary layer equations for zero pressure gradient:

$$C_f = 1.32824/R_e^{1/2}$$

where  $R_e = \frac{U_\infty}{\nu_\infty} \ell$  and  $\ell$  is the distance from the stagnation point to the transition zone.

Transition takes place when the length Reynolds number nominally exceeds  $3.5 \times 10^5$  to  $10^6$  for a flat plate.<sup>123</sup> This is the critical Reynolds number, often assumed to be one-half million for many flows, although pressure gradients strongly influence the location of transition in the boundary layer. It is the objective of boundary-layer stability theory to predict the value of the critical Reynolds number for a prescribed main flow. Success in the calculation of the critical Reynolds number for flows of general aeronautical interest has eluded workers in this field for many decades despite many dedicated efforts.

Many correlations of turbulent boundary-layer data exist. In Fig. 14 the variation of  $C_f$  with Reynolds number, predicted by five different methods, is displayed. Significant changes in  $C_f$  can occur when scaling from wind tunnel ( $R_n = 3 \times 10^6$ ) to flight ( $R_n = 40 \times 10^6$ ) if different correlations are used. Two well-known and widely-used formulas are:

Prandtl-Schlichting:

$$C_f = \frac{0.455}{(\log R_e)^{2.58}} \frac{A}{R_e}$$

where A depends on the position of transition and

Karman-Schoenherr:

$$C_f^{-1/2} = 4.13 \log (R_e C_f)$$

The Prandtl-Schlichting formula, being explicit in  $C_f$ , has been more widely used in the past, although Paterson<sup>108</sup> has shown that the Karman-Schoenherr formula is a good representation of existing test data (Fig. 15). Both formulas have been used as the basis for aircraft drag prediction methods.<sup>63, 107, 135</sup> A new method, based on explicit Prandtl-Schlichting type relations, has been developed by White and Christoph<sup>153, 154</sup> for compressible turbulent skin friction. Their explicit approximation

$$C_f = 0.42/\ln^2 (0.056 R_e)$$

is accurate to  $\pm 4\%$  in the Reynolds number range  $10^5 - 10^9$ . It is the formula selected by Schemensky<sup>122</sup> for his complete drag prediction method.

The reference length used in the Reynolds number computation is the body length for near bodies of revolution and MacWilkinson, et. al.<sup>86</sup> recommend use of the mean aerodynamic chord for lifting surfaces. This choice of reference length will be less accurate (about 2% low) for highly swept delta wings. A strip method, where a reference length is calculated for each streamwise strip of the wing, should be used.<sup>63</sup>

Compressibility corrections to the skin friction are less than 10% at Mach numbers less than one and are often ignored at subsonic speeds unless continuity with supersonic predictions is desired.

### 2.2.2 Form Drag

Subsonic minimum drag is the sum of the friction, form and interference drag when the component buildup method is used. The form drag, or pressure drag, resulting from the effects of nonzero pressure gradient (component thickness) is usually accounted for by a multiplicative factor applied to the skin friction drag. Following Schemensky's<sup>122</sup> drag accounting system for example,

$$C_D = \underbrace{C_f \frac{A_{wet}}{S_{ref}} * FF * IF}_{\text{Components}} + C_{D_{camber}} + C_{D_{base}} + C_{D_{misc}} \quad \text{Eq. 1}$$

where  $A_{wet}$  is the component wetted area

FF is the component form factor, also called the shape factor, SF

IF is the component interference factor

The interference, camber, base, and miscellaneous drags are treated in later sections.

The prediction of the form drag, or FF, is dependent on empirical correlations as given by Hoerner<sup>64</sup>, Schemensky<sup>122</sup>, DATCOM<sup>63</sup>, O'Conner<sup>107</sup>, Snodgrass<sup>135</sup>, MacWilkinson<sup>86</sup>, and others. Example formulas for the computation of FF are:

$$\text{for bodies: } FF = 1 + 60/FR^3 + 0.0025 * FR$$

$$\text{for nacelles: } FF = 1 + 0.35/FR$$

$$\text{where } FR = \frac{\text{Component Length}}{\text{Width} * \text{Height}}$$

and for airfoils:

$$FF = 1 + K_1 (t/c) + K_2 (t/c)^2 + K_3 (t/c)^4$$

where  $t/c$  is the streamwise thickness to chord ratio and the  $K_i$  depend on airfoil series. An additional term, dependent on the section design camber is added for supercritical airfoils.

MacWilkinson, et.al.<sup>86</sup> have shown that fuselage profile drag (the sum of skin friction drag and form drag) can be correlated for bodies of revolution by the method of Young<sup>169</sup>, Fig. 16. This theory agreed with experimental data from four transport fuselages that are radical departures from the ideal body of revolution, if the proper fineness ratio is used as shown in Fig. 17. However, excess drag due to upsweep<sup>93</sup>, which may amount to ten percent of the total cruise drag of military transport aircraft, is not apparent from these correlations. A new prediction method for reasonable estimates of the drag of afterbodies for military airlifters has recently been published by Kolesar and May<sup>72</sup> to replace the method of Hahn, et.al.<sup>50</sup>.

Methods of estimating airfoil shape factors (or form factors) were also compared by MacWilkinson, et.al.<sup>86</sup>. There is wide scatter in both the theoretical and experimental values of the shape factor, as shown in Fig. 18, particularly at twelve percent thickness to chord ratio, a nominal value for modern transport wings. The data on the earlier NACA airfoils were not suited to accurate assessment of airfoil form drag because of the testing techniques used. This earlier data, however, forms the basis of many older shape factor correlations.

Formulas for computing the form factors for other aircraft components, canopies, stores, struts, etc., are available from Hoerner<sup>64</sup>, Schemensky<sup>122</sup>, DATCOM<sup>63</sup>, O'Conner<sup>107</sup>, and Snodgrass<sup>135</sup>, along with examples illustrating their use for drag estimation.

Formally, the form drag follows the same dependence on Reynold's number and Mach number as the skin friction since the form factors are constant for a given geometry in most drag prediction methods. Hoerner<sup>64</sup> has developed compressible form factors that explicitly account for Mach number effects by transforming the appropriate thickness or slenderness ratio using the Prandtl-Glauert transformation factor,  $(1 - M^2)^{1/2}$ . The magnitude of these corrections, however, precludes verification of their accuracy due to lack of precision in experimental data.

### 2.2.3 Interference Drag

Aerodynamic interference in aircraft is the change in flow over given components of the configuration due to the presence of one or more of the other components. Interference can be unfavorable with an attendant drag increase, or in the case of skillful design, favorable where the sum of component drags is greater than the total drag of the configuration. The importance of interference to the optimization of aircraft to meet performance requirements was delineated at a recent AGARD conference<sup>167</sup>. Generally, important interference effects involve fluid dynamic phenomena that is far too complex to be analyzed by existing computational methods.

Interference factors, to account for the mutual interference between aircraft components, are given constants based on experimental evidence for the smaller components and are usually presented as plotted data for the major components. Representative examples of this can be found in Schemensky<sup>122</sup> and DATCOM<sup>63</sup>.

The interference factors, unlike the form factors, are correlated as functions of Mach and Reynolds numbers for the major aircraft components. These factors are usually greater than unity at flight Reynolds number since the resultant total drag is usually larger than the sum of the component drags

when tested singly. The factors also increase with Mach number to account for compressibility effects. The interference factors for the smaller components are constants!

#### 2.2.4 Camber Drag

This increment to the minimum drag accounts for camber and twist in the wing, and, in some drag accounting systems, the fact that all aircraft components are not mounted relative to each other to attain zero lift simultaneously. This increment is also related to the drag due to lift methodology through the drag accounting. A correlation consistent with Equation 1 is

$$C_{D_{\text{CAMBER}}} = \frac{e}{1-e} K (C_L)^2$$

where  $e = 1/(\pi * AR * K)$  span efficiency factor

$K =$  induced drag factor

$C_L =$  a constant. The lift coefficient for a minimum drag. Often the design lift coefficient.

The factors  $e$  and  $K$  are determined from the variation of drag with lift, to be considered later.

A different drag predicting method has been shown in Fig. 2. In that system, all changes in profile drag with lift are derived from experimental data correlations and the basic profile drag is not incremented for camber directly. The method of Fig. 2 is most accurate when the aircraft designs are closely related members of the same series, for example, transports from a single manufacturer.

Thus, drag data reduced using one bookkeeping system may not include all the interference, camber, etc., effects in the resulting correlations that the drag buildup method assumes are included, unless extreme care is taken to achieve consistency.

### 2.2.5 Base Drag

This term is a weak function of Mach number at low speed and is given by Hoerner<sup>64</sup> as:

$$C_{D_{BASE}} = (0.1 + 0.1222M^8) S_{BASE}/S_{REF}$$

It obviously gains significance with increasing Mach number, however, it is independent of lift and is often not correlated separately from the body drag.

### 2.2.6 Miscellaneous Drag

This term accounts for the differences between the corrected aerodynamic reference model drag and the full-scale airplane drag due to surface irregularities, such as gaps, mismatches, fasteners and small protuberances<sup>23</sup>, and leakage due to pressurization. It is estimated, from experience and aircraft type, as some percentage of the total friction, form and interference drags in the preliminary design stages. In the later design stages, when configuration details are known, each of these small drag terms may be accounted for separately. An AGARD conference<sup>170</sup>, devoted to this subject, was held in 1981. The transfer of wind tunnel data to full-scale flight conditions is discussed under wind tunnel/flight correlation of lift, drag, and pitching moment.

It would be highly desirable to assess the creditability of each term in the drag buildup equations. Unfortunately, for complete aircraft configurations, this would require the ability to determine accurately the variation, with Reynolds and Mach numbers, of the drag forces due to viscous and pressure effects of each aircraft component - an intractable task.

### 2.2.7 Drag Due to Lift

Various methods have been used to correlate subsonic drag due to lift, or induced drag, depending upon: the design project phase, the configuration, the anticipated range of angle of attack, and the sophistication of the prediction method.

The complexity of drag due to lift prediction methodology is illustrated in Fig. 19, from Schemensky<sup>122</sup>, based on the extensive systematic correlations of Simon<sup>131</sup>. The drag is predicted in each of the regions, one through seven, by modified or distinct equations and, perhaps, additional correlations (terms) to account for increasing complexity in the flow field. The following section describes drag calculation in regions one, five, and six below the critical Mach number,  $M_{CR}$ . The detailed drag methodology is contained in Schemensky's<sup>122</sup> report.

Classical aerodynamic theory predicts that the drag due to lift is a function of the vortex distribution shed behind the wing (downwash). It is parabolic with lift and is given by

$$C_{D_i} = C_L^2 / \pi AR$$

for an elliptic lift distribution spanwise. Wing taper and sweep produce nonelliptic loadings, thus

$$C_{D_i} = C_L^2 / \pi AR e'$$

where  $e' < 1.0$  is the wing alone efficiency factor. An empirical modification to  $e'$  to account for the presence of the fuselage in the spanwise lift distribution results in

$$C_{D_i} = C_L^2 / \pi AR e = N C_L^2$$

where

$$e = e' [1. - (d/b)^2]$$

and  $d/b$  is the body diameter to wingspan ratio. The effects of camber are not included in these equations. Camber causes a shift in the polar so that minimum drag occurs at a finite lift coefficient,  $C_{L_0}$  or  $\Delta C_L$  depending on the author of the method. Simon, et.al.<sup>131</sup> illustrated this camber effect and the nonparabolic nature of the "drag polar" at higher lift coefficients where flow separation effects become important, as shown in Fig. 20.



Simon<sup>131</sup> found a further empirical modification to this equation was necessary to account for local supervelocities at the wing leading edge, while Schemensky<sup>122</sup>, using the camber drag term, found that

$$K = \frac{1-R}{C_L} + \frac{R}{\pi AR e}$$

Here R is the leading-edge suction parameter and properly bounds K between  $1/\pi AR e_0$  for full leading-edge suction ( $R = 1.$ ), and the upper bound of drag,  $1/C_{L\alpha}$ , for zero leading-edge suction, or  $C_{D_i} = C_L \tan \alpha$ . The suction parameter, R, is significantly affected by airfoil camber, conical camber, leading-edge radius, Reynolds number, and sweep. The proper determination of R is an involved procedure.<sup>122</sup>

It is within region one, bounded by the onset of leading-edge separation with reattachment, i.e., the  $C_L$  for initial polar break boundary, and the critical Mach number boundary that surface paneling methods are accurate and can be applied. These methods are all based on the Prandtl-Glauert equation, a linearized form of the complete fluid dynamics equations of motion, and can predict the lift coefficient for minimum drag and the variation of drag with lift for complex, complete aircraft configurations quite accurately.

Four panel methods were systematically evaluated in 1976 at an AGARD meeting<sup>140</sup>; however, many new methods are currently in use; for example: DOUGLAS-HESS<sup>58, 59</sup>, MCAERO<sup>16</sup>, PAN AIR<sup>26, 39, 130, 146</sup>, QUADPAN<sup>171</sup>, USSAERO<sup>41, 165</sup>, and VSAERO<sup>38, 88</sup>. Each has its particular advantages and limitations<sup>143</sup>, in addition to those due to the Prandtl-Glauert equation, because of the particular numerical method used. An evaluation of these six newer methods against the datum cases of Reference 140 would be enlightening. Drag prediction, not specifically considered during that meeting, should be added as an evaluation criteria.

Basically, all newer panel methods use Green's theorem and assume an algebraic form for the source and doublet singularity strengths on each of the panels that are used to represent the surface of the aircraft. Higher-order methods<sup>16, 26, 59</sup> use polynomials to represent the singularities while lower-order methods<sup>38, 41, 171</sup> assume that the singularities are constant (or vary linearly in one direction) over each panel. Even though the accuracy of each type of representation increases as the paneling density is increased, so does the computer time and cost, thus forcing the usual trade-off between accuracy, schedule and cost.

Panel methods have primarily been used as flow diagnostic tools<sup>31, 146</sup> by performing systematic comparative studies of alternative geometries and noting regions of high velocity or velocity gradient for further detailed analysis.

The proper application of any panel method remains an art due to the myriad of paneling layouts that can be used to represent the configurations<sup>26, 149</sup>, the impact of various types of boundary conditions<sup>28, 142</sup>, and the many numerical ways of enforcing the Kutta condition<sup>59, 143, 146, 171</sup>. The calculation of the induced drag from the velocity potential also presents problems. The near-field summation of pressure multiplied by the area projected in the drag direction results in differences of large numbers and a loss of significant figures. Control volume<sup>26</sup> and the associated far-field or Trefftz plane wake methods<sup>68, 74</sup> for drag calculations also present conceptual and numerical problems when applied to complete wing, fuselage and tailplane configurations. The optimum panel method primarily depends upon the skill of the user, the computational resources available, the geometric configuration to be analyzed, and the type and accuracy of the results desired.

Although, drag prediction results are not often published in the open literature, two examples have been found to demonstrate the induced drag prediction capabilities of panel methods.

The first, from Miller and Youngblood<sup>98</sup>, is shown in Fig. 21. The intricate paneling required for the advanced fighter configuration is shown, along with the drag polars predicted using PAN AIR<sup>130</sup> and a lower-order method, USSAERO-B<sup>165</sup>. The minimum drag was predicted using the empirical methods of the previous sections. The comparison with experimental data is good, with the results favoring use of the higher-order PAN AIR method; however, the computer resources necessary to achieve the increased accuracy were considerably higher. Modeling studies, particularly with respect to the placement of the canard wake, were also necessary to achieve these results<sup>98</sup>.

The second example is from Chen and Tinoco<sup>31</sup>. The versatility of the PAN AIR method in predicting the effects of engine power on the lift and drag of a transport aircraft wing, body, strut, and nacelle wind tunnel model is shown in Fig. 22. The computed lift and drag increments on various components of the aircraft due to increasing the fan nozzle pressure ratio from "ram" to "cruise" shows that the wing, the fuselage, and the strut all had favorable contributions, while the nacelle was the only component that contributed to a drag penalty. When the lost lift was restored and the associated induced drag was included, the computed blowing drag was 1.3 drag counts. About two drag counts were measured in the wind tunnel.

Additional applications of panel methods include: fighter aircraft with externally carried stores<sup>28</sup> (mutual interference effects), transport aircraft with flaps deployed<sup>102</sup>, and separated flow modeling using free vortex sheets<sup>88</sup>. Panel methods have also been used with boundary-layer calculation methods<sup>31, 70</sup> to simulate viscous displacement effects and the parabolized

Navier-Stokes equations<sup>111</sup>. These hybrid methods, designed to conserve computer resources by using only the equations necessary to analyze the flow in each appropriate zone, have had limited success in predicting the fluid velocities and pressure<sup>111</sup> and lift loss due to viscous effects<sup>70</sup>. Drag prediction is presently well beyond their grasp.

Drag due to lift prediction in regions five and six of Fig. 19 is an empirical art and it is likely to be many years before satisfactory physical and mathematical models are achieved for the complex separated flows that occur in these regions<sup>61</sup>. For example, the lift coefficient for polar break,  $C_{L_{PB}}$ , and the initial-stall lift coefficient,  $C_{L_{DB}}$ , coincide for thin wings, low Reynolds number, or highly swept wings, and region five does not exist<sup>122</sup>.

The lower bound for region five is the lift coefficient at which leading-edge separation and subsequent reattachment occur - the bubble-type separations. The upper bound is reached when stall occurs and the entire upper surface flow is separated. Blunt, thick airfoils generally exhibit trailing-edge separation, while very thin airfoils exhibit leading-edge separation. Airfoils of moderate thickness are likely to separate and reattach at the leading-edge, followed by trailing-edge separation and stall at higher lift coefficients. The leading-edge bubble separation produces an increase in drag due to lift because of decreased leading-edge suction. Above drag break, the flow separates completely from the wing and the drag rapidly increases.

The drag correlations developed by Schemensky<sup>122</sup>, Simon, et.al.<sup>131</sup>, and Axelson<sup>4</sup> can be used for rough estimates during the preliminary design phase, but lack the logical and consistent framework necessary for confident, detailed design trade-off studies. As shown in Fig. 20, the drag due to lift in region five varies with lift at a greater rate than in region one. The

additional drag in region six is a separation drag increment that has been correlated with the lift coefficient at drag break<sup>131</sup>.

Numerous symposia have been devoted to the prediction of viscous-inviscid interactions, separation and stall. Gilmer and Bristow<sup>45</sup> accurately predicted the lift and drag of three airfoils through stall by combining a two-dimensional panel method, an integral boundary-layer method and an empirical relationship for the pressure in the separated zone and wake recovery region. Maskew, Rao, and Dvorak<sup>89</sup>, also using a panel method with a simple wake model with prescribed separation line and wake geometry, were able to predict the pressure distribution over an aspect ratio six, 10° swept wing at 21° angle of attack.

The subject of leading-edge separation from slender wings has recently been summarized by Hitzel and Schmidt<sup>62</sup>. Potential flow methods that model the leading-edge vortex and recently-developed Euler methods can predict the flowfield and lift, but drag comparisons are not included. The Pohlhamus suction analogy in conjunction with linear lifting surface theory<sup>24</sup> has produced excellent comparisons with experimental drag data for thin slender wings. However, the method fails for higher aspect ratio wings typical of subsonic transport aircraft.

The use of strakes and other leading-edge devices to reduce the drag at high lift and transonic speeds typical of maneuvering fighter aircraft was the subject of an extensive AGARD conference<sup>61</sup>. Design guidelines and empirical rules for strakes were determined from extensive wind tunnel data bases. A fundamental understanding of the effects of strakes on the wing flowfield, lift and drag was not evident in the proceedings.

High angle of attack aerodynamics<sup>61</sup> is certainly one area of aerodynamics that is not a mature science. Considerable theoretical and experimental

effort will be required to develop accurate force and moment prediction methods for general configurations.

### 3 Transonic Drag

The format of this section parallels that of Section 2. A rapid, strictly empirical method for determining the overall drag rise for preliminary design is presented, followed by a drag component buildup method to assess drag targets for each aircraft component. The section concludes with a summary of the status of numerical aerodynamics methods for detailed drag cleanup during the later design phases.

#### 3.1 The Drag Rise (C.R. James)

A correlation of the point drag difference between Mach numbers 1.2 and 0.8 for many fighter aircraft is shown in Fig. 23. The shape of the drag curve between these Mach numbers, where the drag may attain a maximum, cannot be determined by this method.

The increase in minimum drag coefficient at transonic speeds is determined primarily by configuration slenderness. Body fineness ratio (length/diameter), lifting surface sweeps, and thickness ratio (thickness/chord length) are primary parameters for expressing slenderness of major configuration elements. The area rule concept<sup>97, 167</sup> provides a convenient approach to combining body and wing cross-sectional areas to define an equivalent body of revolution. Fineness ratio of this equivalent body is used as an index of configuration slenderness to derive a correlation of transonic drag rise.

Historic data from twenty-eight aircraft, where the cross-sectional area distribution normal to the body centerline (Mach 1.0 cut) is used to define an equivalent body fineness ratio ( $\lambda/d$ ), is compared in Fig. 23. In all air-breathing configurations, the inlet capture area is subtracted from the body total area aft of the inlet station to define the equivalent body shape.

Minimum drag coefficient,  $C_{D\pi}$ , is based on the maximum cross-sectional area of the equivalent body and the difference between drag values at  $M = 1.20$  and  $M = 0.80$  is defined here as the drag rise.

Three generations of aircraft are shown: (1) early experimental aircraft, (2) the Century series aircraft, and (3) subsequent developments. Most of the data are taken from flight test results, although data for some aircraft (the NASA LFAX configurations and the XFY-1, for example) are taken from wind tunnel tests. The theoretical slender body values determined for Sears-Haack<sup>126</sup> minimum drag body shapes, pointed on both ends, is indicated as a lower limit. An overall progression toward this lower limit is discernable. The first generation supersonic aircraft with fineness ratios of the order of 7.0 had drag rise values about 60% higher than the Sears-Haack limit, the second generation about 50%, and the third, about 25%. The B-58 with an external store pod is the configuration nearest the lower limit.

Unfortunately, some of the currently operational aircraft depart from the trends established by the earlier generations. The F-15, for example, with a fineness ratio of 8.7 has a drag rise 200% higher than the Sears-Haack lower limit and the F-18 with a fineness ratio of 9.5 is 225% above this limit.

### 3.2 Detailed Drag Estimates - Component Buildup

#### 3.2.1 Zero-Lift Drag

A schematic diagram of the component buildup method is shown as Fig. 24. The skin friction drag may be computed by the methods of Section 2.2 at the appropriate Reynolds and Mach numbers for the flow. The friction drag is nearly invariant over the small range of Mach number that is considered transonic, unless the localized details of shock boundary-layer interactions are considered.

While the form and interference drags are also computed by the methods of Section 2.2, both are assumed to terminate abruptly at sonic speed. Recall that some form factors are constants over the entire subsonic range while others are functions of both Reynolds and Mach numbers. Similarly, the wave drag, to be treated in Section 4.2, is assumed to begin abruptly as Mach one is exceeded. Since neither assumption is physically realistic, the zero-lift drag curve is forced to be continuous through the first derivative by fitting a polynomial through the zero-lift drag value at critical, or drag divergence, Mach number. Drag creep is accounted for by the variation of form and interference factors with subsonic Mach number given in Section 2.2. Thus, the drag rise and the interference plus form drag are replaced by wave drag beyond Mach one.

The decrease in critical Mach number with increasing lift for most airfoils causes the subsonic drag polar to begin its rise earlier at higher lift coefficients. The drag rise is usually separated into a minimum drag contribution and a contribution due to lift to account for this change. The drag rise due to lifting surfaces begins at  $M_{CR}$  while the drag rise due to all other components begins at  $M_{CR0}$  as correlated by Schemensky<sup>122</sup>.

Certainly, many unresolved problems and contradictions are evident in this method. It is merely an acceptable artifice to provide continuous drag curves through the transonic regime. For example, the component critical Mach numbers depend on airfoil section, thickness ratio, or body slenderness ratio<sup>122</sup>. It may be different for each aircraft component, causing each to enter the transonic regime at a different free stream Mach number, or interference between closely spaced components, such as aft pylon-mounted engines, may dominate the entire flow field and drag<sup>167</sup>. The drag curves generated by this curve fitting also do not account for the pressure drag slope relationships



derived from transonic similarity theory<sup>105</sup>, and so on. Transonic drag prediction is not yet a reliable, consistent art!

### 3.2.2 Drag Due to Lift

In the transonic region three of Fig. 19, bounded by the critical Mach number and the limit Mach number  $M_{L1}$ , where  $0.95 \leq M_{L1} \leq 1.00$ , the induced drag is computed in the same manner as described for region one, Section 2.2. The drag rise for lifting surfaces from the previous section shifts the basic polar, depending upon  $M_{CR}$ . In the transonic region four above  $M_{L1}$ , the drag polar is calculated by interpolation of the polar shape factors,  $K$ , in regions two and three.

A newer method for transonic drag due to lift prediction to extremely high angles of attack has been programmed by Axelson<sup>4</sup>. This method is based on new forms of compressible wing theory covering potential and nonpotential flows and requires, in addition to the usual geometric inputs, the limiting forward and aft chordwise locations of the shock wave. The method predicts the drag due to lift reasonably well for quite general, assumed limit shock positions, as shown in Fig. 25. The drag at zero lift is not calculated by this program and must be supplied by the user.

### 3.3 Numerical Transonic Aerodynamics

The progress in computational transonic aerodynamics has been reviewed in several recent publications<sup>105, 145, 167, 168</sup>. The book, edited by Nixon<sup>105</sup>, describes steady transonic flow research from both an industry viewpoint and a research viewpoint and includes recent advances in experimental techniques and prediction methods. Yoshihara's AGARD reports<sup>167, 168</sup> review transonic aerodynamics for the applied aerodynamicist engaged in the design of combat and airlift aircraft with proper emphasis on aircraft component interference<sup>167</sup>.

The numerous authors in the field of numerical transonic aerodynamics have reached a consensus -- transonic drag predictions are currently unreliable by any method. Neither the polar shape nor drag levels are acceptably predicted. The uncertainty in the magnitude and often, even the sign, of incremental drag due to small geometric changes precludes the use of drag as an object function in minimization procedures. The surrogate transonic design criteria is the pressure distribution which places a heavy burden on the aerodynamicist. The target pressure distribution must be chosen such that boundary-layer separation is avoided, wave and vortex drag are minimized, and the resulting geometry is acceptable.

Transonic flow is highly three-dimensional and inherently nonlinear. A hierarchy of approximate equations, in addition to the full Navier-Stokes equations, have been used to analyze these flows with varying degrees of success<sup>168</sup>. Unfortunately, the geometric fidelity of the numerical representation, necessary to distinguish drag differences due to design changes, diminishes as the higher approximations are used. This is a result of increased grid generation and computational storage requirements. Grid resolution has been a primary cause for poor drag prediction using even the full Navier-Stokes equations with various turbulence models<sup>32</sup>.

The theoretical and numerical bases for drag calculations based on the approximate equations (transonic small disturbance, full potential and Euler) have been questioned<sup>103, 167, 172</sup> and remain controversial. The addition of a coupled boundary-layer solver to the inviscid transonic flow calculation further complicates the problem of accurate drag determination<sup>168</sup>.

Transonic flow calculations are presently limited in geometric capability to various collections of aircraft components and lack the full configuration

geometric capability of panel methods. The following examples indicate the current limitations and progress that is being made in this area.

Longo, Schmidt, and Jameson<sup>84</sup> illustrated the improvement in transonic airfoil drag prediction produced by modifying the original Bauer-Garabedian-Korn-Jameson (BGKJ) nonconservative full potential method with weak viscous interaction to account for strong viscous interactions (VGK) as shown in Fig. 26. The Dofoil method consists of a conservative, full-potential flow solver coupled to a set of integral boundary-layer methods with special models for separation bubbles at the trailing edge. Further improvements (unpublished) have been obtained by substituting a finite volume Euler flow solver for the inviscid method.

Henne, Dahlin and Peavey<sup>57</sup>, also using the Bauer, Garabedian and Korn method, obtained an excellent correlation of drag divergence Mach number. They found significant scatter in the drag level and compressibility drag increment results for eight airfoils.

Hicks<sup>60</sup> extensive review of transonic wing design using both conservative and nonconservative potential flow codes did not use drag as an evaluation criteria since it was considered to be the least accurate quantity calculated by the aerodynamic codes. Poor experiment to theory correlations of the wing pressure distributions were found for configurations with low fineness ratio bodies. Henne, Dahlin, and Peavey<sup>57</sup> again found drag divergence Mach number could be correlated while drag level and compressibility drag increment could not, for three high aspect ratio transport-type wings, as shown in Fig. 27. Waggoner<sup>150</sup>, using a small disturbance transonic analysis code coupled with a two-dimensional boundary-layer code for the analysis of a supercritical transport wing-body configuration found the method sensitive to design changes, but an increment of 41 drag counts was added to the predicted drag

level to obtain agreement with test data. The computational grid resolution was coarse, particularly on the body nose and boattail region which may account for this drag increment.

The preceding results show that transonic aerodynamics has enjoyed limited success when applied to high aspect ratio transport configurations. However, when applied to a high-performance fighter configuration with a wide complex fuselage, or canards, none of the full-potential methods is capable of straight-forward prediction of the wing pressures, even at the outboard span stations.

With the possible exception of the development of a new transonic method based on paneling technology<sup>39</sup>, geometric generality has been limited to the small disturbance equations. Shanker and Goebel<sup>127</sup> have developed a numerical transformation capable of modeling the closely-coupled canard-wing interactions typical of proposed highly maneuverable fighter configurations. Drag minimization for these complex configurations has been addressed by Mason<sup>90</sup> using a modified vortex lattice method.

Transonic aerodynamic theory and the associated numerical methods are currently employed for design guidance. It will be some time until transonic drag predictions are accurate and reliable enough for detailed design data.

#### 4 Supersonic Drag

Somewhat contrary to the state of transonic drag prediction, supersonic drag is firmly based on theoretical and numerical methods. In the early 1970s, the supersonic transport and the B-70 programs provided the impetus for the extensive development and numerical implementation of linearized supersonic theory that had begun in the 1960s. The dedicated, pioneering efforts of Bonner<sup>10, 11, 12</sup>, Carlson<sup>21</sup>, Carmichael<sup>25</sup>, Harris<sup>54, 55</sup>, Middleton<sup>97</sup>,

Woodward<sup>165</sup>, and others have produced automated numerical design procedures comprised of many individual computer codes under the control of an executive coupling routine. These numerical procedures are continually evolving to reduce the shortcomings uncovered during the succeeding years of intensive application to fighter, bomber and transport configurations. The drag predictions produced by the current versions of these programs are excellent for many slender supersonic configurations at low lift coefficients and are widely used throughout the aircraft industry for preliminary design.

As shown in Fig. 5a, the supersonic cruise drag components are dramatically different from the subsonic cruise drag components. The large, obvious difference is the wave drag, a component that does not have a counterpart in subsonic flow. The lift-dependent and skin friction drag components are analogous to their subsonic flow counterparts and are calculated by the following modifications to the previous subsonic methods. The supersonic drag buildup, using linearized theory, is illustrated in Fig. 28.

#### 4.1 Friction Drag

The effects of compressibility and heat transfer must be accounted for at supersonic speeds. The mean adiabatic skin friction coefficient decreases by about 30%, regardless of Reynolds number, in changing from incompressible speeds to Mach two, as shown in Fig. 29. The relative predictions from the four theories vary with both Reynolds and Mach numbers, illustrating several drag prediction problems. Certainly, the basic full-scale skin friction drag prediction during initial design depends on the theory selected. The correlation from wind tunnel model scale to full-scale flight, as illustrated by the Concorde<sup>81</sup> data, depends on the theory selected. Finally, the reduction of flight test results, in order to define actual drag as a function of Mach number, altitude, ambient temperature and lift coefficient, is also theory

dependent. The magnitude of the drag change produced by selection of alternate prediction methods is, however, small. Leyman and Markham<sup>81</sup> have shown that compared with the later method of Winter and Gaudet, Michel's method predicted lower aircraft drag directly by 2-1/2%  $C_F$  (0.8% total drag) and lower aircraft drag from extrapolation of the 1/45th scale model data by 5%  $C_F$  (1.5% total drag) for the Concorde. The Winter and Gaudet method is similar to that of Sommer and Short<sup>136</sup>, and each reproduced available, acceptable, experimental results more accurately than Michel's method. However, the scatter in all data precluded changing skin friction prediction methods during the Concorde design process. The same theory should be used for all estimates during the design process to achieve consistent results.

The Sommer and Short method<sup>136</sup> is used to calculate the compressible skin friction coefficient,  $C_F$ , from a reference skin friction coefficient,  $C_F'$ , for a selected free stream Mach number,  $M_\infty$ , and Reynolds number,  $R_\infty$ , and adiabatic wall temperature,  $T_w$ , using the incompressible Karman-Schoenherr formula (Section 2.2). The details of the theory and original experimental verification are given in Reference 136. This method has subsequently been extensively tested against newer experimental data and found to be accurate by Peterson<sup>112</sup>, Sorrells, Jackson and Czarnecki<sup>137</sup>, Stallings and Lamb<sup>138</sup>, and Tendeland<sup>141</sup> for a wide variety of geometries, flow conditions, and heat transfer rates. The method has been programmed for many computers and forms the skin friction module of the Integrated Supersonic Design and Analysis System<sup>97</sup>.

Consistent use of the Sommer and Short method from the preliminary design phase through flight testing will improve drag correlations. Note that drag component correlations used during the preliminary design phase are, ultimately, based on older wind tunnel and flight test data. A considerable

amount of these data were reduced using the Sommer and Short method as a basis. It is consistent to continue use of this method for subsequent drag buildups on new configurations.

#### 4.2 Wave Drag

The wave drag produced by standing pressure waves that are not possible in subsonic flow has been traditionally decomposed into two components<sup>5</sup>: a zero-lift wave drag and a wave drag-due-to-lift. The decomposition is a result of the supersonic area rule method used for wave drag prediction and is not permitted if nonlinear methods are used. These drag components vary as:

|                            |                      |  |
|----------------------------|----------------------|--|
| Zero Lift:                 | $D_{0 \text{ wave}}$ | $(\text{volume})^2/(\text{length})^4$              |
| Lift-dependent or induced: | $D_{i \text{ wave}}$ | $(M^2-1)(\text{lift})^2/(\text{lifting length})^2$ |

and must be added to the supersonic counterparts of the subsonic skin friction drag and induced or vortex drag. Thus, the supersonic design problem of obtaining maximum lift-to-drag ratio is more complicated due to constraints arising from these additional drag terms.

Linear supersonic aerodynamics methods are the mainstay of the aircraft industry and are routinely used for preliminary design because of their simplicity and versatility in spite of their limitations to slender configurations at low lift coefficients. Not surprisingly, most successful supersonic designs to date have adhered to the theoretical and geometrical limitations of these analysis methods. Linearized theory has not been supplanted since second-order theories have not been as successful at predicting experimental data, and practical application of nonlinear methods has been precluded by severe geometrical restrictions, i.e. axisymmetric bodies, conical flow, etc.

The normal pressure drag components, consisting of form drag, vortex drag, lift-dependent wave drag and volume-dependent wave drag, are shown in Fig. 6.

The supersonic form drag, or drag due to adding the boundary-layer displacement thickness to the physical areas to obtain the effect of the boundary layer on the wave drag, is conventionally ignored<sup>19, 81</sup>. Calculations have shown this contribution is small ( $\pm 1\%$ ) and dependent upon longitudinal area distribution for bodies of revolution<sup>19</sup>. This assumption is well within the accuracy of the prediction capability for the body alone<sup>55, 67</sup>, particularly for low fineness ratio bodies<sup>80</sup>. The accuracy of this assumption is unknown for wings.

As shown in Fig. 28, both near- and far-field methods are used to calculate the components of inviscid pressure drag, Fig. 6.

A surface panel method, such as PAN AIR<sup>39</sup>, that represents the configuration's thickness, camber and angle of attack with surface distributions of sources and doublets and sums the resulting pressure times the streamwise component of area (near-field method) obtains the sum of the vortex drag, lift-dependent and volume-dependent wave drags. The use of these methods offer improved geometric representation of the configuration, but do not permit independent consideration of each drag component for optimization purposes.

Far-field methods relate the wave drag to the lateral convection of streamwise momentum through a cylindrical control surface, Fig. 28, placed a large distance (several wingspans) from the configuration. The vortex drag is similarly related to the transverse components of momentum through a crossflow plane far downstream in the wake -- the Trefftz plane. The supersonic vortex drag is identical to the induced drag for subsonic flow since the trailing vorticity remains essentially stationary with the fluid, regardless of flight speed. Due to the inherent theoretical limitations of each approach, a combination of near- and far-field methods, along with semiempirical modifications, are currently used for drag prediction and design optimization<sup>5, 97</sup>.



The zero-lift, or volume-dependent, wave drag is commonly computed using a numerical implementation of the Supersonic Area Rule concept, proposed somewhat independently by Hayes, Jones, and Whitcomb. This far-field method relates the zero-lift wave drag of a wing, fuselage, empennage, nacelles, etc., to a number of developments of the normal components of cross-sectional areas as intersected by inclined Mach planes through the Von Kármán slender-body formula (Fig. 28). The use of linear source-sink distributions to represent the configuration precludes representation of both local lift and total integrated lift. The wave drag due to lift and the vortex drag are, perforce, calculated by another method, conventionally the near-field Mach Box method for thin (zero thickness) wings.

With an additional restriction on the slenderness of the configuration, the Transfer Area Rule can be obtained that permits optimization of the wing-body for minimum wave drag due to volume, independent of the wing. Since the fuselages of military aircraft are usually not slender, the use of the Transfer Area Rule in this case would represent a greater violation of theory than use of the Supersonic Area Rule.

Numerous comparisons of this theory with experimental data from the slender XB-70 and Supersonic Transport models<sup>5, 10</sup> have demonstrated that it is remarkably accurate (less than  $\pm 10\%$  error in total drag) over a range of Mach numbers from 1.2 to 3.0.

Bonner<sup>10</sup>, using an integral similar to Von Kármán's slender body formula derived by Hayes, obtains both the zero-lift and lift-dependent wave drag. This procedure, however, requires a priori knowledge of the longitudinal distribution of lift. The use of this procedure is relatively limited since a

near-field method capable of obtaining both the vortex and lift-dependent wave drags must be used to supply the required lift distribution and lifting surfaces are much less likely to satisfy the slenderness requirements. The distant point of view does, however, incorporate lift-volume interference not reflected in many of the theoretical techniques used to estimate the surface pressure.

#### 4.3 Lift-Induced Drag

The drag due to lift, both wave and vortex, has conventionally been calculated using the Mach Box method of Middleton and Carlson<sup>96</sup>, currently with many semiempirical modifications to alleviate known shortcomings<sup>97</sup>. A comprehensive review of this method, as of 1974, is contained in Ref. 23 and later modifications are contained in Ref. 21 and Ref. 97. The method subdivides the zero-thickness planform, often with the fuselage outline (Fig. 28), into rectangular panels whose diagonals are aligned with the free-stream Mach lines of the flow. Alternatively, the sides of the element could be parallel to the Mach lines and the Mach Diamond or Characteristic Box method would result. Generally, the Mach Box method is more accurate for supersonic edges, while the Characteristic Box gives better results for wings with subsonic edges<sup>81</sup>.

The linear theory integral equation relating camber surface slope to lifting pressure difference,  $\Delta C_p$ , across the planform is numerically evaluated by considering  $\Delta C_p$  a constant within each box or element and reducing the integral equation to an algebraic summation. The summation can be solved for either the camber surface slope for a known pressure distribution (wing design case) or the lifting pressure coefficient in terms of known camber surface slopes (lift analysis case). A number of component loadings (up to seventeen) can be combined in the design mode to determine optimum camber shapes for minimum

drag due to lift at a given lift coefficient, subject to optional pitching moment constraints. The effects of the fuselage and nacelles may be included in the component loadings and additional constraints may be applied to the design pressure distribution and local camber surface to provide physical realism. Linear theory consistently overestimates expansion pressures (to less than vacuum pressure!) and underestimates the compression pressure<sup>114</sup>. Proper selection of the component loadings and constraints requires complete understanding of the computer programs backed by critical operational use, otherwise, occasional "endless loops" may result<sup>97</sup>. There may also be small discrepancies between wing loadings and forces determined for an optimized wing and the loadings and forces for the same shape upon submittal to the evaluation program<sup>23</sup>.

The preceding supersonic aerodynamic design and analysis methods have been substantiated for numerous wings, wing/body and wing/body/nacelle configurations at the lower lift coefficients typical of supersonic cruise conditions. A comparison with wind-tunnel data from the Lightweight Experimental Supercruise Model (LES) at the design Mach number and lower lift coefficients is shown in Fig. 30. Test-theory comparisons for supersonic transport and bomber models at typically higher cruise Mach numbers and lower design lift coefficients are equally as accurate<sup>10, 116</sup>, although only if performed by experienced designers familiar with the methods, Fig. 31.

The major unresolved drag prediction problem of thin, highly swept wings typical of efficient supersonic flight is the evaluation of leading-edge thrust or leading-edge suction. The large influence on the drag polar of the various assumptions used to determine the magnitude of this force is shown in Fig. 32 for the same configuration as shown in Fig. 30. The polar shown

in Fig. 32 is for  $M = 1.35$ , an off-design condition for the  $M = 1.8$  super-cruiser configuration.

The leading edge thrust results from the low pressure induced by the high flow velocities around the leading edge from the stagnation point on the undersurface of the wing to the upper surface. For the high aspect ratio wings typical of low subsonic flight speeds, this force largely counteracts the drag from the pressure forces acting on the remainder of the airfoil<sup>22,116</sup>. The thrust force diminishes with increasing speeds, but exists as long as the leading-edges are subsonic<sup>163</sup>. It was found to be negligible at  $M = 3.0$  for the configuration analyzed by Kulfan<sup>76</sup>. Thus, thrust effects have conventionally been ignored for supersonic wing design and analysis at Mach numbers approaching three<sup>116</sup>, with excellent results, as shown in Fig. 31.

The renewed interest in this phenomena resulted from the increased sophistication in supersonic wing design required to achieve higher design lift coefficients for the lower Mach numbers typical of proposed fighter designs with sustained supersonic cruise capability<sup>164</sup>. The maneuver requirements also demand higher available lift coefficients and the attendant thickness and complex camber shapes to minimize drag.

The current complex of NASA computer programs<sup>97</sup> contains four user selected options to estimate leading-edge thrust, Fig. 32. The basic Mach Box zero-thickness wing design and analysis method provides the zero leading-edge suction drag estimate since the low pressures do not have a forward facing area to act upon. The Polhamus analogy assumes the flow is separated from the entire leading-edge and has formed the spiral vortex sheets characteristic of slender wings at higher angles of attack<sup>76</sup>. The Polhamus analogy has been extended, by Kulfan<sup>76</sup>, to account for airfoil shape, wing warp and

planform effects in order to determine the influence of wing geometry on leading-edge vortices. He demonstrates that, except for very slender wings, lowest drag due to lift is achieved with attached flow.

The attainable thrust option (Fig. 32), developed by Carlson, Mack and Barger<sup>22</sup>, has been found to work well for wings with standard NASA airfoil sections, from which the correlations were developed<sup>163</sup>. However, the attainable thrust forces predicted did not agree with those experimentally measured on wings with sharp and varying leading-edge radii; large differences in both levels and trends were evident<sup>163</sup>.

The magnitude of the full leading-edge thrust is dependent upon the upwash in the vicinity of the leading edge and the effect on the pressure distribution. It is determined by calculating the limit of the pressure coefficient (which theoretically approaches infinity) multiplied by the distance from the leading edge. The evaluation of this limit is difficult because the pressure distributions, as calculated by panel methods, vary from the exact theoretical values required. This limit problem and the resulting impact on wing design and drag prediction have been extensively studied by Carlson and Mack<sup>21</sup>.

Calculations using near-field surface-panel methods should predict the full suction drag polar; however, the pressure-area integral is sensitive to leading-edge paneling density. Near thin wing tips, the paneling may be insufficient for the accurate evaluation of this integral and the resulting force will be bounded between the full and zero leading-edge suction values. The force will thus depend on the numerical representation of the wing, rather than aerodynamic assumptions, a disconcerting situation for the designer.

As observed by several investigators, a reasonable estimate for the drag polar could be obtained by numerically averaging the zero and full leading-edge suction drag polars.

Drag polars calculated by two near-field methods for Mach numbers of 1.196, 1.6, and 2.2 are shown in Fig. 33<sup>98</sup>. The complex canard-wing-fuselage configuration and paneling arrangement are shown in Fig. 21. The skin friction drag was estimated using the methods of Section 4.1. Considerable scatter is evident in the zero lift drag which may be attributed to either the skin friction estimate or, more likely, the zero lift wave drag predictions of the near-field methods. The variation in vortex and lift-dependent wave drag with angle of attack was correctly predicted by the higher-order panel method, PAN AIR<sup>26</sup>. The lower-order method, USSAERO-B, has recently been updated to improve supersonic prediction capability by inclusion of the Triplet Singularity<sup>41, 165</sup>. The wing camber design Mach number for this configuration was 1.8. Many additional test-theory comparisons, exhibiting much closer agreement, are contained in Tinoco, Johnson, and Freeman<sup>144</sup> and Tinoco and Rubbert<sup>146</sup>. The prediction methods included a pilot version of PAN AIR, the Mach Box method and the Woodward Constant-Pressure panel method (USSAERO) for a Mach three Recce-Strike design and the supercruise configuration shown in Figs. 30 and 32.

Correction procedures to remedy the observed shortcomings of linear theory are under continuous development. Stancil<sup>139</sup> has modified near-field linear theory to improve the prediction of compression and expansion pressures and to eliminate local singularities. His modifications, the use of exact tangency surface boundary conditions and the corrected local value of Mach number, cause the solution technique to become iterative. The modifications improve the zero-lift wing wave drag prediction capability of linear theory

for the F-8C<sup>139</sup>. Shroul and Covell<sup>129</sup> compared both Stancil's modified linear theory and the far-field slender-body theory zero lift wave drag predictions with their experimental data for a series of forebody models having various degrees of nose droop. The far-field method correctly predicted trends for Mach numbers of 1.2 and 1.47, but was erroneous at 1.8 for the cambered models. Stancil's method<sup>139</sup> correctly predicted wave drag trends for Mach numbers of 1.47, 1.80 and 2.16.

Another breakdown of linear theory occurs when the crossflow velocities exceed sonic value, a situation encountered on fighter aircraft at maneuver lift coefficients. The formation of crossflow shock waves causes the experimental drag-due-to-lift performance of wings designed by linear theory to fail to meet predicted values. The supercritical conical camber concept<sup>91</sup>, (SC<sup>3</sup>), has been proposed to regain wing performance for wings swept such that the Mach number normal to the leading edge is transonic. The design method employs repetitive application of a transonic full potential flow solver, COREL, and a specially adapted version of the Woodward USSAERO linear theory paneling code<sup>92</sup>. Comparison of this design procedure with data from the wind tunnel tests of a demonstration wing show that substantial reductions in drag-due-to-lift are possible, Fig. 34, at the maneuver design condition<sup>91</sup>.

Bonner and Gingrich<sup>12</sup> approach fighter wing design through the use of variable camber and a design compromise between the transonic maneuver configuration and an optimum supersonic cruise design. The unconstrained supersonic design was initially accomplished by conventional linear theory while both small-disturbance and full-potential theories were used for the transonic design. These designs established the boundaries for the design cycle. Experience then guided the selection of the compromise camber shape, followed by alternating constrained optimizations at the supersonic and transonic

design points. This multipoint design process illustrates the need for accurate drag prediction. Spurious high drag regions entirely due to the use of linear theory, shown in Fig. 35 at the sonic leading-edge condition, could eliminate the optimum design from consideration on the first cycle!

Significant potential for further improvement in wing design for minimum drag-due-to-lift exists through the use of nonlinear computational methods early in the design cycle<sup>46</sup>. A comprehensive set of design constraints for efficient, highly swept wings has been determined by Kulfan<sup>77</sup>.

The problems of fighter design and analysis are further compounded by the fact that linear theory does not apply to relatively large fuselages with nonsmooth area distributions, as shown by Wood, et.al.<sup>164</sup> Four wings were designed and tested with a common fuselage in an effort to adapt supersonic technologies to a  $M = 1.8$  fighter design. Their test-theory comparisons, Fig. 36, clearly show the inaccuracy in zero-lift drag prediction using the Middleton and Lundy<sup>97</sup> complex of computer programs. This fuselage severely violates the assumptions of linear theory concerning smooth, slender area distribution bodies. Further inaccuracies as the configuration is built up are opposite in sign and cancel most of the fuselage error -- illustrating the somewhat forgiving nature of linear aerodynamics. The zero-lift drag comparison for each of the four wings is shown in Fig. 37. The prediction capabilities of linear theory are excellent for the complete configurations and vary with slenderness and smoothness of the area distribution. The drag-due-to-lift comparisons were equally as accurate; however, they were performed using in-house empirical corrections.

Linear theory, as developed by Middleton and Lundy<sup>97</sup>, has become the standard preliminary design tool for supersonic aircraft. Correction procedures to alleviate the well-known restrictions of the theory are under



constant development. Higher-order panel methods, necessary for supersonic flow analyses, along with nonlinear numerical methods, are also used during the latter design stages, particularly for lower design Mach number, blunt fighter configurations.

An innovative, statistical method for the prediction of fighter aircraft drag-due-to-lift was developed by Simon, et.al.<sup>131</sup>, for Mach numbers of 0.4 through 2.5. A large experimental data base was fitted with regression equations based on easily calculated nondimensional geometric parameters. The accuracy of the resulting regression equations was only limited by the expanse of the data base from which they were obtained, as shown by Johnson<sup>69</sup> and Tomasetti<sup>148</sup>.

## 5 Numerical Aerodynamics

Here, the term numerical aerodynamics is used to delineate the full spectrum of aerodynamic methods requiring large computers -- from the linearized theory panel methods to the full Navier-Stokes equations. The term computational fluid dynamics (CFD) is often used in this context, and just as often limited to mean only Navier-Stokes computations, particularly with respect to future goals. Numerical aerodynamics now permeates nearly every stage of the design process, as well as each speed regime.

Many prognostications concerning the possible roles of, primarily, CFD and the wind tunnel have been published (Ref. 27, 29, 30, 42, 48, 53, 73, 79, 83, 99, 110, 115, 121, 124, 125, 132, 167) since Chapman's 1975 article<sup>29</sup> and the prediction that CFD would supplant traditional wind tunnel tests within a decade. The pacing item in CFD technology at that time was computer size and speed. A later article<sup>30</sup> recognized turbulence models to be a pacing item. In addition to the long-term problem of turbulence modeling, the problem of

proper grid generation is of immediate concern to those engaged in the use of CFD codes in the production (as apposed to research) mode. Computer hardware has advanced tremendously in the last decade<sup>79</sup>, as have flow simulations using the Reynolds averaged Navier-Stokes equations. Still, the wind tunnel is the primary tool for design verification and a large portion of design development work. CFD analysis of full three-dimensional configurations capable of flight may still be a decade away<sup>48, 73</sup>. The fundamental limitation of CFD during the last decade -- turbulence modeling -- remains the pacing item. Progress in this area in the next 15 years is not projected to remove this limitation<sup>73</sup> and recent reviews of turbulence models<sup>52, 82, 87, 117, 133</sup> reinforce this contention. The fundamental physics of turbulence is not known well enough to permit accurate mathematical modeling and flow simulation. If the present is any indication of the future, drag prediction and design optimization with drag as an objective function using CFD are even further in the future.

Recent publications recognize the complementary roles of wind tunnels and CFD<sup>73</sup>, while the role of the lower-order approximations (linear, potential, Euler) is often understated. Each of these methods will be found in a complementary place in the design process depending on configuration, schedule, cost, availability of hardware and software, and the persuasion of the designer and his management. Confidence in the accuracy of the predictions is tantamount<sup>79, 99</sup>. Aircraft design departments should evolve a full spectrum of numerical aerodynamics methods, coupled through a data management system, to provide accurate, timely, cost-effective design data<sup>110,121, 124, 168</sup>.

## BIBLIOGRAPHY

- 1) Abercrombie, J.M., "Flight Test Verification of F-15 Performance Predictions," AGARD-CP-242, 1977, pp. 17-1 - 17-13.
- 2) Aidala, P.V., Davis, W.H., and Mason, W.H., "Smart Aerodynamic Optimization," AIAA-83-1863, Applied Aerodynamic Conference, Danvers, MA, July 1983.
- 3) Arnaiz, H.H., "Flight-Measured Lift and Drag Characteristics of a Large, Flexible, High Supersonic Cruise Airplane," NASA TM X-3532, May 1977.
- 4) Axelson, John A., "AEROX - Computer Program for Transonic Aircraft Aerodynamics to High Angles of Attack," Vol I, II, and III, NASA TM X-73,208, February 1977.
- 5) Baals, D.D., Robins, A.W., and Harris, R.V., Jr., "Aerodynamic Design Integration of Supersonic Aircraft," J. Aircraft, September-October 1970.
- 6) Baldwin, A.W., Editor, "Symposium on Transonic Aircraft Technology (TACT)," AFFDL-TR-78-100, August 1978.
- 7) Bills, G.R., Hink, G.R., and Dornfeld, G.M., "A Method for Predicting the Stability Characteristics of an Elastic Airplane," AFFDL-TR-77-55, 1977.
- 8) Blackwell, J.A., Jr., "Preliminary Study of Effect of Reynolds Number and Boundary Layer Transition Location on Shock Induced Separation," NASA TN D-5003, 1969.
- 9) Blasius, H., "Boundary Layers in Fluids of Small Viscosity," Dissertation, Gottinger, 1907.
- 10) Bonner, E., "Expanding Role of Potential Theory in Supersonic Aircraft Design," J. Aircraft, May 1971, pp. 347-353.
- 11) Bonner, E., Clever, W., and Dunn, K., "Aerodynamic Preliminary Analysis II Part I - Theory," NASA CR 165627, April, 1981.
- 12) Bonner, E., and Gingrich, P., "Supersonic Cruise/Transonic Maneuver Wing Section Development Study," AFWAL-TR-80-3047, June 1980.
- 13) Bowes, G.M., "Aircraft Lift and Drag Prediction and Measurement," AGARD-LS-67, May 1974, pp. 4-1 - 4-44.
- 14) Braslow, A.L., "Use of Grit-Type Boundary-Layer-Transition Trips on Wind Tunnel Models," NASA TN D-3579, September 1966.
- 15) Braslow, A.L., and Knox, E.C., "Simplified Method for Determination of Critical Height of Distributed Roughness Particles for Boundary Layer Transition at Mach Numbers from 0 to 5," NACA TN-4363, 1958.

- 16) Bristow, D.R., and Hawk, J.D., "Subsonic Panel Method for the Efficient Analysis of Multiple Geometry Perturbations," NASA CR-3528, March 1982.
- 17) Brown, S.W., and Bradley, D., "Uncertainty Analysis for Flight Test Performance Calculations," AIAA-81-2390, AIAA/SETP/SAE Flight Testing Conf., Las Vegas, NV, November 1981.
- 18) Buckner, J.K., and Webb, J.B., "Selected Results from the YF-16 Wind Tunnel Test Program," AIAA-74-619, 8th Aerodynamic Testing Conf., Bethesda MA, July 1974.
- 19) Butler, S.F.J., "Aircraft Drag Prediction for Project Appraisal and Performance Estimation," AGARD-CP-124, 1973, pp. 6-1 - 6-50, with Appendix.
- 20) Butler, S.F.J., "Technical Evaluation Report," AGARD-CP-124, 1973, pp. vii-xv.
- 21) Carlson, H.W., and Mack, R.J., "Estimation of Wing Nonlinear Aerodynamic Characteristics at Supersonic Speeds," NASA TP-1718, November 1980.
- 22) Carlson, H.W., Mack, R.J., and Barger, R.L., "Estimation of Attainable Leading-Edge Thrust for Wings at Subsonic and Supersonic Speeds," NASA TP 1500, October, 1979.
- 23) Carlson, H.W., and Miller, D.S., "Numerical Methods for the Design and Analysis of Wings at Supersonic Speed," NASA TN D-7713, December 1974.
- 24) Carlson, H.W., and Walkley, K.B., "A Computer Program for Wing Subsonic Aerodynamic Performance Estimates Including Attainable Thrust and Vortex Lift Effect," NASA CR-3515, March 1982.
- 25) Carmichael, R.L., and Woodward, F.A., "An Integrated Approach to the Analysis and Design of Wings and Wing-Body Combinations in Supersonic Flow," NASA TN D-3685, October 1966.
- 26) Carmichael, R.L., and Erickson, L.L., "PAN AIR: A Higher-Order Panel Method for Predicting Subsonic or Supersonic Linear Potential Flows About Arbitrary Configurations," AIAA-81-1255, June 1981.
- 27) Caughey, D.A., "A (Limited) Perspective on Computational Aerodynamics," FDA-80-07, Fluid Dynamics and Aerodynamics Program - Cornell University, July 1980.
- 28) Cenko, A., "PAN AIR Applications to Complex Configurations," AIAA-83-0007, Aerospace Sciences Meeting, Reno NV, January 1983.
- 29) Chapman, D.R., Mark, H., and Pirtle, M.W., "Computers vs. Wind Tunnels for Aerodynamic Flow Simulations," Astronautics and Aeronautics, April 1975, pp. 21-30.
- 30) Chapman, D.R., "Computational Aerodynamics Development and Outlook," AIAA-79-0129R, 17th Aerospace Sciences Meeting, January 1979.

- 31) Chen, A.W., and Tinoco, E.N., "PAN AIR Applications to Aero-Propulsion Integration," AIAA-83-1368, 19th Joint Propulsion Conference, Seattle WA, June 1983.
- 32) Coakley, T.J., "Turbulence Modeling Methods for the Compressible Navier-Stokes Equations," AIAA-83-1693, 16th Fluid and Plasma Dynamics Conf., Danvers MA, July 1983.
- 33) Cooper, J.M., Hughes, D.L., and Rawlings, K., "Transonic Aircraft Technology - Flight-Derived Lift and Drag Characteristics," AFFTC-TR-12, July 1977.
- 34) Craig, R.E., and Reich, R.J., "Flight Test Aerodynamic Drag Characteristics Development and Assessment of Inflight Propulsion Analysis Methods for AGM-109 Cruise Missile," AIAA-81-2423, AIAA/SETP/SFTE/SAE/ITEA/IEEE 1st Flight Testing Conf., Las Vegas NV, November 1981.
- 35) Crosthwait, E.L., Kennon, I.G., Jr., and Roland, H.L., ETAL "Preliminary Design Methodology for Air-Induction Systems," SEG-TR-67-1, January 1967.
- 36) Daugherty, J.C., "Wind Tunnel/Flight Correlation Study of Aerodynamic Characteristics of a Large Flexible Supersonic Cruise Airplane (SB-70-1)," NASA TP-1514, November 1979.
- 37) DeLaurier, J., "Drag of Wings with Cambered Airfoils and Partial Landing-Edge Suction," J. Aircraft, October 1983, pp. 882-886.
- 38) Dvorak, F.A., Woodward, F.A., and Maskew, B., "A Three-Dimensional Viscous/Potential Flow Interaction Analysis Method for Multi-Element Wings," NASA CR-152012, 1977.
- 39) Erickson, L.L., and Strande, S.M., "PAN AIR Evolution and New Directions. . . Transonics for Arbitrary Configurations," AIAA-83-1831, Applied Aerodynamics Conf., Danvers MA, July 1983.
- 40) Firmin, M.C.P., and Potter, J.L., "Wind Tunnel Compatibility Related to Test Sections, Cryogenics, and Computer-Wind Tunnel Integration," AGARD-AR-174, April 1982.
- 41) Fornasier, L., "Calculation of Supersonic Flow Over Realistic Configurations by an Updated Low-Order Panel Method," AIAA-83-0010, 21st Aerospace Sciences Meeting, January 1983.
- 42) "Future Computer Requirements for Computational Aerodynamics," NASA Workshop Series -- Mixed Papers, NASA CP-2032, October 1977.
- 43) Gaudet, L., and Winter, K.G., "Measurements of the Drag of Some Characteristic Aircraft Excrescences Immersed in Turbulent Boundary Layers," AGARD-CP-124, 1973, pp. 4-1 - 4-12.
- 44) Geddes, J.P., "Taking an Airliner from Certification to Airline Acceptance - the DC-10-30," INTERAVIA, June 1973, pp. 609-611.

- 45) Gilmer, B.R., and Bristow, D.R., "Analysis of Stalled Airfoils by Simultaneous Perturbations to Viscous and Inviscid Equations," AIAA-81-023, 14th Fluid and Plasma Dynamics Conference, Palo Alto CA, June 1981.
- 46) Gingrich, P.B., and Bonner, E., "Wing Design for Supersonic Cruise/Transonic Maneuver Aircraft," ICAS-82-5.8.2, 13th Congress of the International Council of the Aeronautical Sciences, Seattle WA, August 1982.
- 47) Glauert, H., The Elements of Aerofoil and Airscrew Theory, 2nd ed., Cambridge University Press, New York, 1959.
- 48) Graves, Randolph A., "Computational Fluid Dynamics - The Coming Revolution," Astronautics and Aeronautics, March 1982, pp. 20-28.
- 49) Grellmann, H.W., "YF-17 Full Scale Minimum Drag Prediction," AGARD-CP-242, 1977, pp. 18-1 - 18-12.
- 50) Hahn, M., Brune, G.W., Rubbert, P.E., and Nark, T.C., "Drag Measurements of Upswept Afterbodies and Analytical Study on Axisymmetric Separation," AFFDL-TR-73-153, February 1974.
- 51) Haines, A.B., "Subsonic Aircraft Drag: An Appreciation of Present Standards," The Aeronautical Journal of the Royal Aeronautical Society, Vol. 72, March 1968, pp. 253-266.
- 52) Haines, A.B., "Turbulence Modelling," Aeronautical Journal, August/September 1982, pp. 269-277.
- 53) Hall, M.G., "Computational Fluid Dynamics - A Revolutionary Force in Aerodynamics," AIAA-81-1014, 1981.
- 54) Harris, R.V., "An Analysis and Correlation of Aircraft Wave Drag," NASA TMX-947, 1964.
- 55) Harris, R.V., and Landrum, E.J., "Drag Characteristics of a Series of Low-Drag Bodies of Revolution at Mach Numbers from 0.6 to 4.0," NASA TN D-3163, December 1965.
- 56) Henne, P.A., "Inverse Transonic Wing Design Method," J. Aircraft, February 1981.
- 57) Henne, P.A., Dahlin, J.A., and Peavey, C.C., "Applied Computational Transonics - Capabilities and Limitations," Douglas Paper 7025, Transonic Perspective Symposium NASA Ames, February 1981.
- 58) Hess, J.L., "A Higher Order Panel Method for Three-Dimensional Potential Flow," Naval Air Development Center Report No. NADC 77166-30, June 1979.
- 59) Hess, J.L. and Friedman, D.M., "An Improved Higher Order Panel Method for Three-Dimensional Lifting Potential Flow," Naval Air Development Center Final Report, NADC -79277-60, December 1981.
- 60) Hicks, R.M., "Transonic Wing Design Using Potential-Flow Codes -- Successes and Failures," 810565, Society of Automotive Engineers, Inc., 1981.

- 61) "High Angle of Attack Aerodynamics," AGARD-CP-124, 1979.
- 62) Hitzel, S.M., Schmidt, W., "Slender Wings with Leading-Edge Vortex Separation -- A Challenge for Panel-Methods and Euler-Codes," AIAA-83-0562, 21st Aerospace Sciences Meeting, Reno NV, January 1983.
- 63) Hoak, D.E., USAF Stability and Control DATCOM, Revised, April 1978.
- 64) Hoerner, S.F., Fluid-Dynamic Drag, published by the author, 1965.
- 65) Hopps, R.H., and Danforth, E.C.B., "Correlation of Wind Tunnel And Flight Test Data for the Lockheed L-1011 Tristar Airplane," AGARD-CP-242, 1977, pp. 21-1 - 21-12.
- 66) Hunt, B.L., Gowadia, N.S., "Determination of Thrust and Throttle-Dependent Drag for Fighter Aircraft," AIAA-81-1692, Aircraft Systems and Technology Conference, Dayton OH, August 1981.
- 67) Jackson, C.M., Jr., and Smith, R.S., "A Method for Determining the Total Drag of a Pointed Body of Revolution in Supersonic Flow with Turbulent Boundary Layer," NASA TN D-5046, March 1969.
- 68) James, R.M., "An Investigation of Induced Drag for Field Calculation Methods for Planar Distributions," MDC J7046, December 1975.
- 69) Johnson, J. Kenneth, "Accuracies and Limitations of a Statistical Method for Computing Lift and Drag Due to Lift of Fighter Type Wing-Body Configurations," AFFDL/FXM-TM-73-46, August 1973.
- 70) Kjelgaard, S.O., "Evaluation of a Surface Panel Method Coupled with Several Boundary Layer Analyses," AIAA-83-0011, 21st Aerospace Sciences Meeting, Reno NV, January 1983.
- 71) Knaus, A., "A Technique to Determine Lift and Drag Polars in Flight," J. Aircraft, Vol. 20, July 1983, pp. 587-593.
- 72) Kolesar, C.E., and May, F.W., "An Aftbody Drag Prediction Technique for Military Airlifters," AIAA-83-1787, Applied Aerodynamics Conf., Danvers MA, July 1983.
- 73) Korkegi, R.H., "The Impact of CFD on Development Test Facilities - A National Research Council Projection," AIAA-83-1764, 16th Fluid and Plasma Dynamics Conf., Danvers MA, July 1983.
- 74) Kuhlman, J.M., and Ku, T.J., "Numerical Optimization Techniques for Bound Circulation Distribution for Minimum Induced Drag of Nonplanar Wings: Computer Program Documentation," NASA CR-3458, August 1981.
- 75) Kulfan, R.M., "Application of Hypersonic Favorable Aerodynamic Interference Concepts to Supersonic Aircraft," AIAA-78-1458, Aircraft Systems and Technology Conference, August 1978.
- 76) Kulfan, R.M., "Wing Geometry Effects on Leading-Edge Vortices," AIAA-79-1872 Aircraft Systems and Technology Meeting, NY, August 1979.

- 77) Kulfan, R.M., and Sigalla, A., "Real Flow Limitations in Supersonic Airplane Design," AIAA-78-147, January 1978.
- 78) Kulfan, R.M., Yoshihara, H., Lord, B.J., and Friebel, G.O., "Application of Supersonic Favorable Aerodynamic Interference to Fighter Type Aircraft," AFFDL-TR-78-33, April 1978.
- 79) Kutler, P., "A Perspective of Theoretical and Applied Computational Fluid Dynamics," AIAA-83-0037, 21st Aerospace Sciences Meeting, Reno NV, January 1983.
- 80) Landrum, E.J., and Miller, D.S., "Assessment of Analytic Methods for the Prediction of Supersonic Flow over Bodies," AIAA-80-0071R, AIAA Journal, February 1981.
- 81) Leyman, C.S. and Markham, T., "Prediction of Supersonic Aircraft Aerodynamic Characteristics," AGARD-LS-67, May 1974, pp. 5-1 - 5-52.
- 82) Liepmann, H.W., "The Rise and Fall of Ideas in Turbulence," American Scientist, Vol. 67, March-April 1979, pp. 221-228.
- 83) Lomax, H., "Some Prospects for the Future of Computational Fluid Dynamics," AIAA-81-0991R, AIAA Journal, Vol. 20, No. 8, August 1982.
- 84) Longo, J., Schmidt, W., and Jameson, A., "Viscous Transonic Airfoil Flow Simulation," Z. Flugwiss Wettraumforsch. 7, 1983, Heft 1.
- 85) Lotz, M., and Friedel, H., "Analysis of Error Sources in Predicted Flight Performance," Performance Prediction Methods, AGARD-CP-242, 1977, pp. 14-1 - 14-11.
- 86) MacWilkinson, D.G., Blackerby, W.T., and Paterson, J.H., "Correlation of Full Scale Drag Prediction with Flight Measurements on the C-141A Aircraft - Phase II, Wind Tunnel Test, Analysis, and Prediction Techniques. Volume I - Drag Predictions, Wind Tunnel Data Analysis and Correlation," NASA CR-2333, February 1974.
- 87) Marvin, J.G., "Turbulence Modeling for Computational Aerodynamics," AIAA-82-0164, 20th Aerospace Sciences Meeting, Orlando FL, January 1982.
- 88) Maskew, B., "Prediction of Subsonic Aerodynamic Characteristics - A Case for Low-Order Panel Methods," AIAA-81-0252, January 1981.
- 89) Maskew, B., Rao, B.M., and Dvorak, F.M., "Prediction of Aerodynamic Characteristics for Wings with Extensive Separations," AGARD-CP-291, February 1981, pp. 31-1 - 31-15.
- 90) Mason, W.H., "Wing-Canard Aerodynamics at Transonic Speeds - Fundamental Considerations on Minimum Drag Span Loads," AIAA-82-0097, 20th Aerospace Sciences Meeting, January 1982.
- 91) Mason, W.H., "SC<sup>3</sup> A Wing Concept for Supersonic Maneuvering," AIAA-83-1858, July 1983.



- 92) Mason, W.H., and Rosen, B.S., "The COREL and W12SC3 Computer Programs for Supersonic Wing Design and Analysis," NASA CR-3676, 1983.
- 93) McCluney, B. and Marshall, J., "Drag Development of the Belfast," Aircraft Engineering, October 1967, pp. 33-37.
- 94) McGreer, T., and Shevell, R.S., "A Method for Estimating the Compressibility Drag of an Airplane," SUDAAR 535, January 1983.
- 95) McKinney, L. Wayne, Editor, "Wind Tunnel/Flight Correlation - 1981," NASA Miniworkshop Series, NASA Publication 2225, November 1981.
- 96) Middleton W.D., and Carlson, H.W., "Numerical method of Estimating and Optimizing Supersonic Aerodynamic Characteristics of Arbitrary Planform Wings," J. Aircraft, July-August 1965.
- 97) Middleton, W.D., and Lundry, J.L., "A System for Aerodynamic Design and Analysis of Supersonic Aircraft," NASA CR-3351, December 1980.
- 98) Miller, S.G., and Youngblood, D.B., "Applications of USSAERO-B and the PAN AIR Production Code to the CDAF Model - A Canard/Wing Configuration," AIAA-83-1829, Applied Aerodynamics Conf., Danvers MA, July 1983.
- 99) Miranda, L.R., "A Perspective of Computational Aerodynamics from the Viewpoint of Airplane Design Applications," AIAA-82-0018, Orlando FL, January 1982.
- 100) Miranda, L.R., Elliott, R.D., and Baker, W.M., "A Generalized Vortex Lattice Method for Subsonic and Supersonic Flow Applications," NASA CR-2865, December 1977.
- 101) Morris, S.J., Neums, W.P., and Bailey, R.O., "A Simplified Analysis of Propulsion Installation Losses for Computerized Aircraft Design," NASA TM X-73,136, August 1976.
- 102) Murillo, L.E., and McMasters, J.H., "A Method for Predicting Low-Speed Aerodynamic Characteristics of Transport Aircraft," AIAA-83-1845, Applied Aerodynamics Conf., Danvers MA, July 1983.
- 103) Murman, E.M., and Cole, J.D., "Inviscid Drag at Transonic Speeds," AIAA-74-540, 7th Fluid and Plasma Dynamics Conference, Palo Alto CA, June 1974.
- 104) Nelson, D.W., Gornstein, R.J., and Dornfeld, G.M., "Prediction of Maneuvering Drag Polars Including Elasticity Effects for AFTI-F-111," AIAA-81-1658, August 1981.
- 105) Nixon, D., Transonic Aerodynamics, Vol. 81, Progress in Astronautics and Aeronautics, AIAA, NY, 1982.
- 106) Norton, D.A., "Airplane Drag Prediction," Annals New York Academy of Sciences, 1968, pp. 306-328.

- 107) O'Conner, W.M., "Lift and Drag Prediction in Computer Aided Design," Vols. I and II, ASD/XR-73-8, April 1973.
- 108) Paterson, J.H., "Scaling Effects on Drag Prediction," AGARD-LS-37-10, June 1970, pp. 4-1 - 4-12.
- 109) Paterson, J.H., MacWilkinson, D.G., and Blackerby, W.T., "A Survey of Drag Prediction Techniques Applicable to Subsonic and Transonic Aircraft Design," AGARD-CP-124, 1973, pp. 1-1 - 1-38.
- 110) Perrier, P., "Computational Fluid Dynamics Around Complete Aircraft Configurations," ICAS Paper 82.6.11, 13th Congress of the International Council of the Aeronautical Sciences, Seattle WA, August 1982.
- 111) Paynter, G.C., Vaidyanathan, T.S., Maskew, B., and Dvorak, F.A., "Experience with Hybrid Aerodynamic Methods," AIAA-83-1819, Applied Aerodynamics Conference, Danvers MA, July 1983.
- 112) Peterson, J.B., "A Comparison of Experimental and Theoretical Results for the Compressible Turbulent-Boundary-Layer Skin Friction with Zero Pressure Gradient," NASA TN D-1795, March 1963.
- 113) Peterson, J.B., Jr., "Wind Tunnel/Flight Correlation Program on XB-70-1," NASA CP-2225, November 1981.
- 114) Pittman, J.L., "Preliminary Supersonic Analysis Methods Including High Angle of Attack," AIAA-82-0938, AIAA/ASME 3rd Joint Thermophysics, Fluids, Plasma, and Heat Transfer Conference, St. Louis MO, June 1982, J. Aircraft, Vol. 20, No. 9, September 1983, pp. 784-790.
- 115) Poisson-Quinton, P., "From Wind Tunnel to Flight, the Rule of the Laboratory in Aerospace Design," J. Aircraft, May-June 1968, pp. 193-214.
- 116) Robins, A.W., Carlson, H.W., and Mack, R.J., "Supersonic Wings with Significant Leading-Edge Thrust at Cruise," NASA TP-1632, April 1980.
- 117) Rodi, W., "Progress in Turbulence Modeling for Incompressible Flows," AIAA-81-0045, 19th Aerospace Sciences Meeting, January 1981.
- 118) Rooney, E.C., "Development of Techniques to Measure In-Flight Drag of a U.S. Navy Fighter Airplane and Correlation of Flight Measured Drag with Wind Tunnel Data," AGARD-CP-124, October 1973.
- 119) Rooney, E.C., and Craig, R.E., "Development of Techniques and Correlation of Results to Accurately Establish the Lift/Drag Characteristics of an Air Breathing Missile from Analytical Predictions, Subscale and Full Scale Wind Tunnel Tests and Flight Tests," Performance Prediction Methods, AGARD-CP-242, 1977, pp. 16-1 - 16-18.
- 120) Rooney, E.C., Craig, R.E., and Lauer, R.F., "Correlation of Full Scale Wind Tunnel and Flight Measured Aerodynamic Drag," AIAA-77-996, AIAA/SAE 13th Propulsion Conf., Orlando FL, July 1977.

- 121) Rubbert, P.E., and Tinoco, E.N., "Impact of Computational Methods on Aircraft Design," AIAA-83-2060, Atmospheric Flight Mechanics Conf., Gatlinburg TN, August 1983.
- 122) Schemensky, R.T., "Development of an Empirically Based Computer Program to Predict the Aerodynamic Characteristics of Aircraft," Vols. I and II, AFFDL-TR-73-144, November 1973.
- 123) Schlichting, H., Boundary-Layer Theory, Sixth Edition, McGraw-Hill, New York, 1968.
- 124) Schmidt, W., "Advanced Numerical Methods for Analysis and Design in Aircraft Aerodynamics," Int. J. of Vehicle Design, Technological Advances in Vehicle Design Series, SP6, Applications of New Techniques for Analysis and Design of Aircraft Structures, 1983, pp. 2-37.
- 125) Schmidt, W., Jameson, A., "Euler Solvers as an Analysis Tool for Aircraft Aerodynamics," Recent Advances in Numerical Methods in Fluids, Vol. 4, 1983.
- 126) Sears, W.R., "On Projectiles of Minimum Wave Drag," Quarterly Journal of Applied Mathematics, January 1947, pp. 361-366.
- 127) Shankar, V. and Goebel, T., "A Numerical Transformation Solution Procedure for Closely Coupled Canard-Wing Transonic Flows," AIAA-83-0502, 21st Aerospace Sciences Mtg, Reno NV, January 1983.
- 128) Shrout, B.L., "Aerodynamic Characteristics at Mach 2.03 of a Series of Curved-Leading-Edge Wings Employing Various Degrees of Twist and Camber," NASA TN D-3827, February 1967.
- 129) Shrout, B.L and Covell, P.F., "Aerodynamic Characteristics of a Series of Bodies with Variations in Nose Camber," NASA TP-2206, September 1983.
- 130) Sidwell, K.W., Baruah, P.K., and Bussoletti, J.E., "PAN AIR - A Computer Program for Predicting Subsonic or Supersonic Linear Potential Flows About Arbitrary Configurations Using a Higher Order Panel Method," NASA CR-3252, May 1980.
- 131) Simon, W.E., Ely, W.L., Niedling, L.G., and Voda, J.J., "Prediction of Aircraft Drag Due to Lift," AFFDL-TR-71-84, July 1971.
- 132) Smelt, R., "The Role of Wind Tunnels in Future Aircraft Development," The Aeronautical Journal, November 1978, pp. 467-475.
- 133) Smith, A.M.O., "The Boundary Layer and I," AIAA Journal 81-4291, November 1981.
- 134) Smith, K.G., "Methods and Charts for Estimating Skin Friction Drag in Wind Tunnel Tests with Zero Heat Transfer," Technical Note No. AERO 2980, Royal Aircraft Establishment, Ministry of Aviation, London, United Kingdom, August 1964.
- 135) Snodgrass, R.R., "A Computerized Method for Predicting Drag and Lift for Aeronautical Systems," ASD-ENF-TM-76-1, October 1976.

- 136) Sommer, S.C., and Short, B.J., "Free-Flight Measurements of Turbulent-Boundary-Layer Skin Friction in the Presence of Severe Aerodynamic Heating at Mach Numbers from 2.8 to 7.0," NACA TN-3391, March 1955.
- 137) Sorrells, R.B., Jackson, M.W., and Czarnecki, K.R., "Measurement by Wake Momentum Surveys at Mach 1.61 and 2.01 of Turbulent Boundary-Layer Skin Friction on Five Swept Wings," NASA TN D-3764, December 1966.
- 138) Stallings, R.L., Jr., and Lamb, M., "Wind Tunnel Measurements and Comparison with Flight of the Boundary Layer and Heat Transfer on a Hollow Cylinder at Mach 3," NASA TP 1789, December 1980.
- 139) Stancil, R.T., "Improved Wave Drag Predictions Using Modified Linear Theory," Journal of Aircraft, January 1979, pp. 41-46.
- 140) Sytsma, H.S., Hewitt, B.L., and Rubbert, P.E., "A Comparison of Panel Methods for Subsonic Flow Computation," AGARD-AG-241, February 1979.
- 141) Tendeland, T., "Effects of Mach Number and Wall Temperature Ratio on Turbulent Heat Transfer at Mach Numbers from 3 to 5," NACA TN 4236, April 1958.
- 142) Thomas, J.L. and Miller, D.S., "Numerical Comparisons of Panel Methods at Subsonic and Supersonic Speeds," AIAA-79-0404, 17th Aerospace Sciences Meeting, New Orleans LA, January 1979.
- 143) Thomas, J.L., Luckring, J.M., and Sellers, W.L. III, "Evaluation of Factors Determining the Accuracy of Linearized Subsonic Panel Methods," AIAA-83-1821, Applied Aerodynamics Conference, Danvers MS, July 1983.
- 144) Tinoco, E.N., Johnson, F.T., and Freeman, L.M., "Application of a Higher Order Panel Method to Realistic Supersonic Configurations," AIAA-79-0274R, January 1980.
- 145) Tinoco, E.N., and Rubbert, P.E., "Experience, Issues, and Opportunities in Steady Transonics," AERO-B8111-P82-006, Computational Methods in Potential Aerodynamics (ICTS) Short Course, Amalf, Italy, May-June 1982.
- 146) Tinoco, E.N., and Rubbert, P.E., "Panel Methods: PANAIR," AERO-B8111-P82005, Computational Methods in Potential Aerodynamics Short Course, Amalf, Italy, May-June 1982.
- 147) Tjonneland, E., Paynter, G., and May, F., "Progress Toward Airframe/Propulsion Design Analysis," Paper 8, AGARD Flight Mechanics panel Symposium on Sustained Supersonic Cruise/Maneuver, Brussels, Belgium, October 1983.
- 148) Tomasetti, T.A., "Statistical Determination of the Lift and Drag of Fighter Aircraft," GAM/AE/73-1, June 1972.
- 149) Towne, M.C., et. al., "PAN AIR Modeling Studies," AIAA-83-1830, Applied Aerodynamics Conf., Danvers MA, July 1983.

- 150) Waggoner, E.G., "Computational Transonic Analysis for a Supercritical Transport Wing-Body Configuration," AIAA-80-0129, 18th Aerospace Sciences Meeting, Pasadena CA, January 1980.
- 151) "Wall Interference in Wind Tunnels," AGARD-CP-335, May 1982.
- 152) Webb, T.S., Kent, D.R., and Webb, J.B., "Correlation of F-16 Aerodynamics and Performance Predictions with Early Flight Test Results," AGARD-CP-242, 1977, pp. 19-1 - 19-17.
- 153) White, F.M., and Christoph, G.H., "A Simple New Analysis of Compressible Turbulent Two-Dimensional Skin Friction under Arbitrary Conditions," AFFDL-TR-70-133, February 1971.
- 154) White, F.M., and Christoph, G.H., "Rapid Engineering Calculation of Two-Dimensional Turbulent Skin Friction," AFFDL-TR-72-136, Sup. 1, November 1972.
- 155) White, F.M., Lessman, R.C., and Christoph, G.H., "A Simplified Approach to the Analysis of Turbulent Boundary Layers in Two and Three Dimensions," AFFDL-TR-136, November 1972.
- 156) Williams, J., "Ground/Flight Test Techniques and Correlation," AGARD-CP-339, October 1982.
- 157) Williams, J., "Technical Evaluation Report on the Flight Mechanics Panel Symposium on Ground/Flight Test Techniques and Correlation," AGARD-AR-191, June 1983. Also AGARD-CP-339, October 1982.
- 158) Williams, J., "Synthesis of Responses to AGARD-FMP Questionnaire on Prediction Techniques and Flight Correlation," AGARD-CP-339, 1982, pp. 24-1 - 24-30.
- 159) Williams, J., "Aircraft Performance - Prediction Methods and Optimization," AGARD-LS-56, Charlotte St, London.
- 160) Williams, J., "Prediction Methods for Aircraft Aerodynamic Characteristics," AGARD-LS-67, May 1974.
- 161) Wood, R.A., "Brief Prepared Remarks for Session II, Performance Correlation," AGARD-CP-339, 1982, pp. 9A-1 - 9A-4.
- 162) Wood, R.M., Dollyhigh, S.M., and Miller, D.S., "An Initial Look at the Supersonic Aerodynamics of Twin-Fuselage Aircraft Concepts," ICAS-82-1.8.3, 13th Congress of the International Council of the Aeronautical Sciences with AIAA Aircraft Systems and Technology Conference, Seattle WA, August 1982.
- 163) Wood, R.M. and Miller, D.S., "Experimental Investigation of Leading-Edge Thrust at Supersonic Speeds," NASA TP-2204, September 1983.
- 164) Wood, R.M., Miller, D.S., Hahne, D.E., Niedling, L., and Klein, J., "Status Review of a Supersonically Biased Fighter Wing-Design Study," AIAA-83-1857, Applied Aerodynamics Conference, Danvers MA, July 1983.

- 165) Woodward, F.A., "Development of the Triplet Singularity for the Analysis of Wings and Bodies in Supersonic Flow," NASA CR-3466, September 1981.
- 166) Wu, J.C., Hackett, J.E., Lilley, D.E., "A Generalized Wake-Integral Approach for Drag Determination in Three-Dimensional Flows," AIAA-79-0279, Aerospace Sciences Meeting, New Orleans LA, January 1979.
- 167) Yoshihara, H., "Special Course on Subsonic/Transonic Aerodynamic Interference for Aircraft," AGARD-R-712, May 1983.
- 168) Yoshihara, H. and Spee, B.M., "Applied Computational Transonic Aerodynamics," AGARD-AG-266, August 1982.
- 169) Young, A.D., "The Calculation of the Total and Skin Friction Drags of Bodies of Revolution at Zero Incidence," A.R.C. R&M 1874, April 1939.
- 170) Young, A.D., Patterson, J.H., and Jones, J.L., "Aircraft Excrescence Drag," AGARD-AG-264, July 1981.
- 171) Youngren, H.H., Bouchard, E.E., Coopersmith, R.M., and Miranda, L.R., "Comparison of Panel Method Formulation and its Influence on the Development of QUADPAN, an Advanced Low Order Method," AIAA-83-1827, Applied Aerodynamics Conference, Danvers MA, July 1983.
- 172) Yu, N.J., Chen, H.C., Samant, S.S., and Rubbert, P.E., "Inviscid Drag Calculations for Transonic Flows," AIAA-83-1928, Computational Fluid Dynamics Conference, Danvers MA, July 1983, pp. 283-292.
- 173) Friedman, L.M., "Performance Evaluation of the F-15C," AFFTC-TR-83-32, Dec 1983.

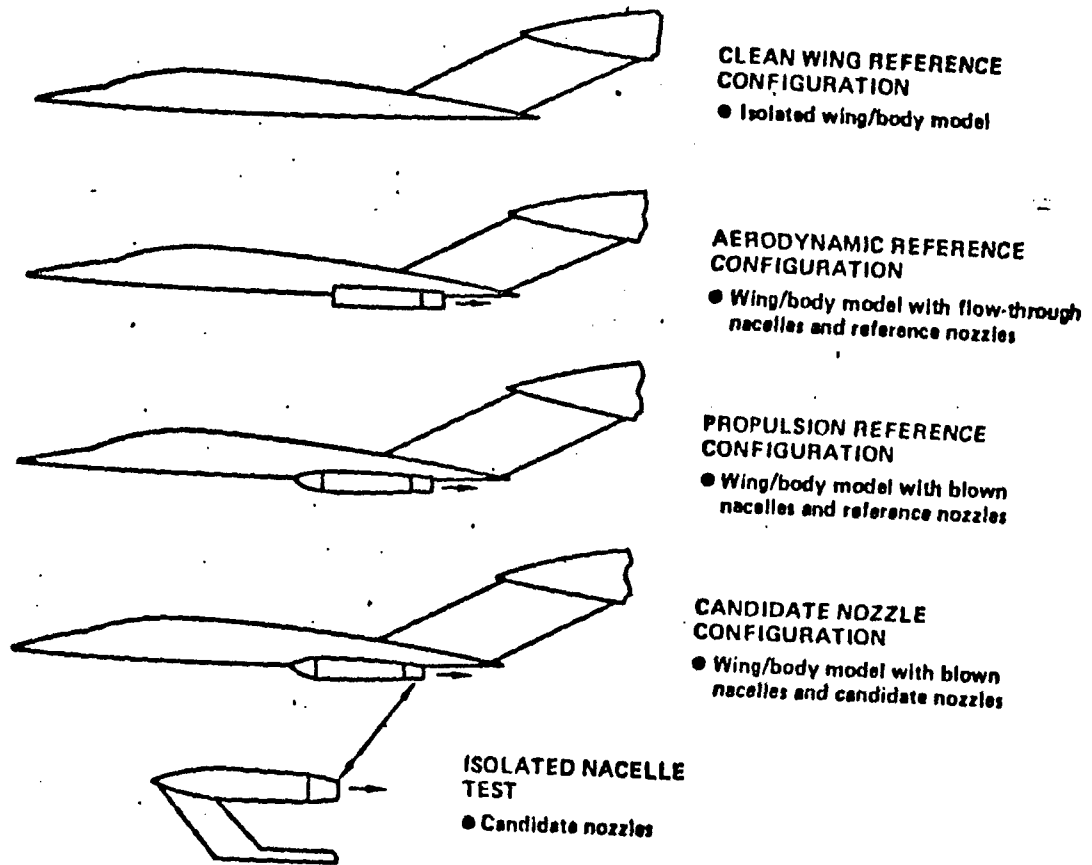


Figure 1. Test Approach  
 (from Tjonneland, et al, Ref. 147)

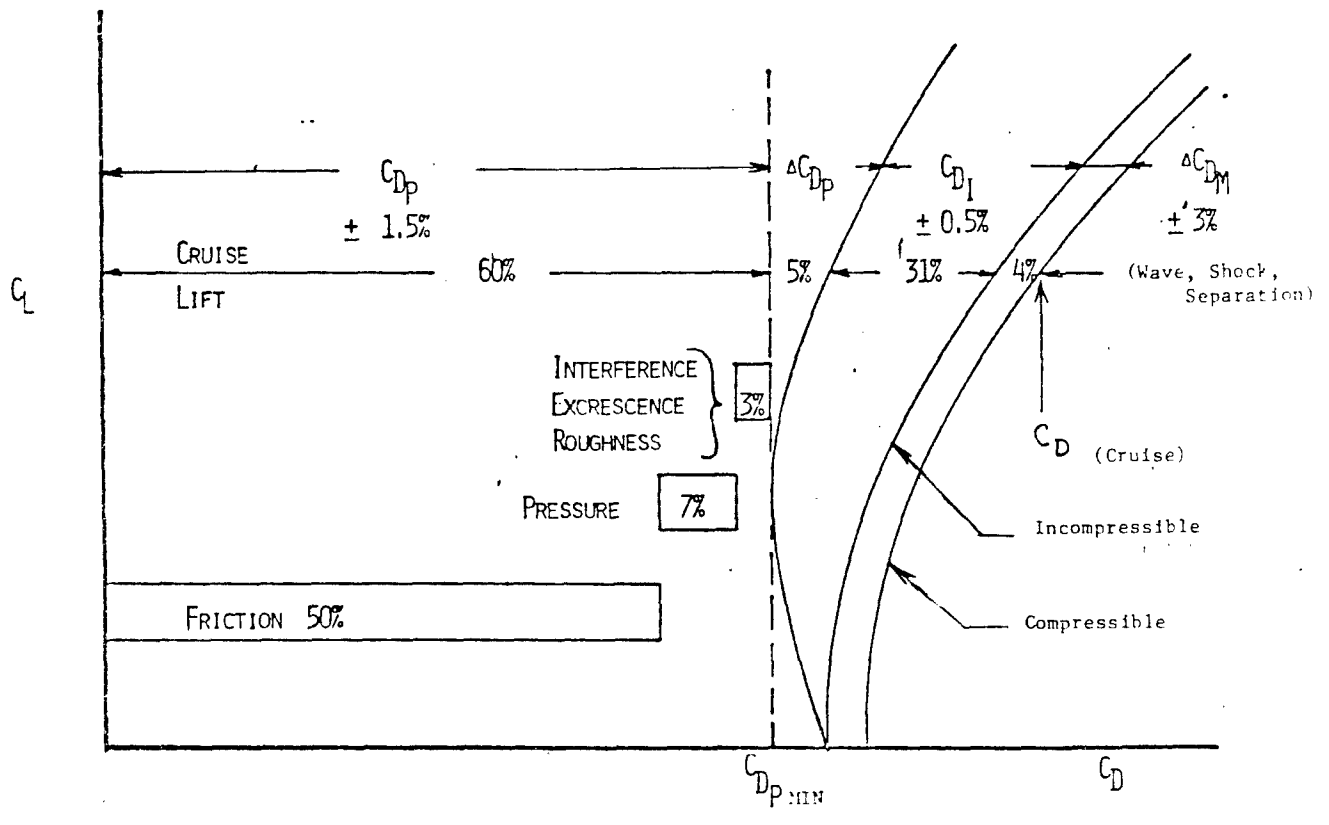


Figure 2. Transport Aircraft Drag Buildup  
(Full Scale,  $M = 0.8$ )



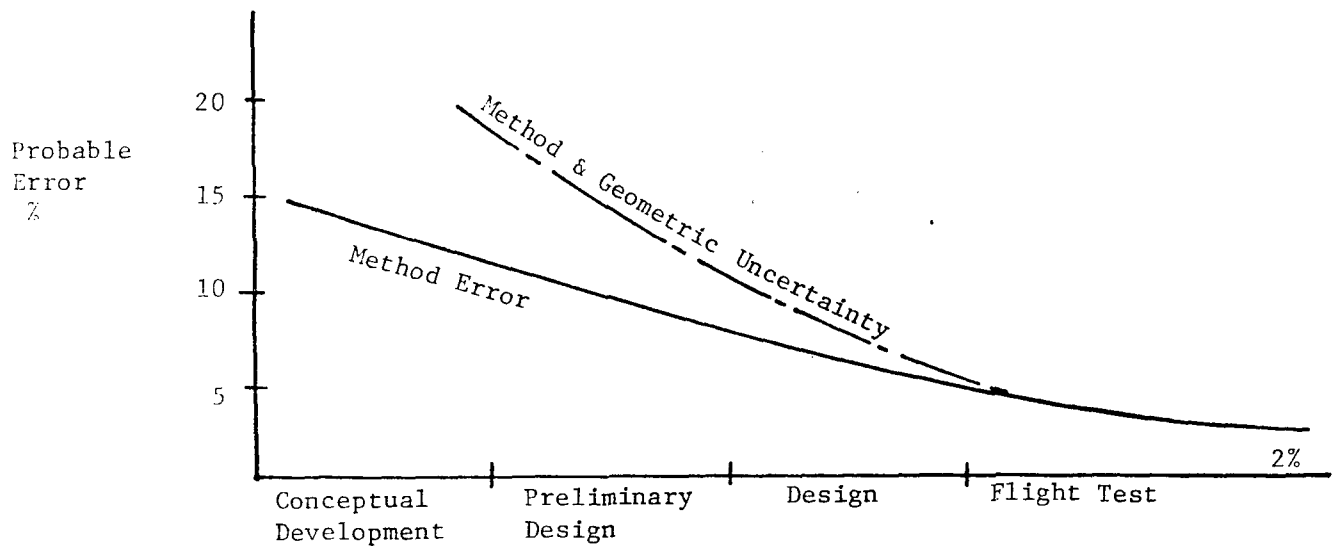


Figure 3. Probable Error During Design

(from Bowes, Ref. 13)

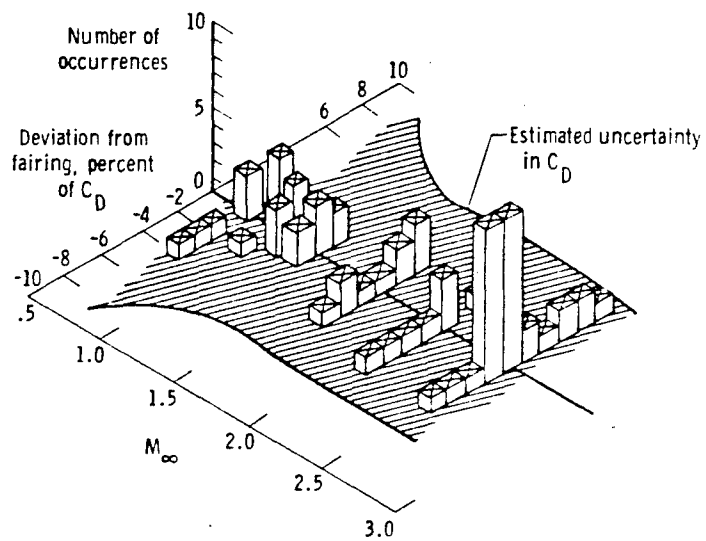


Figure 4. Drag Data Scatter About Drag Polar Fairings with Mach Number.

(From Arnaiz, Ref. 3)

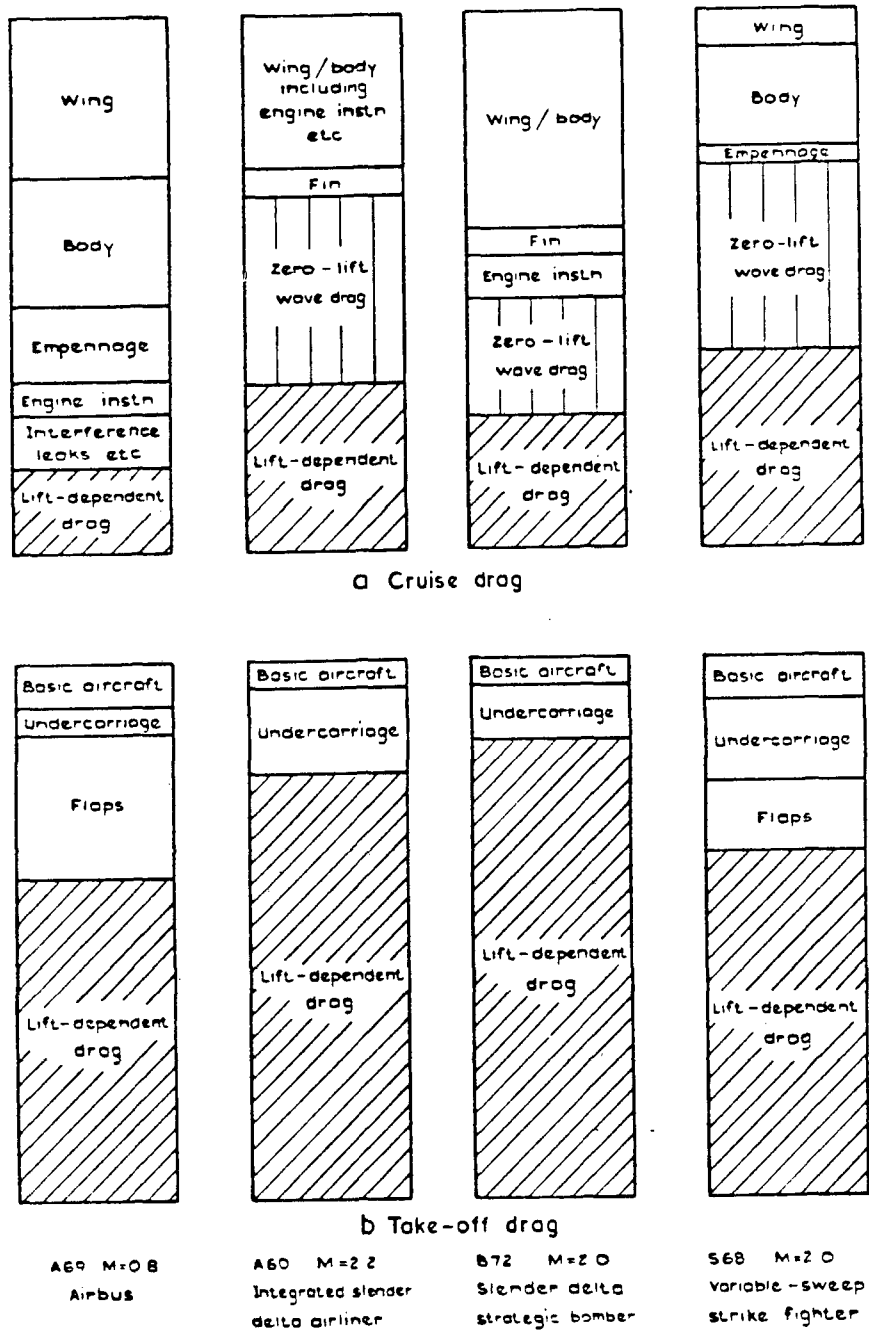


Figure 5. Typical Aircraft Drag Breakdowns  
(from Butler, Ref. 19)

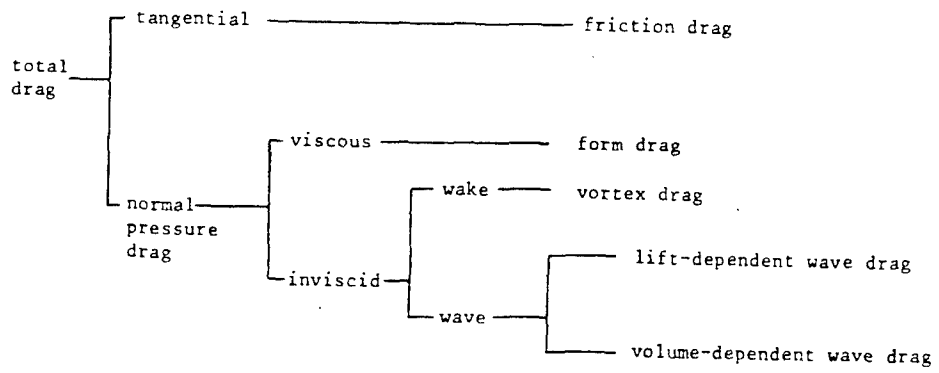


Figure 6. Components of Aircraft Drag  
 (from Butler, Ref. 19; See also Leyman, Ref. 81)

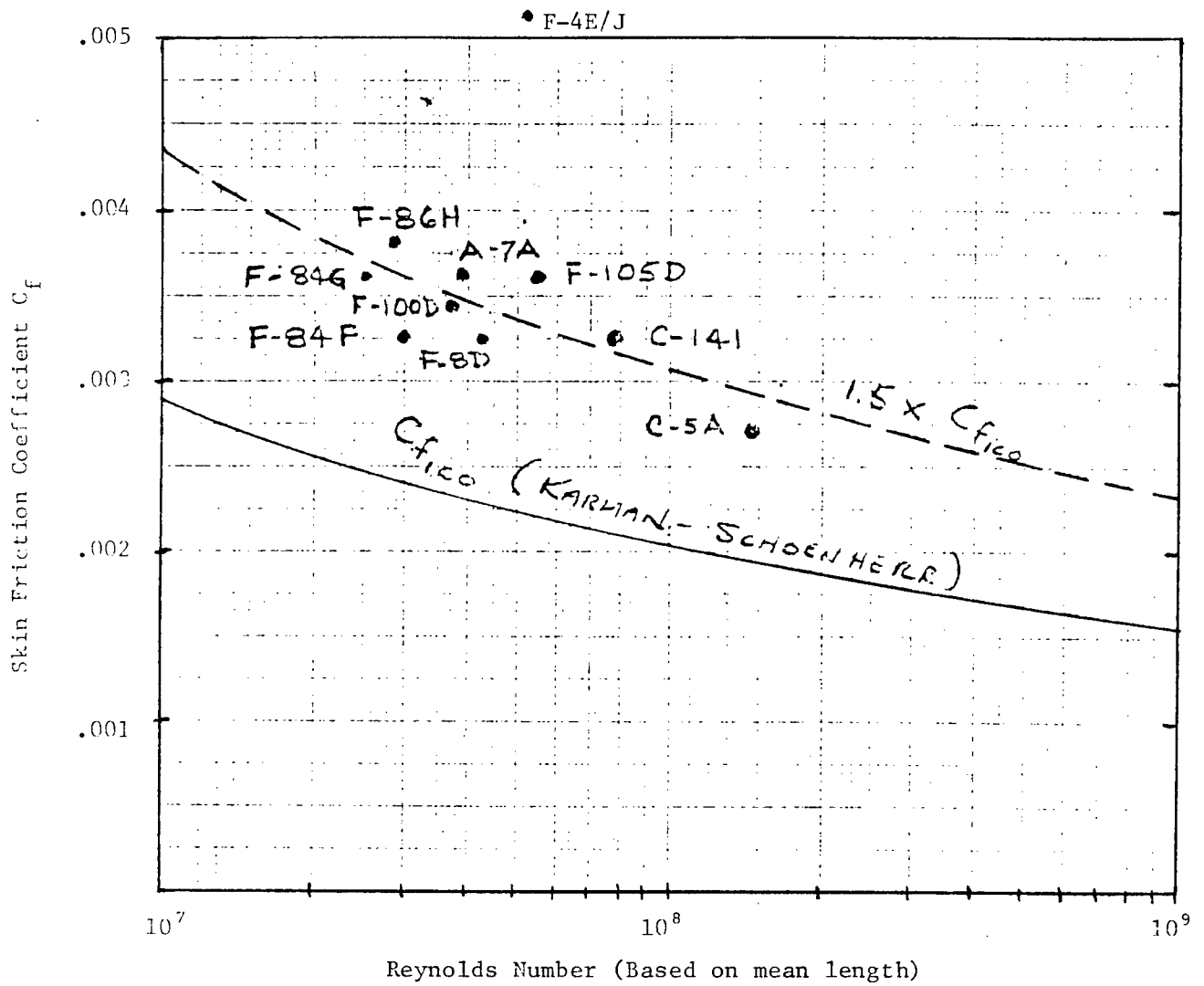


Figure 7. Equivalent Skin Friction

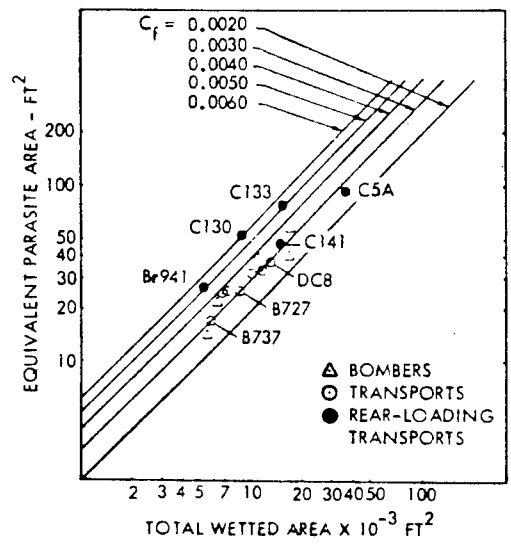


Figure 8. Subsonic Parasite Drag-Bomber/Transport

(from Paterson, et al, Ref. 109)

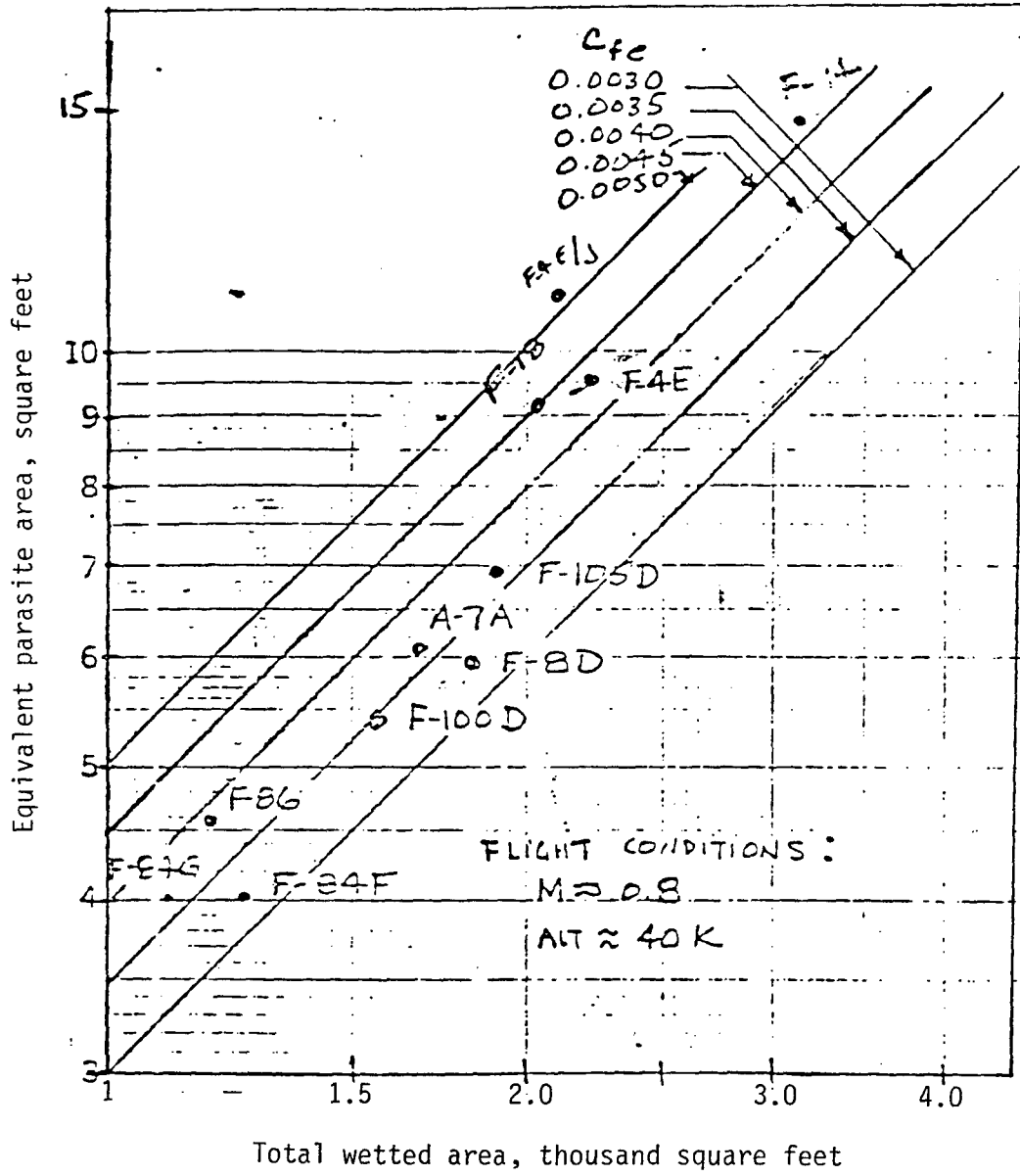


Figure 9. Subsonic Parasite Drag-Fighter/Attack

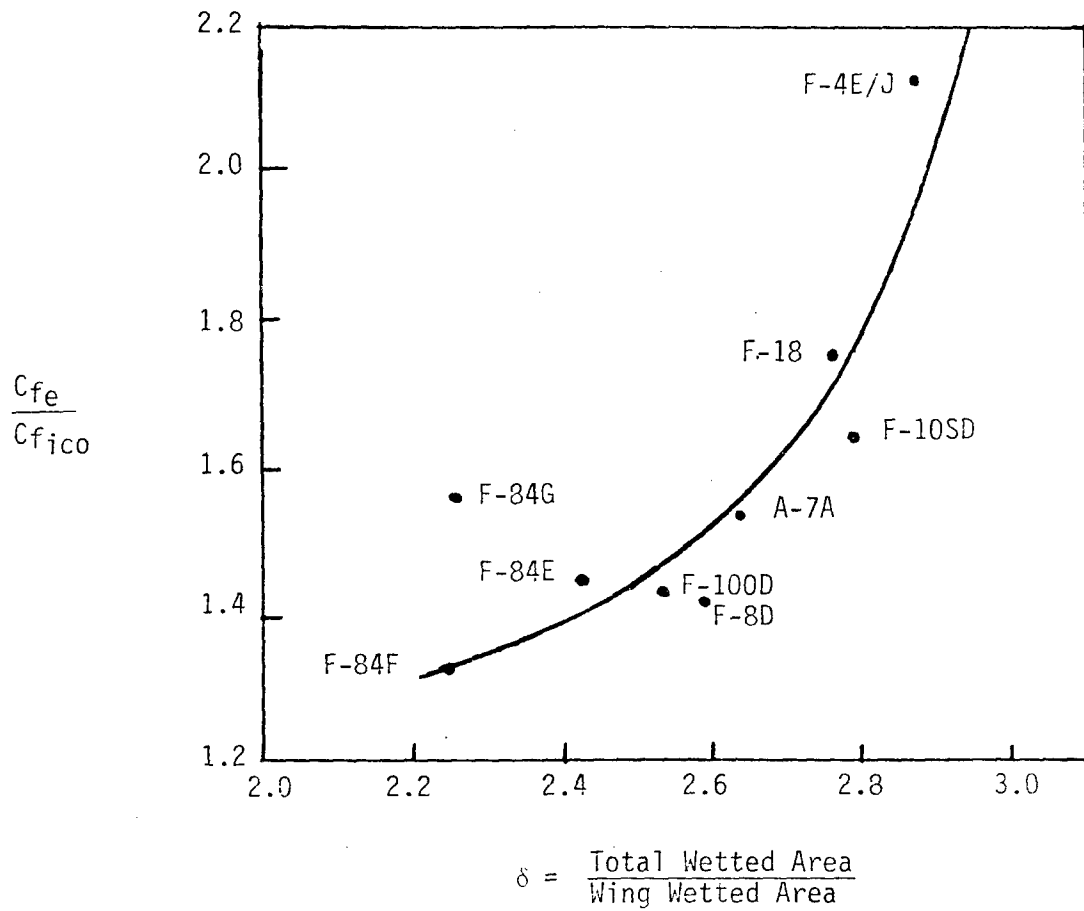


Figure 10. Relative Wing Size



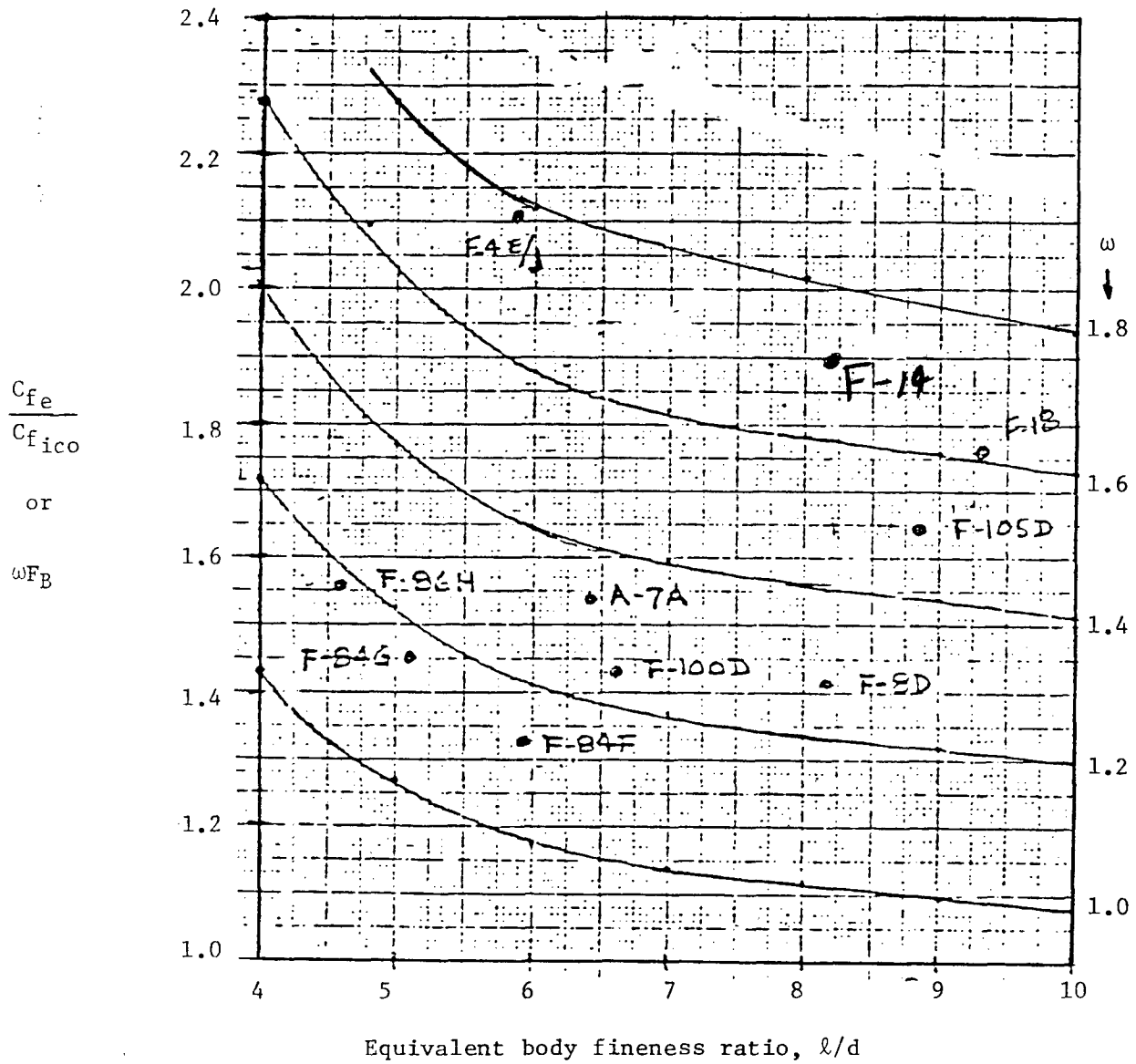
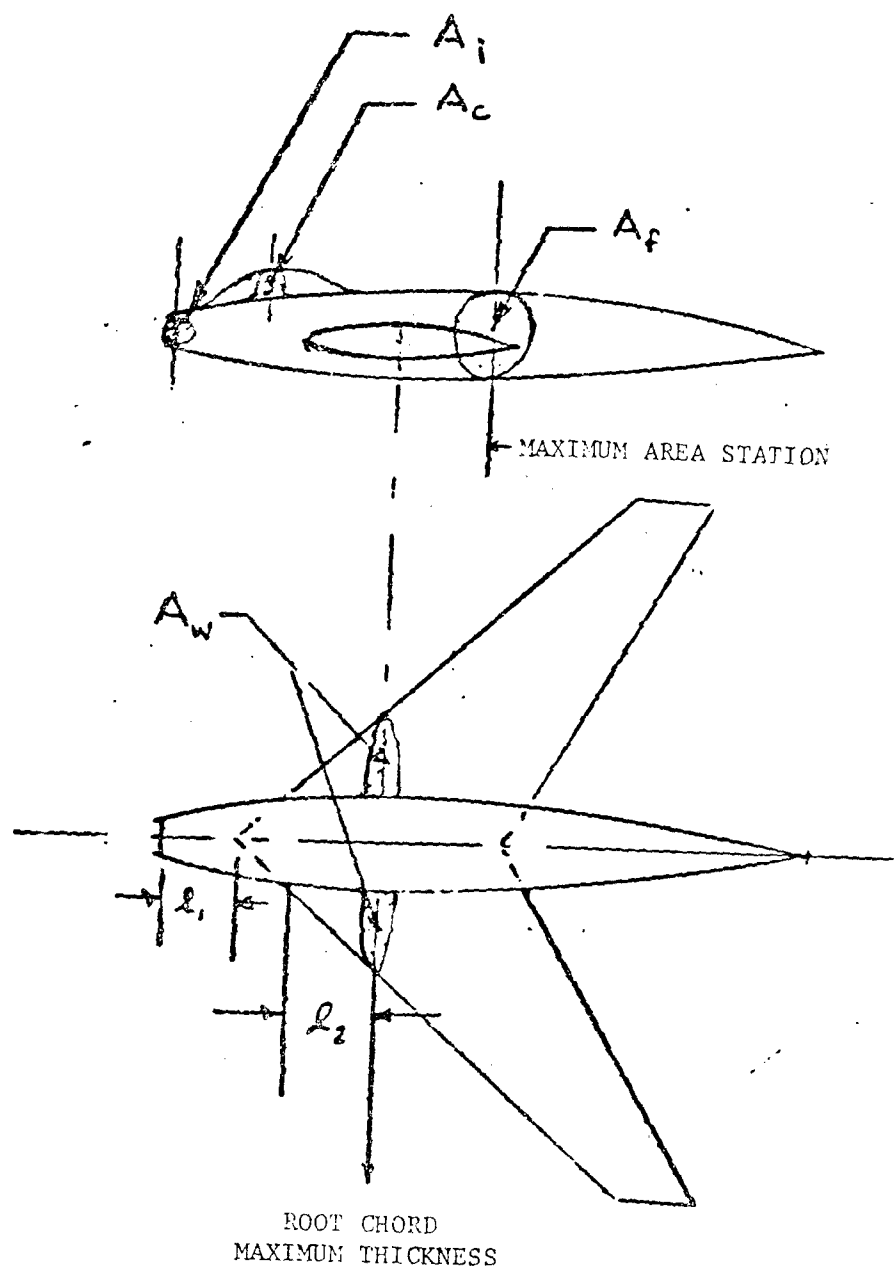


Figure 11. Equivalent Body Shape



$$\left(\frac{l}{d}\right)_{\text{equiv}} = 2 * \bar{l}_f / \left(\frac{4 * A_{\text{eq}}}{\pi}\right)^{1/2}$$

$$\bar{l}_f = l_1 + l_2$$

$$A_{\text{eq}} = A_f + A_c + A_w - A_i$$

Figure 12. Equivalent Body Concept

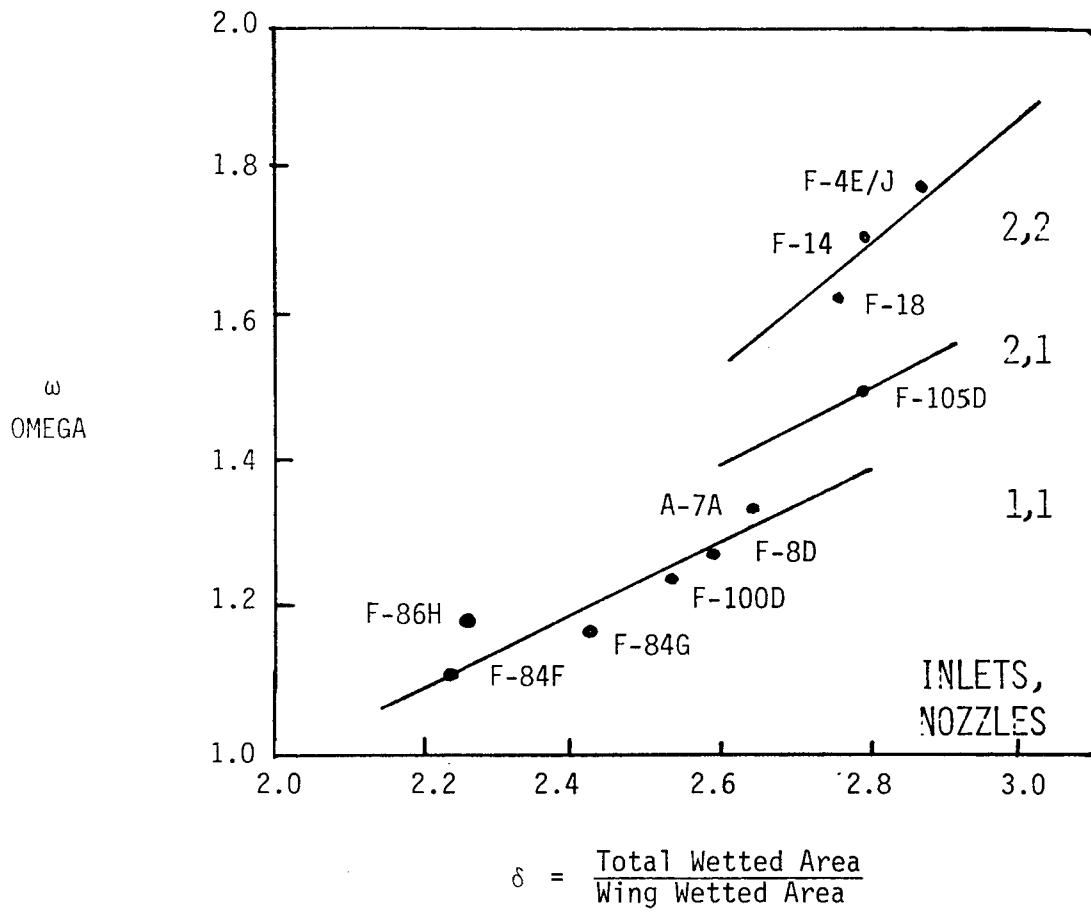


Figure 13. Aerodynamic Cleanness

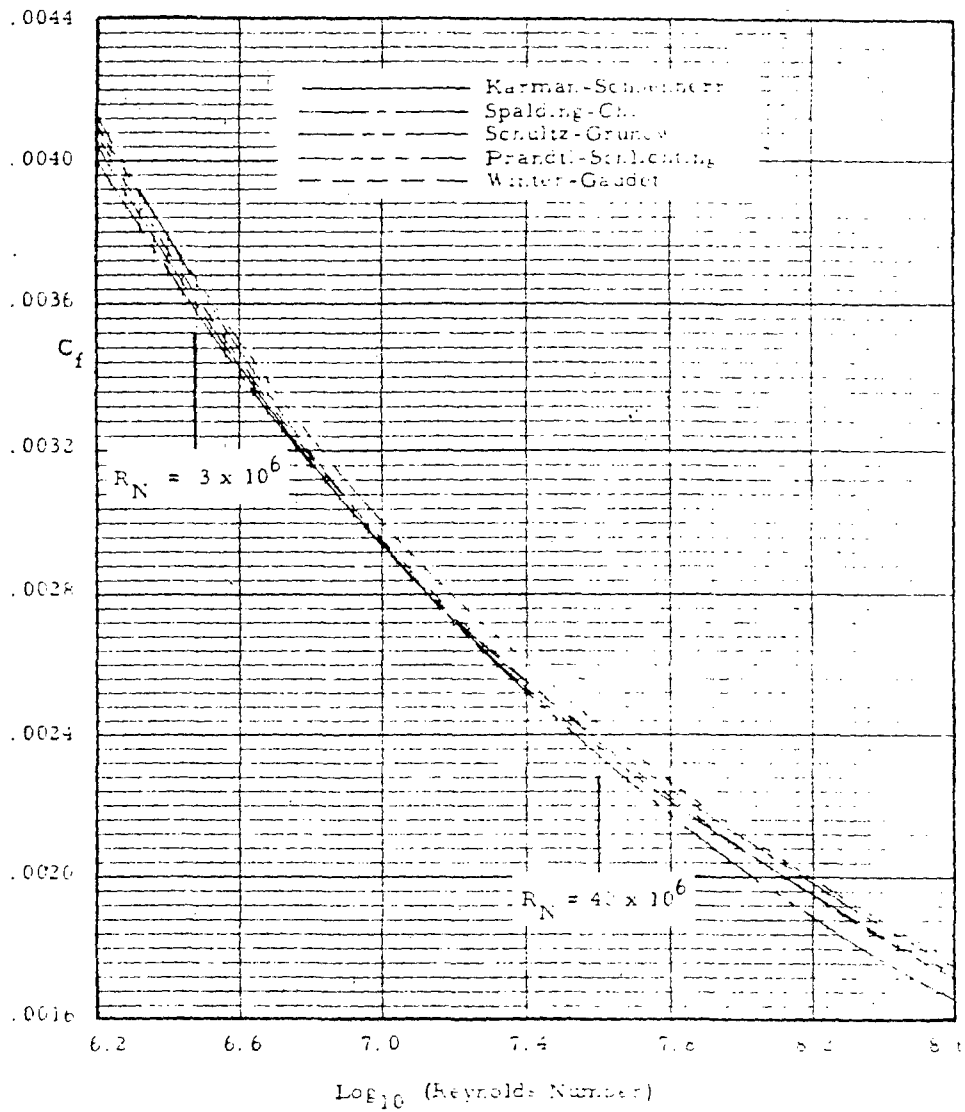


Figure 14. Comparison of Empirical Flat Plate Skin Friction Formulae for Incompressible Turbulent Flow.

(from MacWilkinson, et al, Ref. 86)

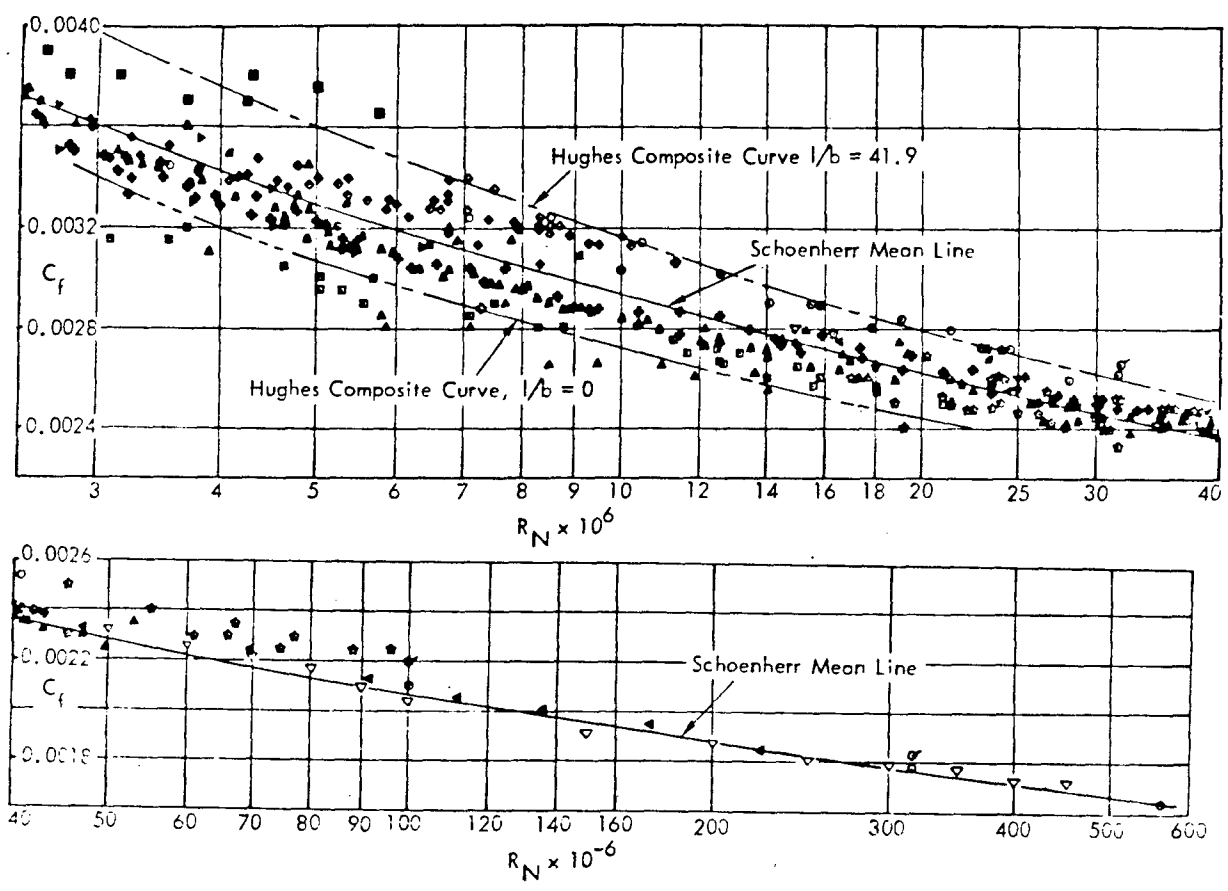


Figure 15. Summary of Experimental Research on Flat Plate Skin Friction, Incompressible Speeds.

(from MacWilkinson, et al, Ref. 86)

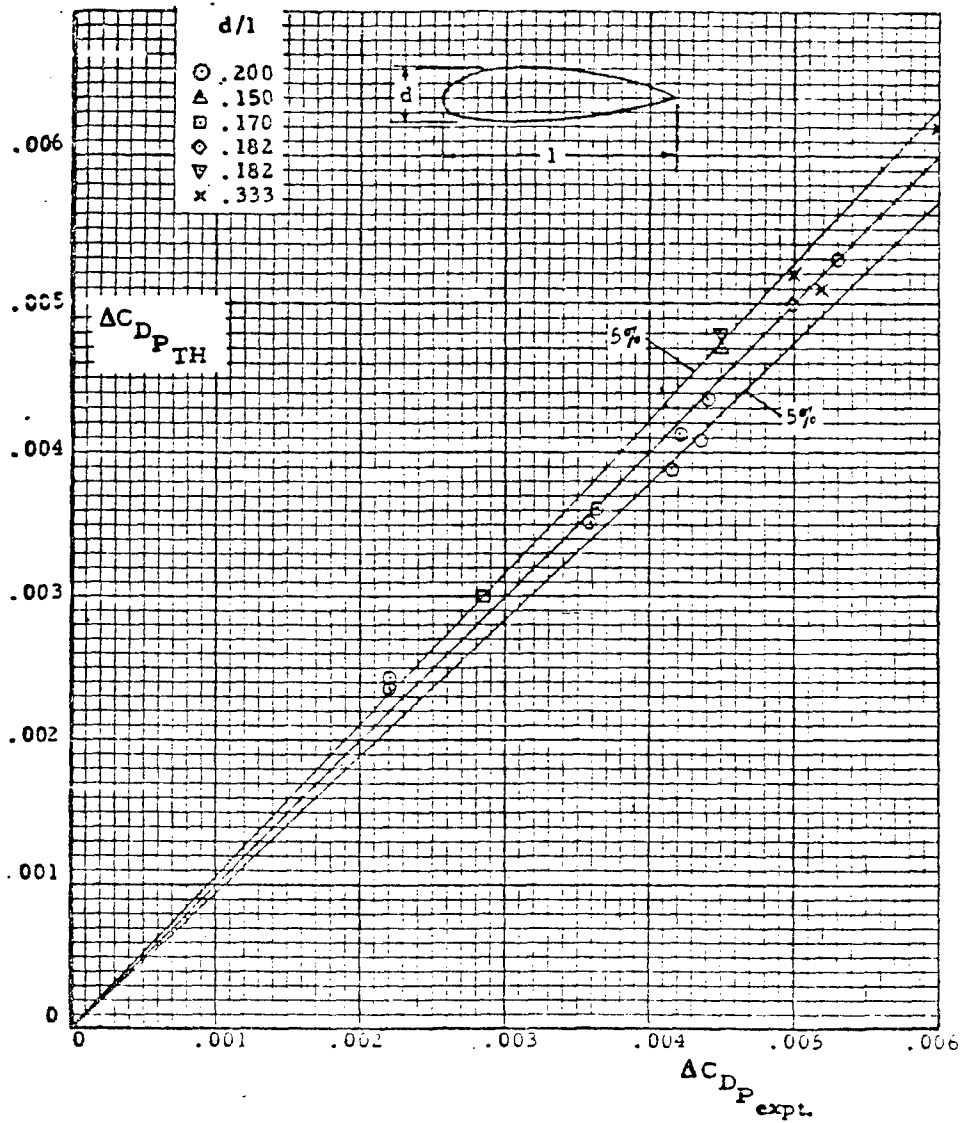


Figure 16. Fuselage Profile Drag-Bodies of Revolution

(from MacWilkinson, et al, Ref. 86)

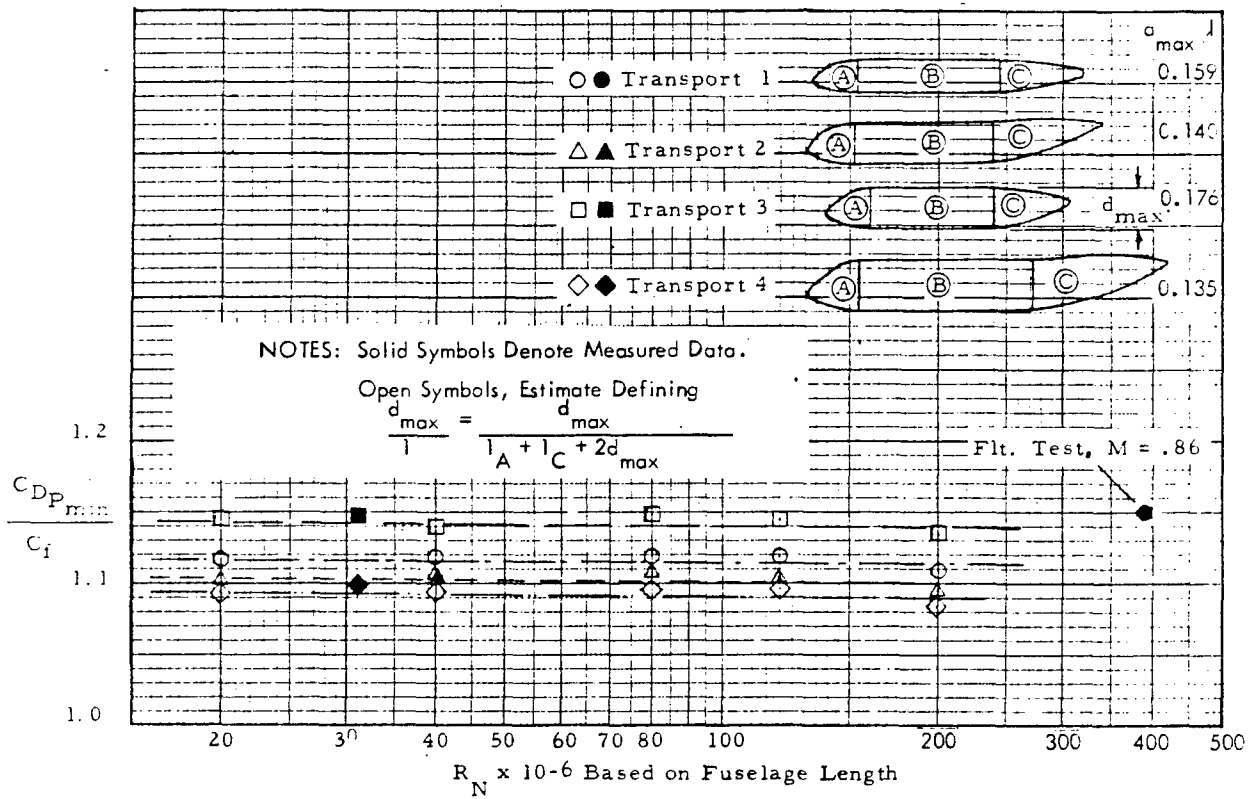


Figure 17. Fuselage Shape Factors,  $M \leq 0.70$

(from MacWilkinson, et al, Ref. 86)

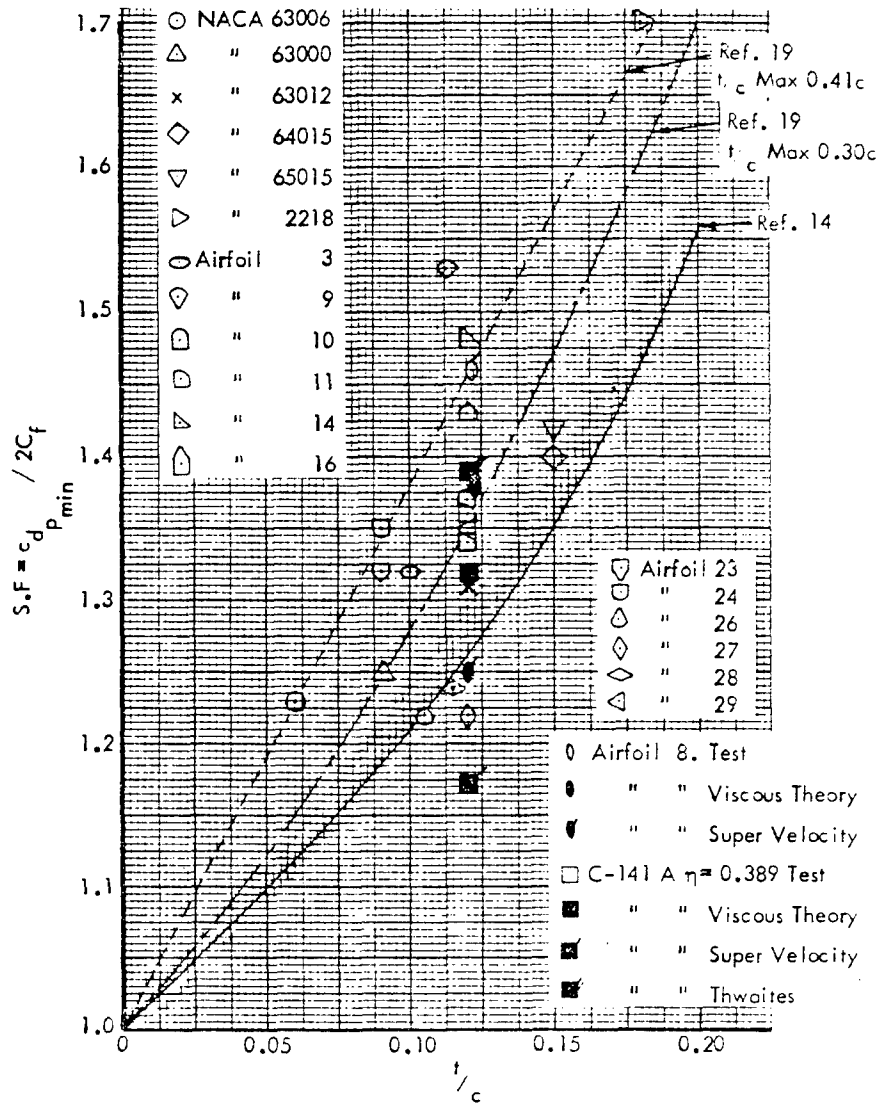


Figure 18. Airfoil Shape Factors  
 (from MacWilkinson, et al, Ref. 86)



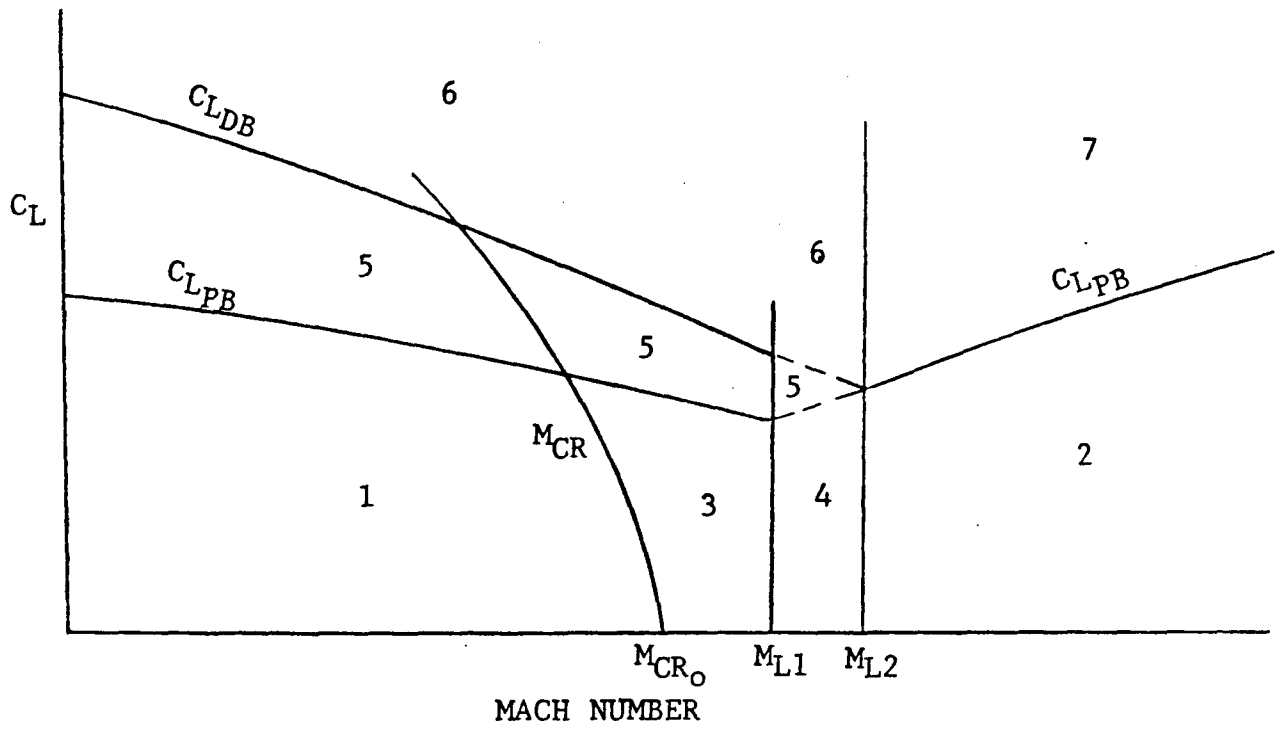
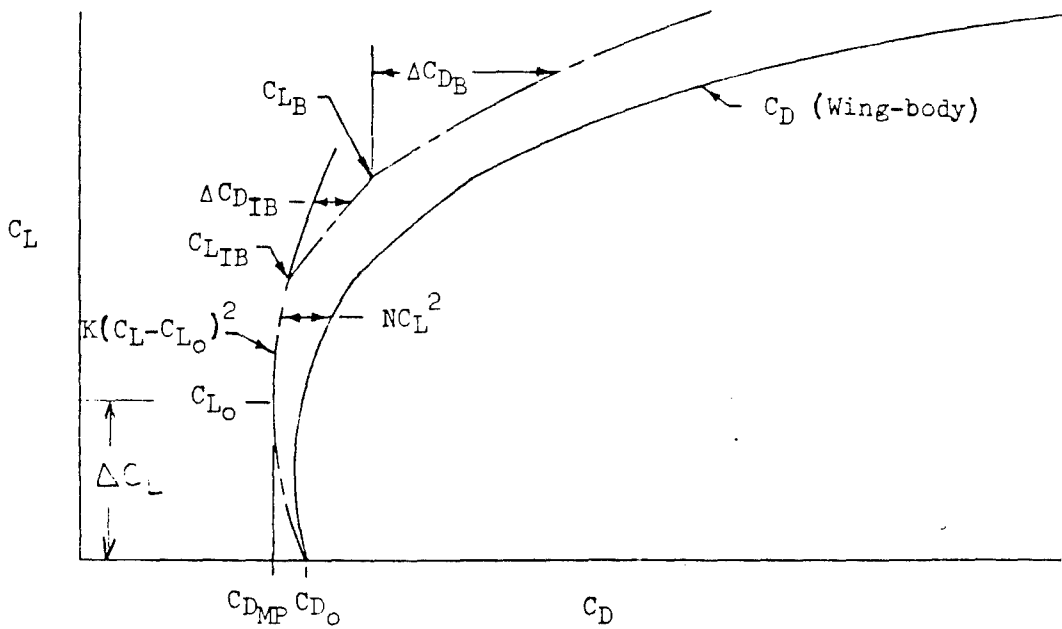


Figure 19. Lift and Speed Regions for Calculation of Drag Due to Lift

(from Schemensky, Ref. 122)



$C_{DMP}$  is the minimum profile drag  $C_{DMP} = C_{D0} - KC_{L0}^2$

$C_{D0}$  is the zero lift drag coefficient

$NC_L^2$  is the theoretical drag due to lift =  $\frac{C_L^2}{\pi A R e}$

$K(C_L - C_{L0})^2$  is the additional profile drag

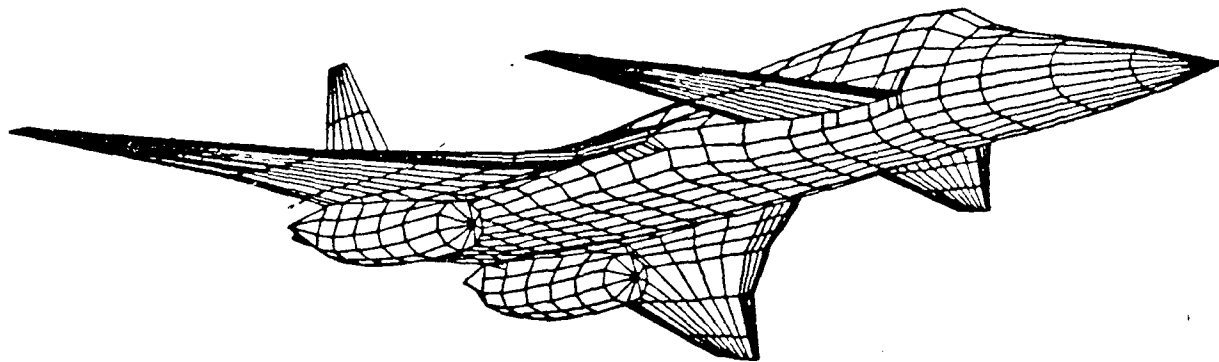
$C_{LB}$  is the lift coefficient for drag break, also  $C_{LDB}$

$\Delta C_{DIB}$  is the intermediate drag break increment, also  $\Delta C_{DPB}$

$\Delta C_{DB}$  is the drag variation for  $C_L > C_{LBR}$

Figure 20. The Subsonic Drag Polar

(from Simon, et al, Ref. 131)



MACH NUMBER = .6

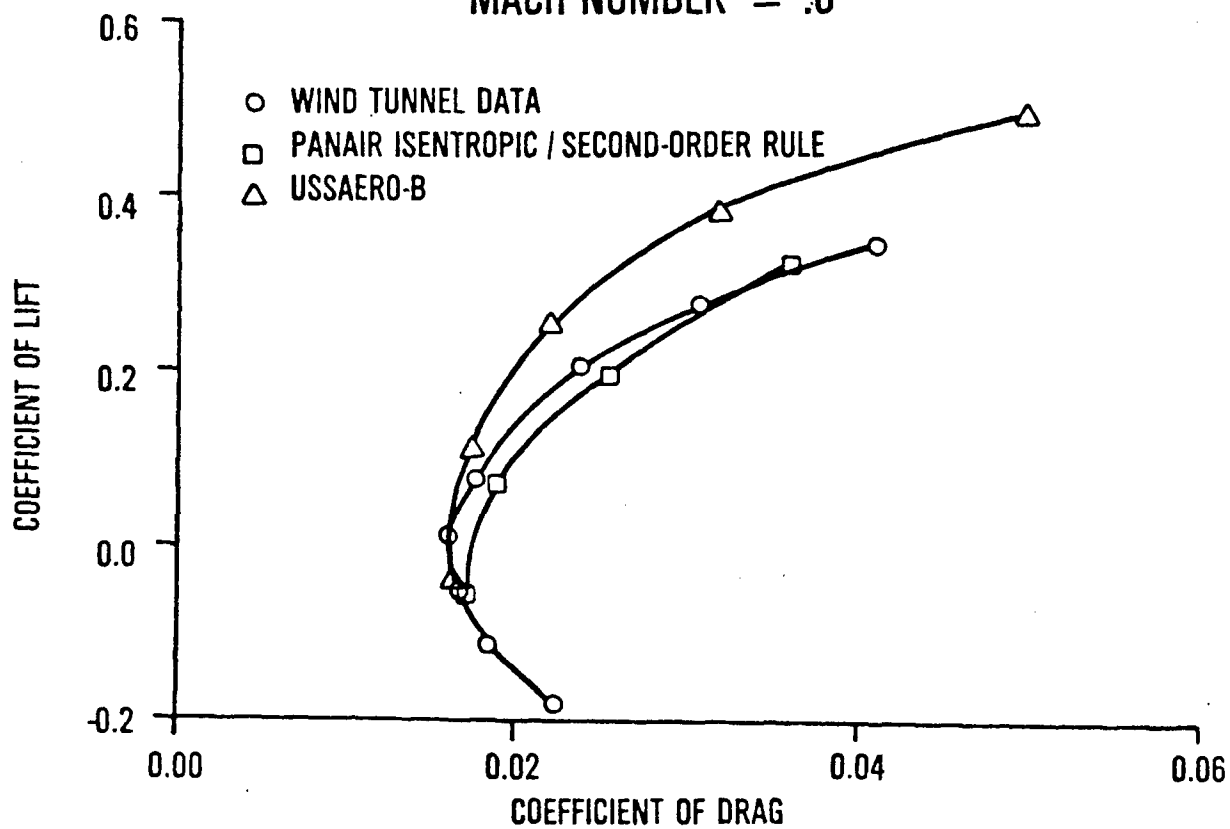


Figure 21. Drag Predictions Using Panel Methods

(from Miller, et al, Ref. 98)

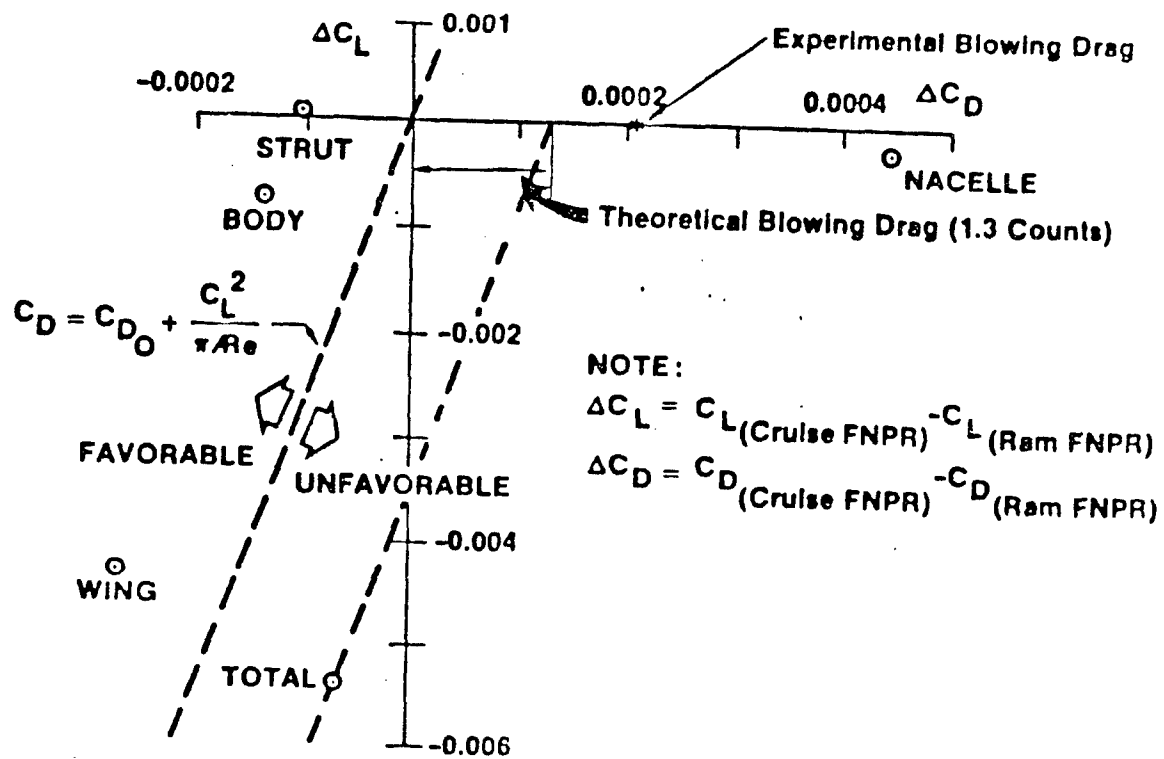


Figure 22. Effects of Engine Power on Lift and Drag of Various Aircraft Components

(from Chen, et al, Ref. 31)

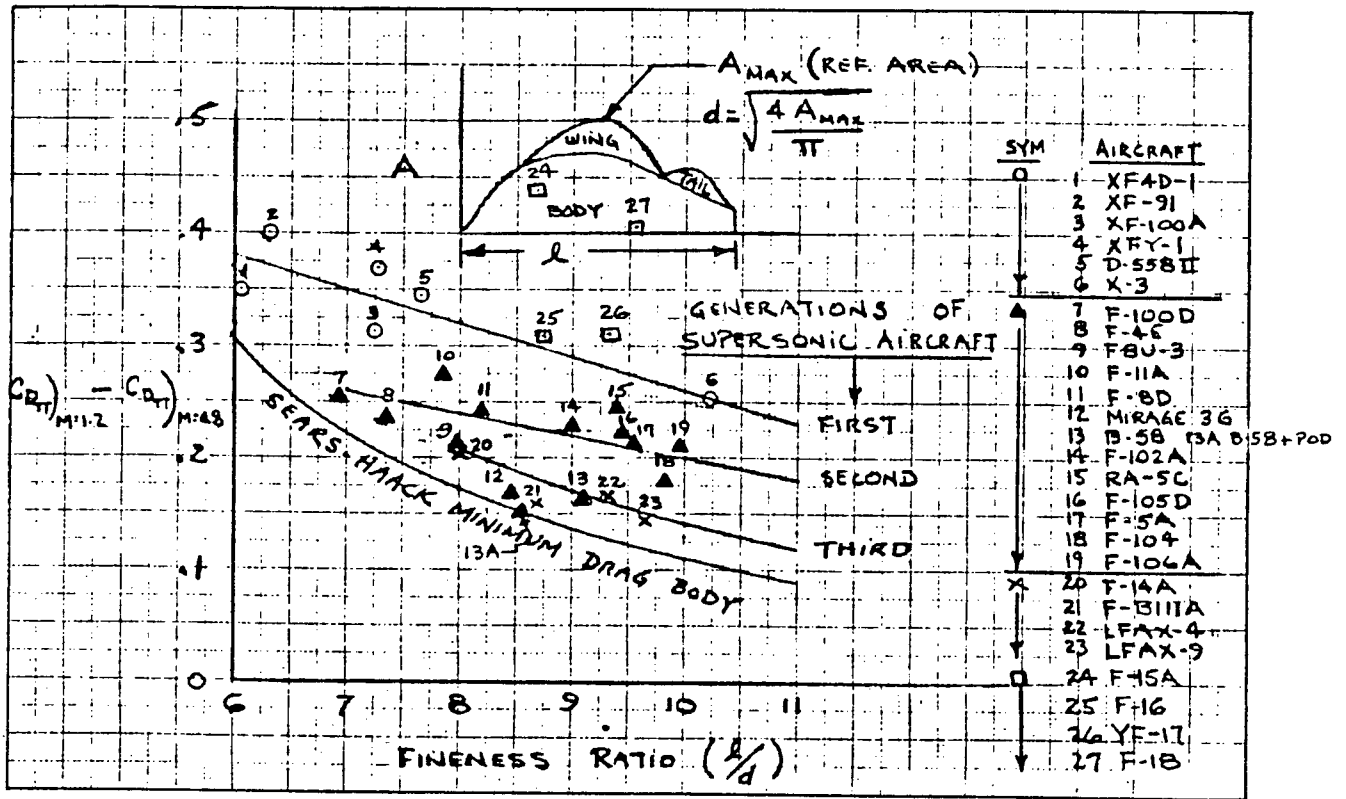


Figure 23. Historic Correlation of Transonic Drag Rise

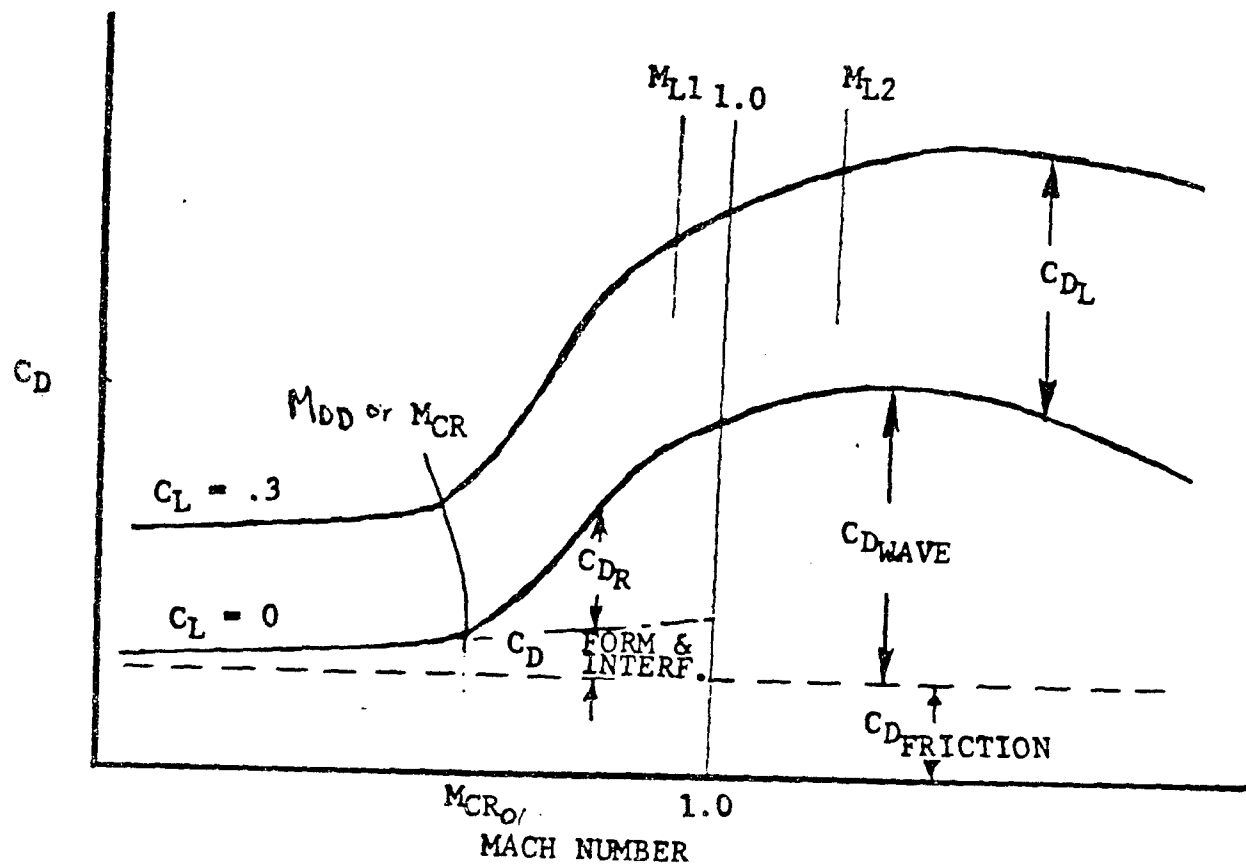


Figure 24. Transonic Drag Buildup

(from Schemensky, Ref. 122)

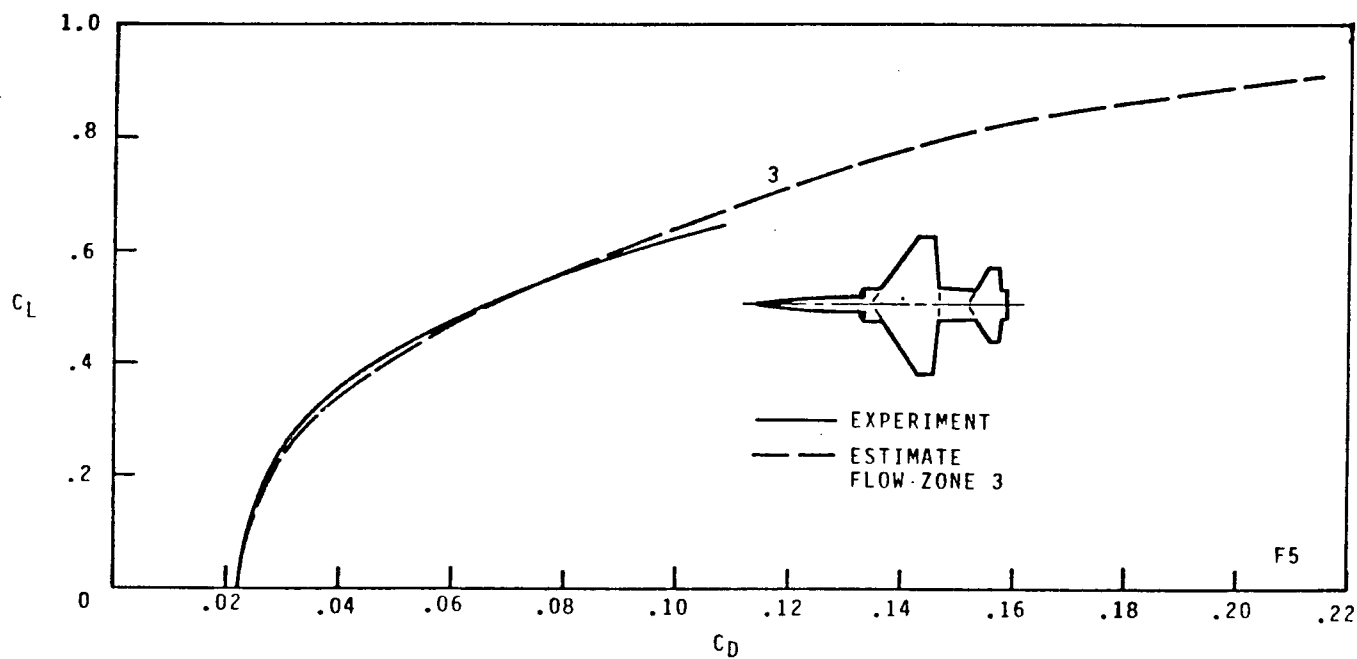


Figure 25. F-5  $C_L$  versus  $C_D$ ;  $M = 0.9$

(from Axelson, Ref. 4)

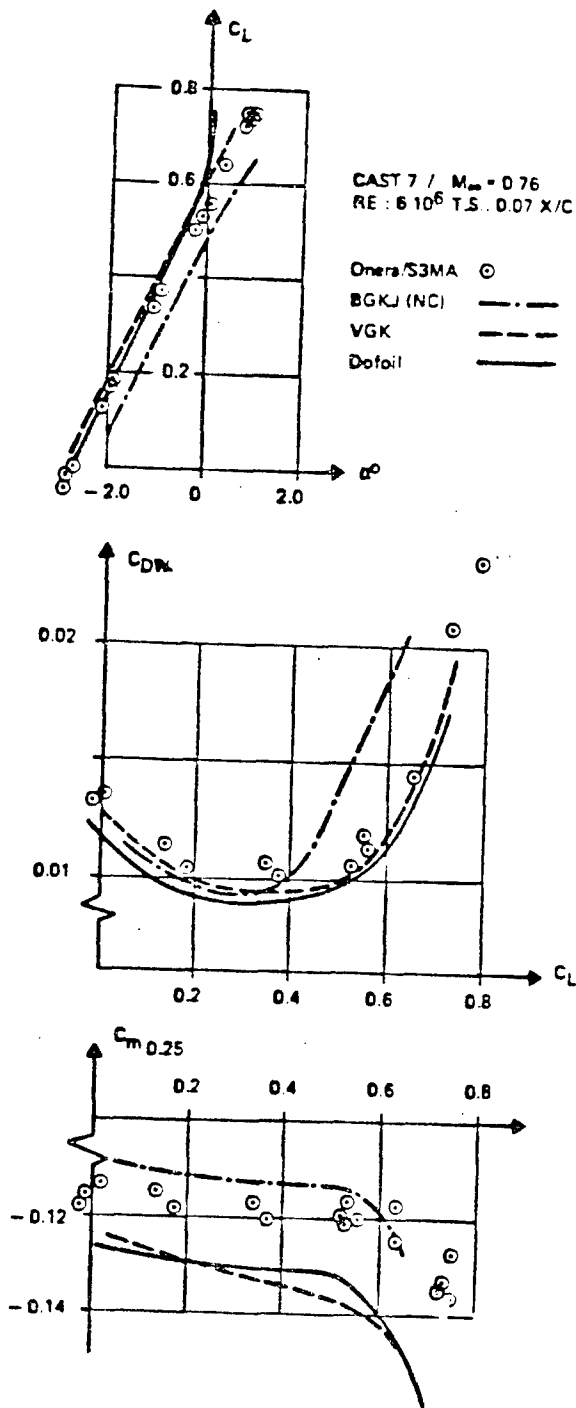


Figure 26. Total Forces and Moments Comparison Between Different Computer Programs

(from Longo, et al, Ref. 84)



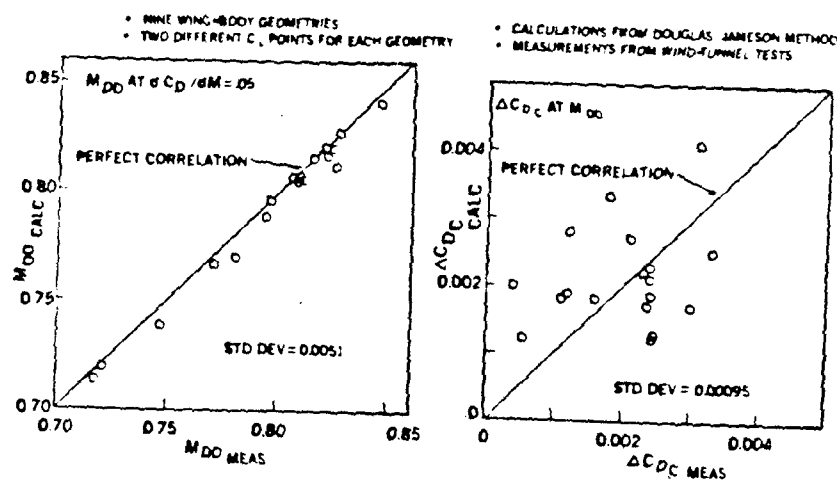
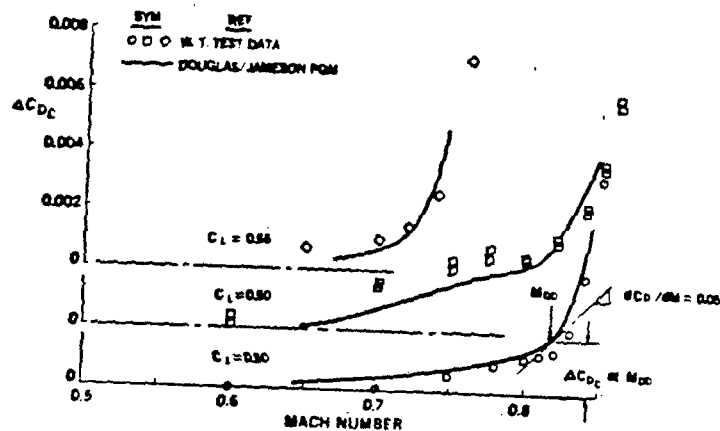


Figure 27. Correlation of Calculated and Measured Wing-Body Drag Divergence Mach Number, Compressibility Drag, and Drag Rise for Three Supercritical Wings.

(from Henne, et al, Ref. 57)

SUPERPOSITION METHOD OF DRAG ANALYSIS

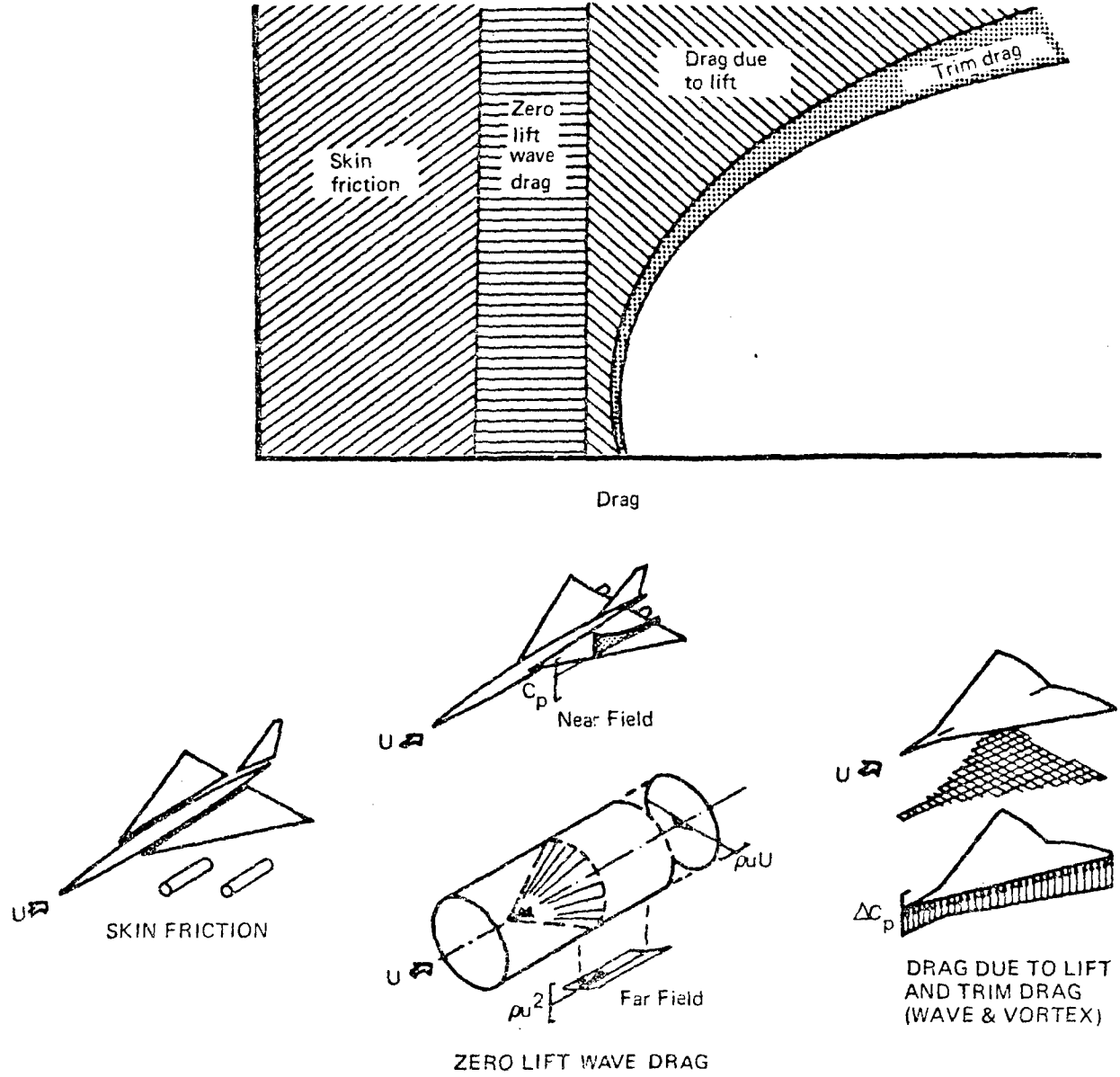


Figure 28. Supersonic Drag Buildup  
 (from Middleton, et al, Ref. 96)

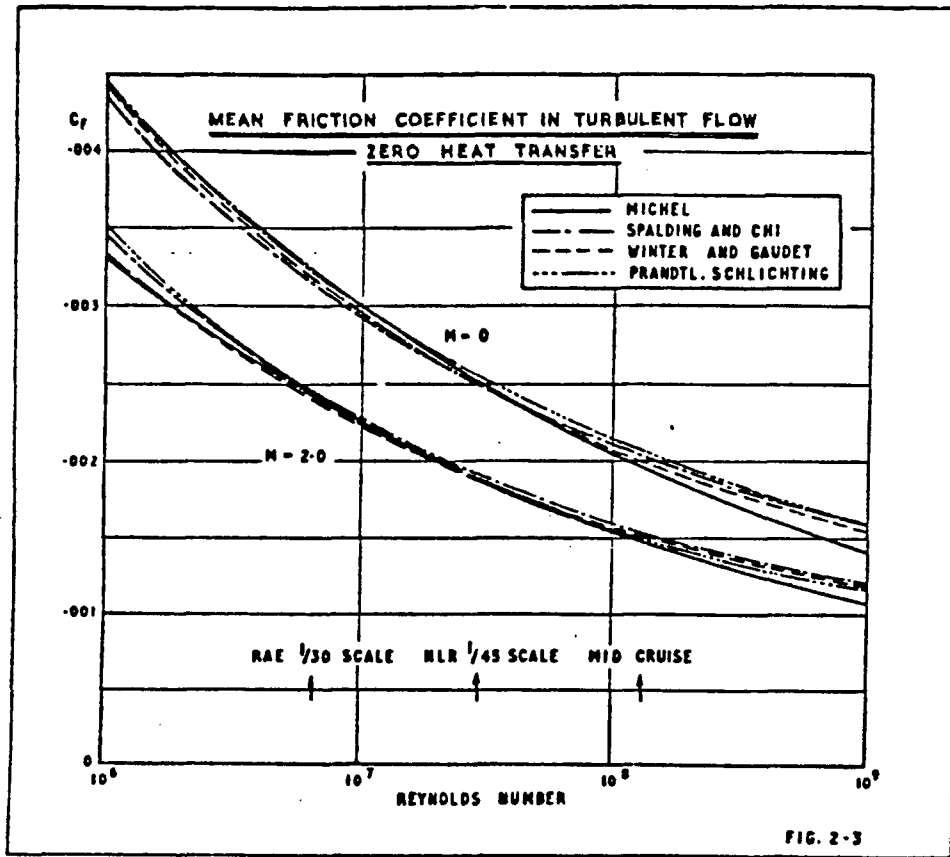


Figure 29. Supersonic Skin Friction

(from Leyman, et al, Ref. 81)

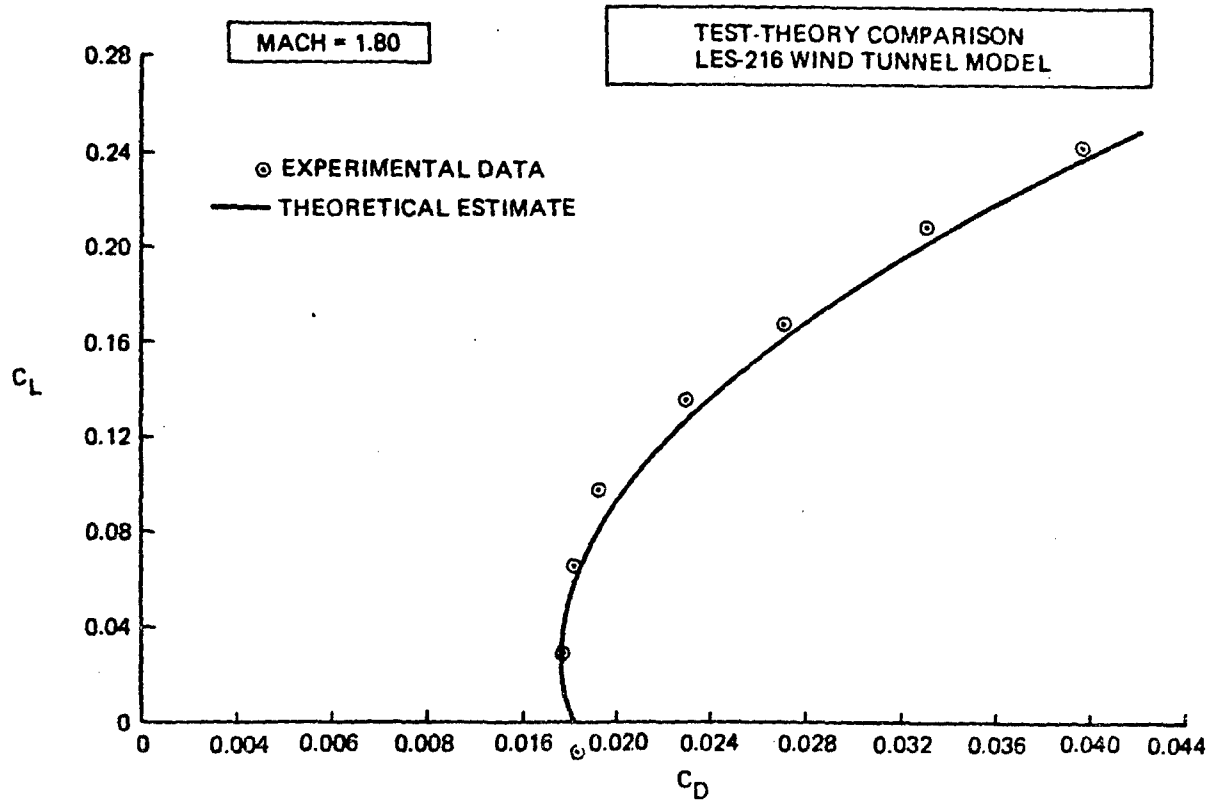
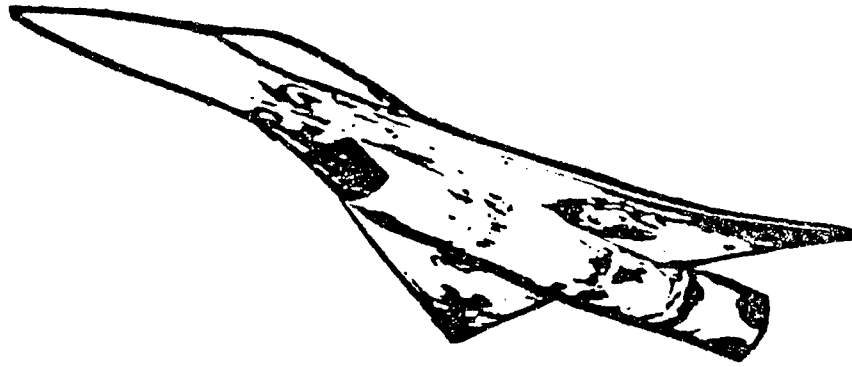


Figure 30. Supercruiser Type Configuration Test-Theory Comparison

(from Kulfan, et al, Ref. 78)

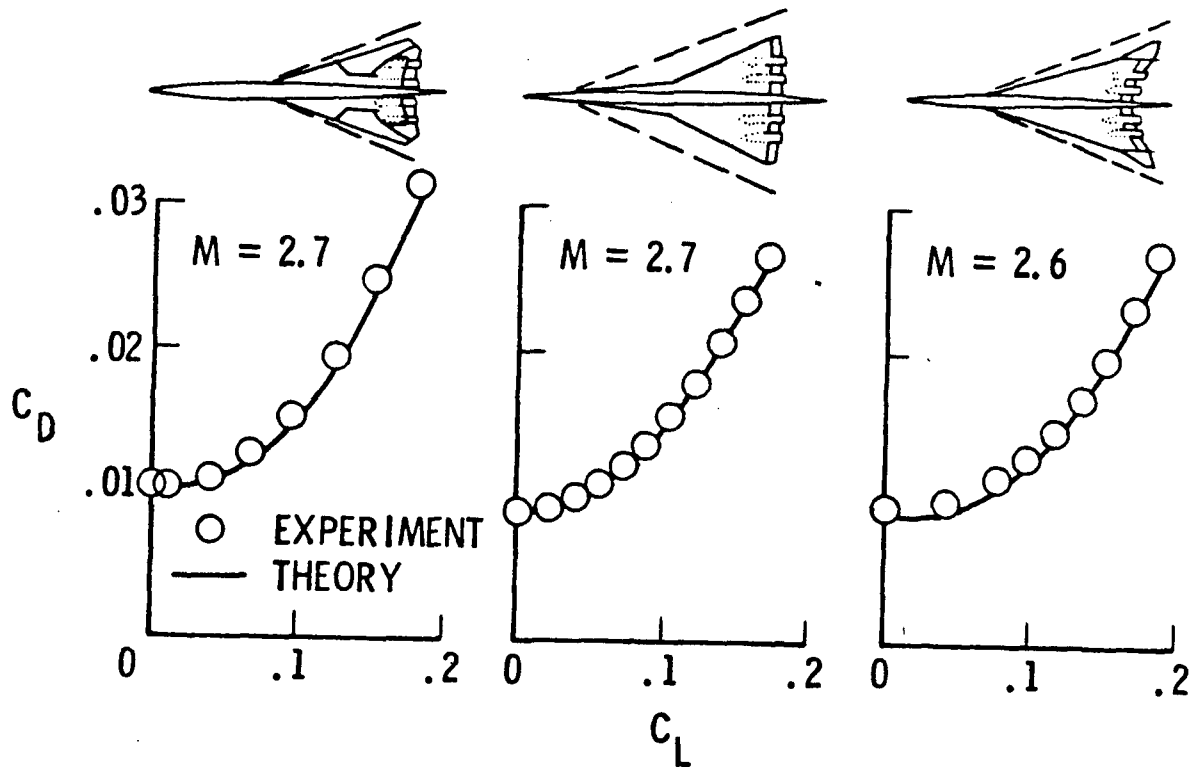


Figure 31. Experimental and Theoretical Drag Polars of Supersonic-Cruise Airplanes,  $R_c = 4.8 \times 10^6$

(from Robins, et al, Ref. 116)

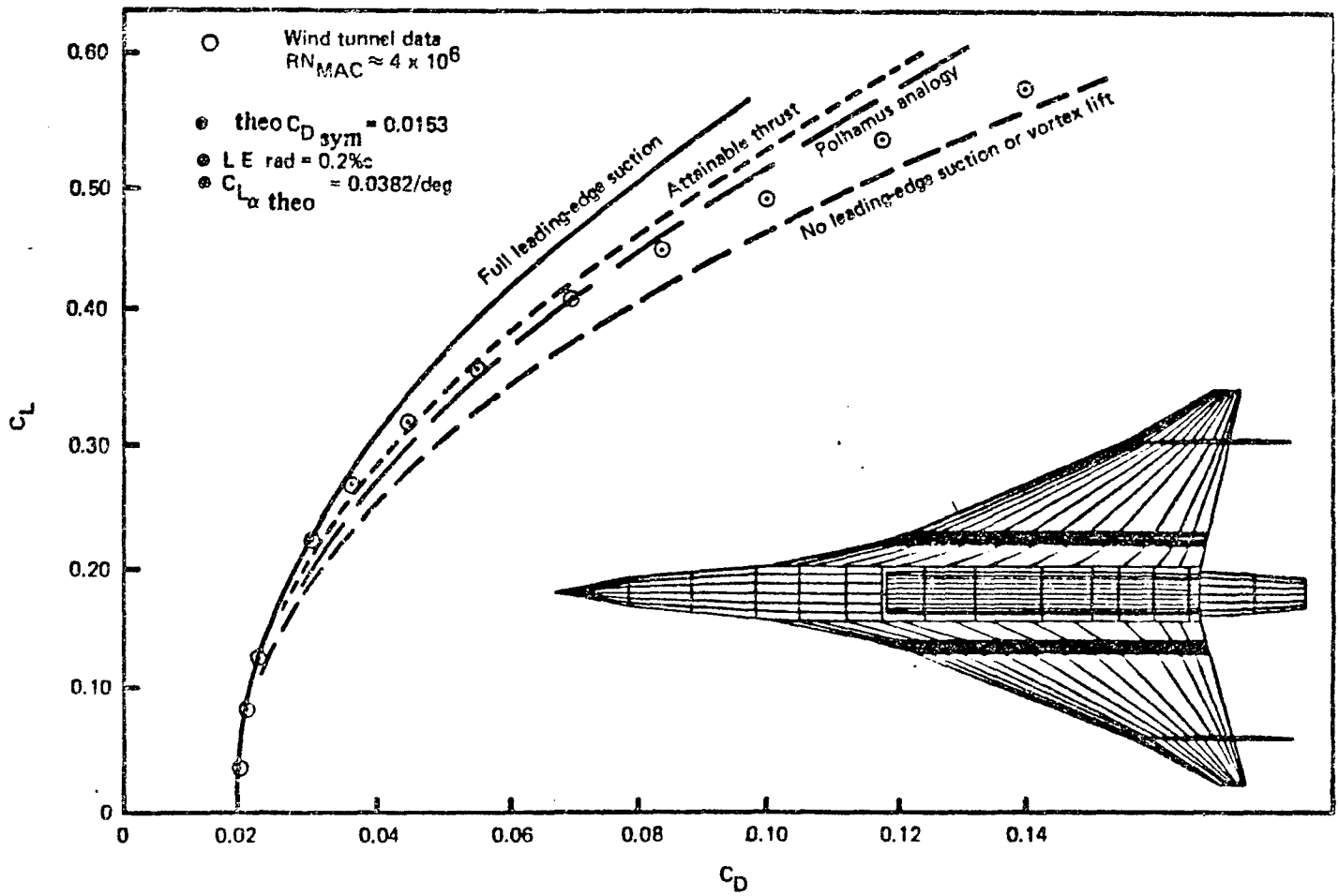


Figure 32. Leading Edge Suction Effects, LES 216

(from Middleton, et al, Ref. 97)

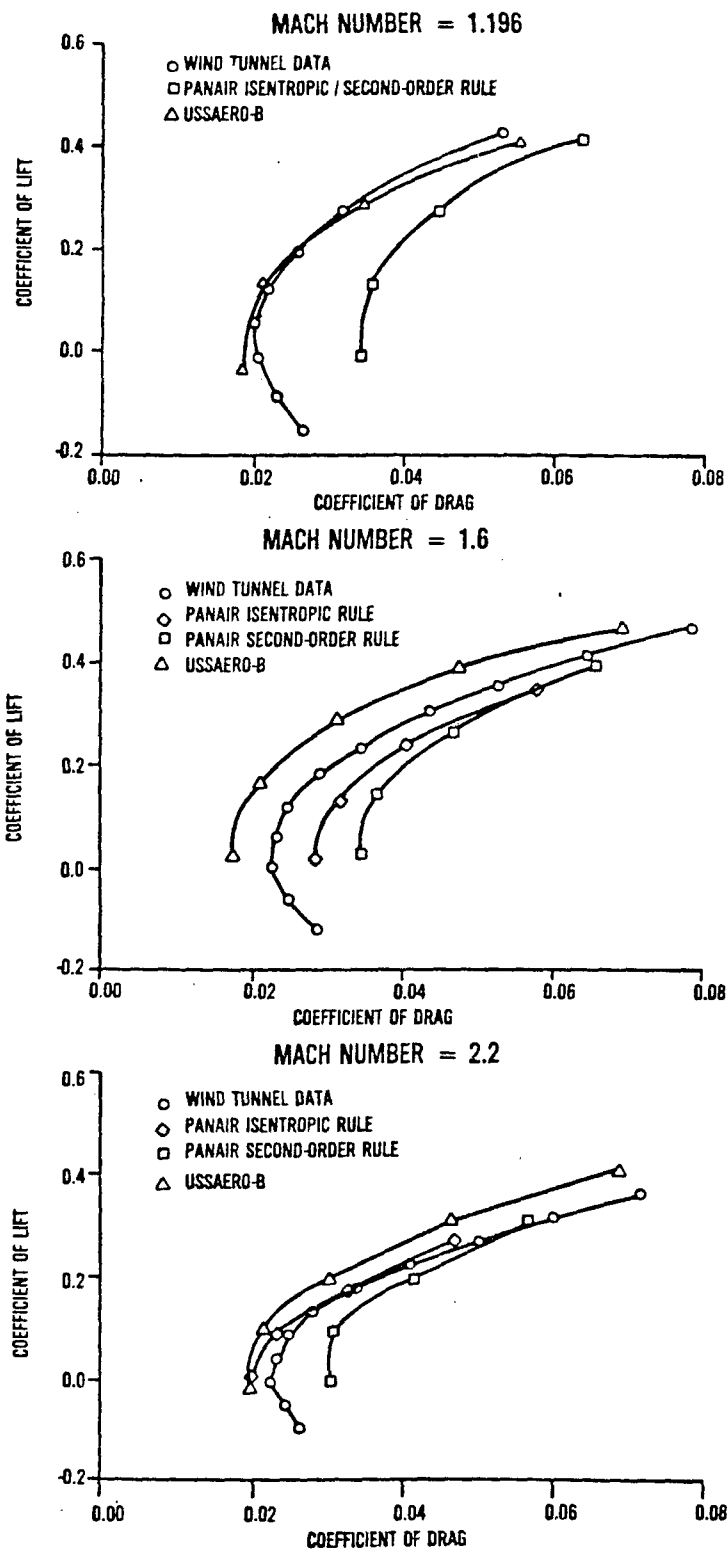


Figure 33. Drag Polars, CDAF Configuration  
 (from Miller, et al, Ref. 98)

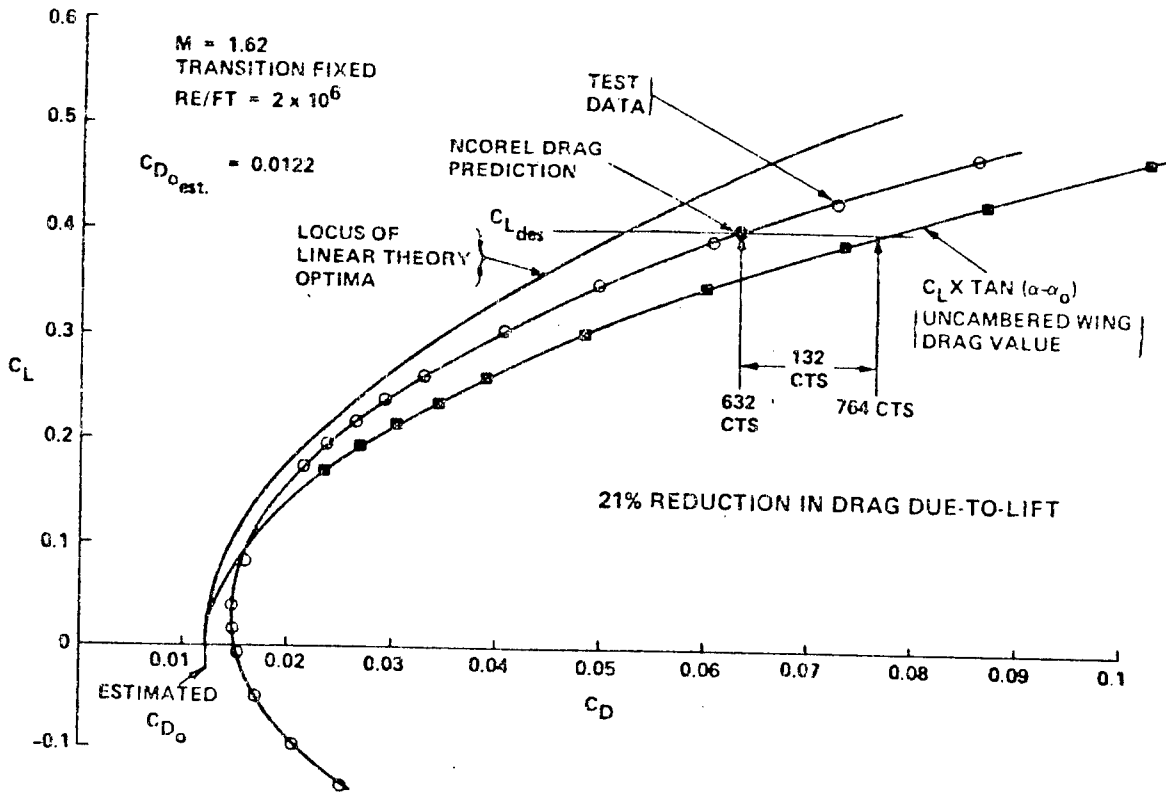


Figure 34. SC<sup>3</sup> Drag Performance  
 (from Mason, Ref. 91)



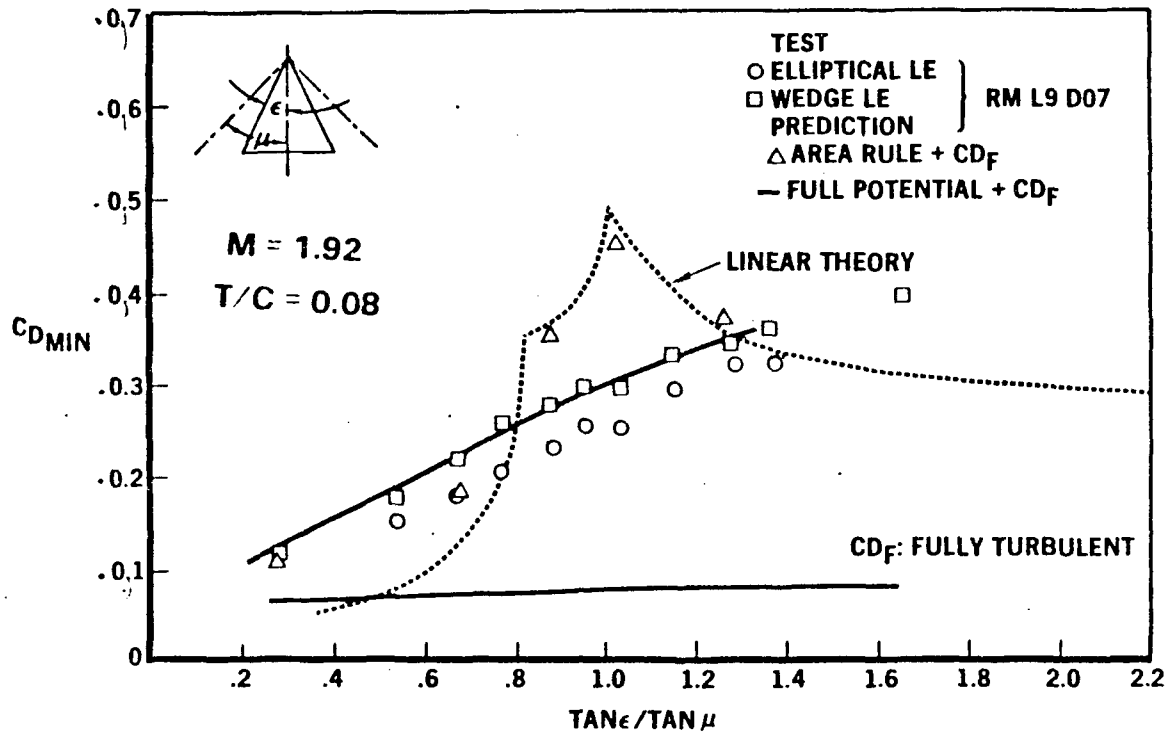


Figure 35. Supersonic Volumetric Efficiency

(from Bonner, et al, Ref. 12)

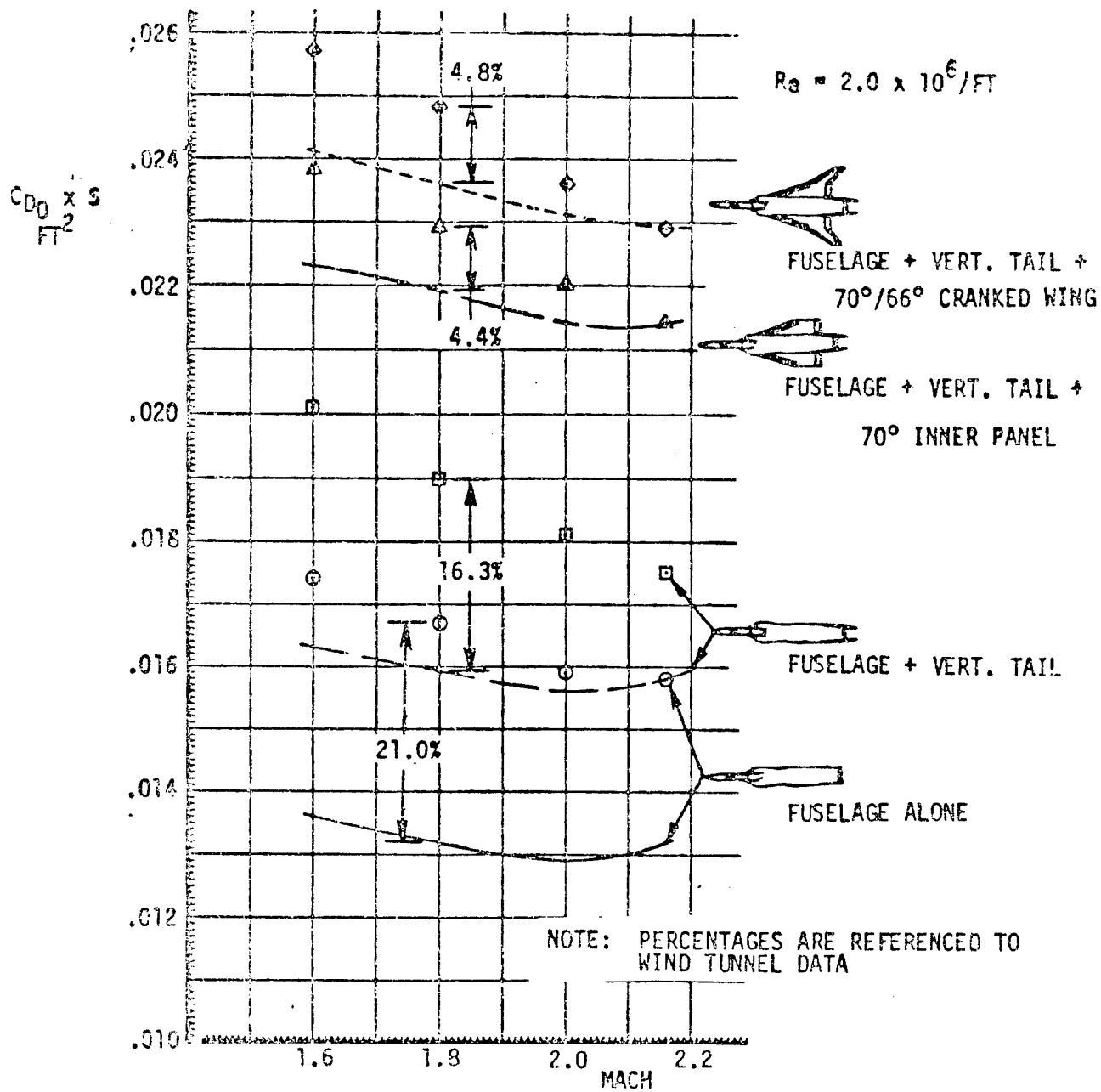
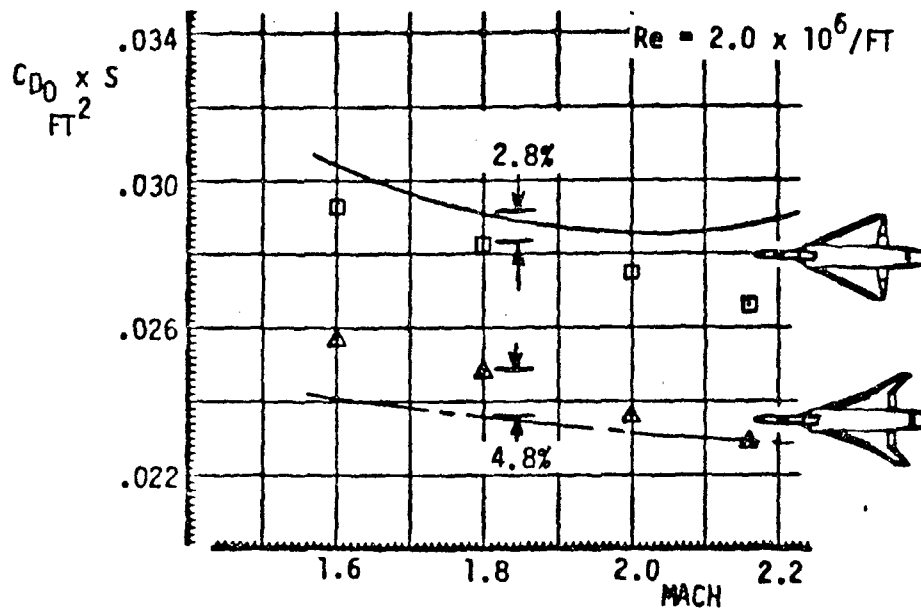
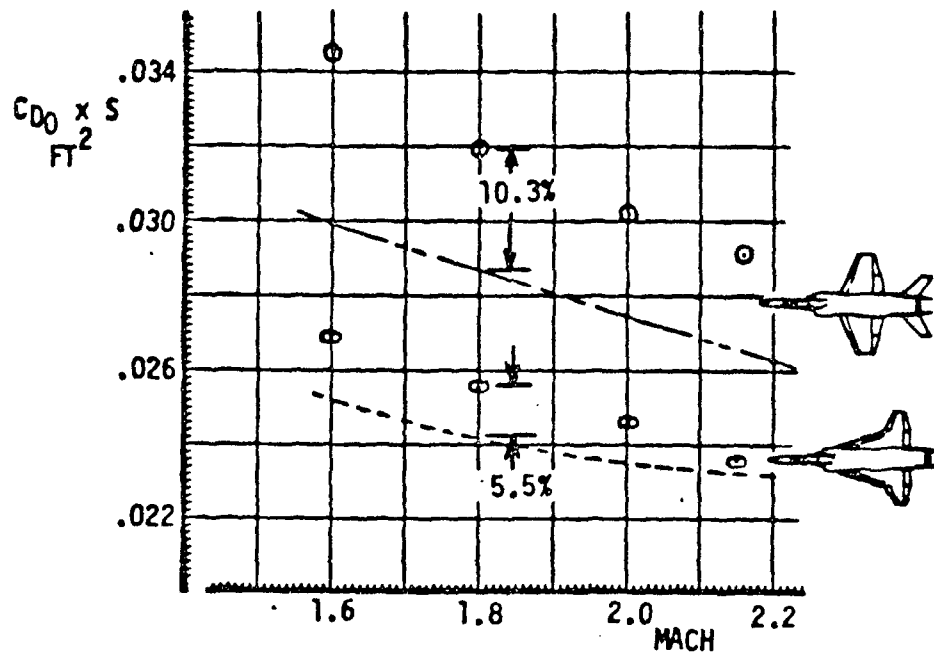


Figure 36. Zero Lift Drag Buildup

(from Wood, et al, Ref. 164)



NOTE: PERCENTAGES ARE REFERENCED TO WIND TUNNEL DATA

Figure 37. Zero Lift Drag Comparison

(from Wood, et al, Ref. 164)